DEVELOPMENT OF A COMPUTER PROGRAM FOR THREE DIMENSIONAL FREQUENCY DOMAIN ANALYSIS OF ZERO SPEED FIRST ORDER WAVE BODY INTERACTION

A Thesis

by

AMITAVA GUHA

Submitted to the Office of Graduate Studies of
Texas A&M University
in partial fulfillment of the requirements for the degree of

MASTER OF SCIENCE

Approved by:

Chair of Committee,   Jeffrey M. Falzarano
Committee Members, Moo-Hyun Kim
                   Alan B. Palazzolo
Head of Department, John Niedzwecki

December 2012

Major Subject: Ocean Engineering

ABSTRACT

Evaluation of motion characteristics of ships and offshore structures at the early stage of design as well as during operation at the site is very important. Strip theory based programs and 3D panel method based programs are the most popular tools used in industry for vessel motion analysis. These programs use different variations of the Green's function or Rankine sources to formulate the boundary element problem which solves the water wave radiation and diffraction problem in the frequency domain or the time domain.

This study presents the development of a 3D frequency domain Green's function method in infinite water depth for predicting hydrodynamic coefficients, wave induced forces and motions. The complete theory and its numerical implementation are discussed in detail. An in house application has been developed to verify the numerical implementation and facilitate further development of the program towards higher order methods, inclusion of forward speed effects, finite depth Green function, hydro elasticity, etc. The results were successfully compared and validated with analytical results where available and the industry standard computer program WAMIT v7.04 for simple structures such as floating hemisphere, cylinder and box barge as well as complex structures such as ship, spar and a tension leg platform.

To my loving parents

ACKNOWLEDGEMENTS

TABLE OF CONTENTS

LIST OF FIGURES

Page

x

xi

LIST OF TABLES

Page

1   INTRODUCTION

1.1 Motivation

Potential-flow methods are widely used in marine hydrodynamics to calculate the forces and corresponding motion responses of floating bodies due to ocean waves. The 2D-Strip theory based methods has been the most commonly used approach for solving motions and loads of slender bodies in waves, e.g. ships (McTaggart (1997)). With the increasing computational power, three dimensional boundary element methods became feasible. These methods remove the requirement of slenderness of the body which make them useful in the hydrodynamic analysis of offshore structures. Recently Computational Fluid Dynamics (CFD) approaches have provided hydrodynamic analysis of floating structures in a fully non-linear wave environment possible. However, long duration CFD simulation in the time domain is still unrealistic due to computational limitations. Potential flow methods give us the means to simulate floating structure behavior accurately for long duration predictions such as motion, loads and even maneuvering and slamming analysis.

The purpose of this work is to develop an in house capability to compute three dimensional hydrodynamic coefficients in the frequency domain using the infinite depth Green's function for zero speed. This has then been extended to convert the frequency domain hydrodynamic coefficients from time domain impulse response functions.

This effort gives us a platform which can be used to further improve on the capability of potential flow methods such as the effect of forward speed or performing higher order drift force calculations, etc.

1.2 Background

The computational methods for calculation of wave loads on floating bodies have been developed over many decades. At first ships were modeled in potential flow using linear strip theory which enabled us to predict the wave loads with reasonable accuracy. However, at a low frequency of encounter, or for full form ships such as tankers, or ships with large Froude Numbers, the result obtained using strip theory were not very satisfactory.

For high sea states, nonlinear effects become important which can be considered in nonlinear strip theory methods where the instantaneous immersion of section shapes are used to obtain the wave loads.

With the increase in computer power, it became possible to develop three dimensional methods to obtain wave loads. Of these, the boundary element method or panel method has become most popular. Panel methods solve the Laplace equation in the fluid domain by distributing sources and dipoles on the body and in some cases on the free surface. These surfaces are divided into triangular or quadrilateral panels with a constant or linearly varying source or dipole with unknown strength. The boundary condition is then applied which is often linearized for simplicity to solve for these unknown strengths. Green's theorem relates the source and dipole distribution strength

to the potential and normal velocity on each panel. Once the potential is obtained we can obtain the velocity and pressure at any point in the fluid domain. The wave forces are found by integrating pressure over the submerged body surface and then applying Newton's law to determine the motions.

The three dimensional methods developed so far can be categorized in two groups: Green's Function Methods and Rankine Source Methods.

1.2.1   Green's Function Methods

The Green's function method determines the velocity potential by distributing sources over the hull surface only. There is no need to discretize and distribute sources over the fluid free surface in this method. The Green's function satisfies the continuity condition and all other boundary conditions including the free surface and radiation conditions but not the body surface boundary condition. LAMP (Lin, Shin, Chung, Zhang and Salvesen (1997)) and WAMIT (Lee and Newman (2005)) are example applications which use this approach.

1.2.2   Rankine Source Methods

The Rankine source methods have been used both in the frequency-domain and in the time domain. In the frequency domain, the velocity potential is determined by distributing Rankine or simple sources $(1/r)$ over the body. Since the Rankine source does not satisfy the free surface condition, a source distribution on the free surface is needed as well,(Nakos, Kring and Sclavounos (1994)).

1.3 Literature Survey

Theoretical development of potential theory started as early as 1950 when John (1950) obtained the infinitesimal motion of fluid in presence of an obstacle. Three dimensional methods came to existence when Hess and Smith (1964) first introduced flow calculation about arbitrary, non-lifting, three dimensional bodies using Rankine source. Later they Hess and Wilcox (1969) extended this theory to include presence of free surface with a small oscillating body. The theory of wave diffraction and scattering is described by Wehausen (1971) to formulate potential flow method for solving motions of floating bodies. Webster (1975) suggested another modification to Hess & Smiths method by discretizing the body surface using triangular panels instead of quadrilaterals. The use of Green's function to represent the source potential in calculating wave loads on large floating bodies is given by Garrison (1978) and Garrison (1984). Two other numerical techniques called the integral-equation method and the hybrid-element method were compared by Mei (1978). Sclavounos and Lee (1985) discuss various topics on boundary element methods such as the properties of spectral techniques and the removal of irregular frequencies. They also show that the hydrodynamic forces predicted by the distribution of source is identical to the force calculated from the direct solution of velocity potentials. The panel method based program is then optimized for large number of panels with controlled accuracy by Newman (1986) and Newman and Sclavounos (1988). Many researchers including Faltinsen (1990) ,Newman (1992), Lee and Newman (2005) presented comprehensive reviews of the panel method for deep water applications.

4

The numerical implementation of the panel method is also well described by McTaggart (2002) and Islam, Islam and Baree (2009). Lin and Liao (2011) attempted a Fast Multiple Boundary Element Method (FEBEM) to solve the wave radiation problem for simple structures.

The efficient evaluation of Green's function and its derivatives are of significant importance in implementing boundary element methods. The computing time involved in the boundary-integral-equation methods almost varies linearly with the computing time required for evaluating the Green's function and its derivatives. The numerical evaluation of Green function was explained in Newman (1984), Ponizy and Noblesse (1994) and Telste and Noblesse (1986). Bingham (1998) and Ponizy, Guilbaud and Ba (1998) also presented an analytical form of the Green function. Ohkusu and Iwashita (1989) numerically integrated the analytical form of Green function to solve the radiation diffraction problem for ships with forward speed. A comparison of classical and simple free surface Green's function is presented in Yang and Lohner (2004). A multipole expansion of the Green's function for fast numerical evaluation is developed and tested by Borgarino, Babarit, Ferrant, Spinneken, Swan *et al.* (2011).

Higher order methods have been developed to increase accuracy of the force prediction. Zhu (1997), Rahman (1984) and Rahman (1998) gave a detailed description of such methods. Kouh and Suen (2001); Willis, Peraire and White (2006); Hong, Nam, Kim, Kim, Hong *et al.* (2011) are other examples of higher order implementations of panel methods.

The motion of floating bodies in the time domain can be obtained by transforming the frequency domain results. McTaggart (2003) presents the transformation techniques. 3D Time domain Green function has been also developed by Liapis (1986) and Beck and Liapis (1987). Liu, Teng, Gou and Sun (2011) replaced the convolution of the time domain Green function with their Fourier transformations and showed good agreement with published results.

1.4 Description of the Present Work

A 3D frequency domain panel method program is developed based on infinite water depth zero speed Green's function. An open source project named APAME 3d panel method developed by Filkovic (2008) for analyzing airfoil at subsonic speed was studied in detail to understand paneling of the vessel hull. The numerical technique developed by Telste and Noblesse (1986) for numerically calculating the Green's function is used for implementing free surface effects. Formulation of the hydrodynamic problem and numerical solution is then developed based on the overall approach suggested by McTaggart (2002).

The application developed is then tested methodically for fully submerged and then floating bodies for a range of frequencies. Many structures ranging from simple hemisphere, cylinder and box barge to complex hull forms including TLP, USN LMSR ship and DWSC spar has been analyzed.

The results were compared to analytical results where available and the well proven commercial program WAMIT v7.0 and found to be in excellent agreement.

2   MATHEMATICAL MODEL

The hydrodynamic forces acting on the floating structure is solved using potential theory. The coordinate system is defined as explained in McTaggart (2002) with its origin in the still water plane aligned vertically with ship center of gravity and center line (see Fig. 1). The wave heading angle is defined as shown in Fig. 2 where zero degree corresponds to the following sea.
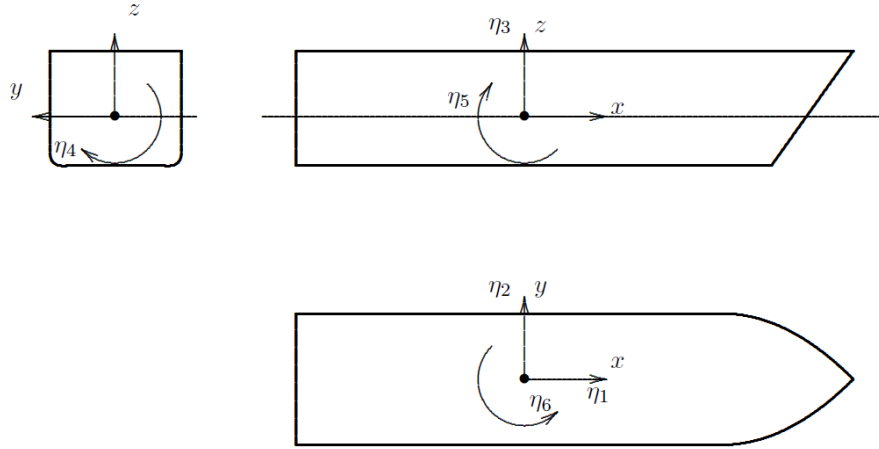
Fig. 1. Coordinate system (As used in McTaggart (2002))
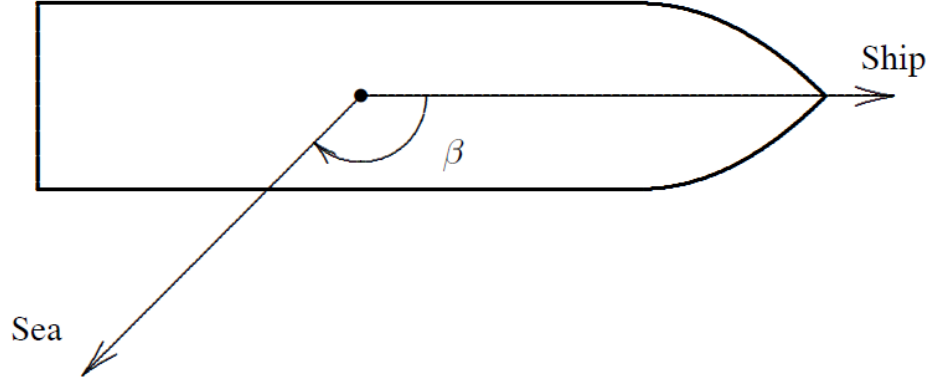
Fig. 2. Sea direction (As used in McTaggart (2002))

2.1 Governing Equations

Assuming the fluid to be irrotational, a velocity potential may be defined as:

$$q = \nabla \Phi(x, y, z, t) \; where, \nabla = \left[\frac{\partial}{\partial x}, \quad \frac{\partial}{\partial y}, \quad \frac{\partial}{\partial z} \right]^{T} \tag{2.1}$$

where q denotes the velocity vector of the fluid and Φ denotes the velocity potential. The total oscillatory velocity potential in the vicinity of a floating body in waves is broken into components as follows:

$$\Phi(x, y, z, t) = \left[\phi_{I}(\vec{x}, \beta) + \phi_{D}(\vec{x}, \beta) + \sum_{j=1}^{6} \eta_{j} \phi_{j}(\vec{x}) \right] e^{i\omega t} \tag{2.2}$$

where Φ is total velocity potential, $\vec{x}$ is location, t is time, ϕ_{I} is incident wave velocity potential, β is the angle of incident waves with respect to positive x axis, ϕ_{D} is

8

diffracted wave velocity potential, η_j is the complex motion amplitude for mode j, ϕ_j is radiation potential for mode j, and ω is the incident wave frequency.

The velocity potential satisfies the Laplace equation in the fluid domain

$$\nabla^2 \phi = 0 \qquad (2.3)$$

The boundary conditions to be satisfied by the potential function are:

1. The linearized combined kinematic and dynamic free surface boundary condition:

$$\frac{\partial \phi}{\partial z} - \frac{\omega^2}{g} \phi = 0 \qquad on \ \ z = 0 \qquad (2.4)$$

2. The sea bottom boundary condition for infinite depth:

$$\frac{\partial \phi}{\partial z} = 0 \qquad on \ \ z = -\infty \qquad (2.5)$$

3. The body surface boundary condition:

$$\frac{\partial \phi}{\partial n} - v_n = 0 \qquad on \ \ S(x, y, z) \qquad (2.6)$$

where v_n denotes the specified complex function which represents the magnitude of normal component of velocity on the immersed surface given by $V_n = Re[v_n(x, y, z)e^{-i\omega t}]$.

2.2 The Solution of Velocity Potentials Using Source Distribution

The potential at some point (x, y, z) in the fluid region may be expressed in terms of a surface distribution of sources.

$$\phi(\vec{x}) = \frac{1}{4\pi} \int_S \sigma(\vec{x}_s) G(\vec{x}; \vec{x}_s) dS \qquad (2.7)$$

9

where $(\vec{x}_s)$ denotes a point on the surface of the body S, and $\sigma(\vec{x}_s)$ denotes the unknown source distribution. The integral is to be carried out over the complete immersed surface of the object. The Greens function satisfies the continuity condition and all boundary conditions including the free surface and radiation boundary conditions, with the exception of the following normal velocity boundary condition on the hull surface:

$$\frac{\partial \phi}{\partial n} = v_n \qquad on \quad S \tag{2.8}$$

where $v_n(x,y,z)$ is the flow normal velocity on the hull surface. The evaluation of Greens function will be discussed in detail in later sections. The source strengths are solved such that following equation is satisfied:

$$-\frac{1}{2}\sigma(\vec{x}) + \frac{1}{4\pi}\int_S \sigma(\vec{x}_s)\frac{\partial G(\vec{x},\vec{x}_s)}{\partial n}dS = v_n(\vec{x}) \qquad on \quad S \tag{2.9}$$

where $\partial G / \partial n$ denotes the derivative of the Green's function in the outward normal direction. This derivative of G may be evaluated from:

$$\frac{\partial G}{\partial n} = \frac{\partial G}{\partial x}n_x + \frac{\partial G}{\partial y}n_y + \frac{\partial G}{\partial z}n_z \tag{2.10}$$

The oscillatory potential components $\phi_k (k = 1, 2...6)$ must satisfy the free-surface condition and the condition that the fluid on the hull surface must move identically to the hull surface.

$$\frac{\partial \phi_k(\vec{x})}{\partial n} = i\omega n_k \tag{2.11}$$

For solution of the wave diffraction potentials, the hull boundary condition is:

10

$$\frac{\partial \phi_D(\vec{x})}{\partial n} = -\frac{\partial \phi_I(\vec{x})}{\partial n} \tag{2.12}$$

2.3 Numerical Solution

The integral Equation (2.9) may be solved numerically by dividing the immersed surface S into N quadrilateral panels of area $\Delta S_j (j = 1, 2, \ldots N)$ and solving the equation at the control point which are at the center of each panel. The discretized form of the Equation (2.9) gives N equations, as given in Garrison (1978).

$$-\frac{1}{2}\sigma_i + \frac{1}{4\pi}\int_S \sigma(\vec{x_s})\frac{\partial G}{\partial n}(\vec{x_i}, \vec{x_s})dS = v_{n_i} \tag{2.13}$$

Furthermore, the surface integral in Equation (2.13) may be written as the sum of the integrals over the N panels of area ΔS_j and, as an approximation, the source strength function $\sigma(x_s, y_s, z_s)$ may be taken as constant over each panel so that Equation (2.13) becomes,

$$-\frac{1}{2}\sigma_i + \frac{1}{2}\sum_{j=1}^{N}\alpha_{ij}\sigma_j = v_{n_i} \qquad i = 1, 2, \ldots N \tag{2.14}$$

where

$$\alpha_{ij} = \frac{1}{2\pi}\int_{\Delta S_j}\frac{\partial G(x, x_s)}{\partial n}dS \tag{2.15}$$

In physical terms, α_{ij} denotes the velocity induced at the ith node point in the direction normal to the surface by a source distribution of unit strength distributed uniformly over the jth panel.

11

In Equation (2.13) the function v_n is considered specified and the elements of the α matrix are defined through the Green's function according to Equation(2.15). The unknown source strength σ_i may, therefore, be obtained through the following equation:

$$[\sigma] = 2[\alpha - I]^{-1}[v_n] \qquad (2.16)$$

where I denotes the unit matrix. Once the inverse of $[\alpha - I]$ matrix is evaluated the vector σ corresponding to several different v_n vectors may be computed with very little computing time. Most computing time is used in evaluating the α matrix and the inversion of $[\alpha - I]$.

Using the same numerical scheme as outlined above, Equation (2.7) may be expressed as the sum

$$\phi_i = \sum_{j=1}^{N} \beta_{ij} \sigma_j \qquad (2.17)$$

in which

$$\beta_{ij} = \frac{1}{4\pi} \int_{\Delta S_j} G(\vec{x}_i, \vec{x}_s) dS \qquad (2.18)$$

Hence, the numerical solution of the surface singularity distribution problem may be expressed as shown in Fig. 3.
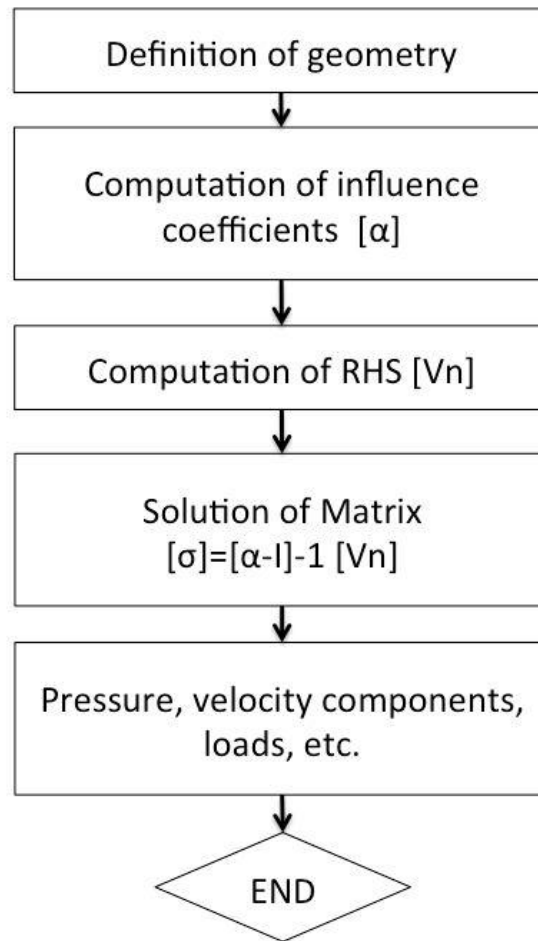
Fig. 3. Steps of obtaining source strength

2.4 Paneling of the Ship Hull

The solution of the three-dimensional velocity potential for a ship hull requires that the hull geometry be modeled using panels. In this work the hull of the structure is divided into quadrilaterals and triangles where triangles are nothing but quadrilateral with two common vertices. The structure can be modeled in any design software like Rhinoceros (McNeel and Associates (2003)) or Solid Works (Planchard and Planchard

13

(2010)). Panelization is done through the meshing program available in most design packages. The mesh created needs to be exported as a GDF file which contains the coordinates of the panel vertices to be used in this program.

The Coordinate of four vertices are $A(x_1,y_1,z_1)$, $B(x_2,y_2,z_2)$, $C(x_3,y_3,z_3)$ and $D(x_4,y_4,z_4)$

Two diagonals of the quadrilateral are calculated as:

$$D_1 = (C - A) = (x_3 - x_1)\hat{i} + (y_3 - y_1)\hat{j} + (z_3 - z_1)\hat{k}$$
$$D_2 = (D - B) = (x_4 - x_2)\hat{i} + (y_4 - y_2)\hat{j} + (z_4 - z_2)\hat{k}$$

$$(2.19)$$

The normal to the panel surface is calculated using vector multiplication of the two diagonal vectors:

$$N = D_1 \times D_2 \tag{2.20}$$

hence the unit normal to the panel surface is

$$n = \frac{N}{|N|} = n_1\hat{i} + n_2\hat{j} + n_3\hat{k} \tag{2.21}$$

Two lengthwise vectors (tangent to the panel surface) are calculated to form the local coordinate system as:

$$L = l_x\hat{i} + l_y\hat{j} + l_z\hat{k} \tag{2.22}$$

where,

$$l_x = \frac{(x_4 + x_3)}{2} - \frac{(x_1 + x_2)}{2}$$
$$l_y = \frac{(y_4 + y_3)}{2} - \frac{(y_1 + y_2)}{2}$$
$$l_z = \frac{(z_4 + z_3)}{2} - \frac{(z_1 + z_2)}{2}$$

$$(2.23)$$

14

and the unit vector is formed as

$$l = l_1 \hat{i} + l_2 \hat{j} + l_3 \hat{k} \tag{2.24}$$

$$l_1 = \frac{l_x}{L}, \ l_2 = \frac{l_y}{L}, \ l_3 = \frac{l_z}{L} \tag{2.25}$$

The other lengthwise vector is perpendicular to the normal and the lengthwise vector as calculated above:

$$P = n \times l \tag{2.26}$$

$$p = \frac{P}{|P|} = p_1 \hat{i} + p_2 \hat{j} + p_3 \hat{k} \tag{2.27}$$

The centroid of the panel is calculated by:

$$
\begin{aligned}
c_x &= \frac{cx_1 d_1 + cx_2 d_2 + cx_3 d_3 + cx_4 d_4}{d_1 + d_2 + d_3 + d_4} \\
c_y &= \frac{cy_1 d_1 + cy_2 d_2 + cy_3 d_3 + cy_4 d_4}{d_1 + d_2 + d_3 + d_4} \\
c_z &= \frac{cz_1 d_1 + cz_2 d_2 + cz_3 d_3 + cz_4 d_4}{d_1 + d_2 + d_3 + d_4}
\end{aligned} \tag{2.28}
$$

where,

$$
\begin{aligned}
d_1 &= \sqrt{(x_2 - x_1)^2 + (y_2 - y_1)^2 + (z_2 - z_1)^2} \\
d_2 &= \sqrt{(x_3 - x_2)^2 + (y_3 - y_2)^2 + (z_3 - z_2)^2} \\
d_3 &= \sqrt{(x_4 - x_3)^2 + (y_4 - y_3)^2 + (z_4 - z_3)^2} \\
d_4 &= \sqrt{(x_1 - x_4)^2 + (y_1 - y_4)^2 + (z_1 - z_4)^2}
\end{aligned} \tag{2.29}
$$

and

15

$$cx_1 = \frac{(x_1 + x_2)}{2}, cx_2 = \frac{(x_2 + x_3)}{2}, cx_3 = \frac{(x_3 + x_4)}{2}, cx_4 = \frac{(x_4 + x_1)}{2},$$

$$cy_1 = \frac{(y_1 + y_2)}{2}, cy_2 = \frac{(y_2 + y_3)}{2}, cy_3 = \frac{(y_3 + y_4)}{2}, cy_4 = \frac{(y_4 + y_1)}{2} \qquad (2.30)$$

$$cz_1 = \frac{(z_1 + z_2)}{2}, cz_2 = \frac{(z_2 + z_3)}{2}, cz_3 = \frac{(z_3 + z_4)}{2}, cz_4 = \frac{(z_4 + z_1)}{2}$$

The panel coordinates $\left[(x_i, y_i, z_i), i = 1 \ldots 4\right]$ are transformed from the body coordinate system $(\hat{i}, \hat{j}, \hat{k})$ to a local coordinate system $(\hat{l}, \hat{p}, \hat{n})$ which lies in the panel surface plane to $\left[(xl_i, yl_i, 0), i = 1 \ldots 4\right]$ using

$$x_{li} = (x_i - c_x)l_1 + (y_i - c_y)l_2 + (z_i - cz)l_3$$
$$y_{li} = (x_i - c_x)p_1 + (y_i - c_y)p_2 + (z_i - cz)p_3 \qquad (2.31)$$
$$i = 1 \ldots 4$$

The source is placed at a point called collocation point which is just below the centroid of the panel lowered by a parameter entered in the configuration file called *COLLDIST* .

$$colx = cx - COLLDIST \cdot n_1$$
$$coly = cy - COLLDIST \cdot n_2 \qquad (2.32)$$
$$colz = cz - COLLDIST \cdot n_3$$

The coordinate of the field point or the center of ith (influenced) panel is calculated in the above local coordinate system which is in the plane of jth (influencing) panel is:

$$cpx = dist_x \cdot l_1 + dist_y \cdot l_2 + dist_z \cdot l_3$$
$$cpy = dist_x \cdot p_1 + dist_y \cdot p_2 + dist_z \cdot p_3 \qquad (2.33)$$
$$cpz = dist_x \cdot n_1 + dist_y \cdot n_2 + dist_z \cdot n_3$$

where

16

$$dist_x = colx(j) - cx(i)$$
$$dist_y = coly(j) - cy(i) \tag{2.34}$$
$$dist_z = colz(j) - cz(i)$$

2.5 Hydrostatics

Hull hydrostatic properties can be computed from the panel properties as given in McTaggart (2002). The volume of a paneled hull is determined by the following discretized equation:

$$\nabla = \sum_{j=1}^{N_p} A_j n_{z-j} z_j \tag{2.35}$$

where N_p is the total number of panels, A_j is the area of panel j, n_{j-z} is the z normal component of the panel j, and z_j is the z value (relative to the waterline) of the centroid of panel j. The location of the center of buoyancy relative to the waterline is:

$$z_{CB} \nabla = \sum_{j=1}^{N_p} A_j n_{z-j} \frac{1}{2} z_j^2 \tag{2.36}$$

The longitudinal center of buoyancy, which corresponds with the longitudinal center of gravity, is given by:

$$x_{CB} \nabla = \sum_{j=1}^{N_p} A_j n_{z-j} z_j x_j \tag{2.37}$$

where x_j is the x value of the centroid of panel j. The hull water plane area, which is used for computing heave stiffness, is given by:

$$A_{wp} = -\sum_{j=1}^{N_p} A_j n_{z-j} \tag{2.38}$$

17

The longitudinal centroid of floatation is given by:

$$x_{wp} A_{wp} = -\sum_{j=1}^{N_p} A_j n_{z-j} x_j \qquad (2.39)$$

Water plane moment terms are:

$$I_{wp-xx} = -\sum_{j=1}^{N_p} A_j n_{z-j} x_j^2 \qquad (2.40)$$

$$I_{wp-yy} = -\sum_{j=1}^{N_p} A_j n_{z-j} y_j^2 \qquad (2.41)$$

Using the above computed values, hydrostatic stiffness terms for motion equations are:

$$
\begin{aligned}
C_{33} &= \rho g A_{wp} \\
C_{35} &= -\rho g A_{wp} x_{wp} \\
C_{44} &= \rho g \left[\nabla z_{CB} - \nabla z_{CG} + I_{wp-yy} \right] \\
C_{53} &= C_{35} \\
C_{55} &= \rho g \left[\nabla z_{CB} - \nabla z_{CG} + I_{wp-xx} \right]
\end{aligned}
\qquad (2.42)
$$

where z_{CG} is the vertical center of gravity obtained from the input parameter VCG.

2.6 Derivation of 3D Green's Function

The deep water Green's function used in eqn. (2.7) has been derived in detail by Kim (2008). The derivation is repeated here for reader's convenience with the coordinate system followed in rest of the thesis.

18

The potential flow due to a 3-D pulsating source at a fixed source point (x_0, y_0, z_0) in the deep water bounded by free surface S_F, bottom surface S_B, and far field cylindrical surface S_∞ will produce 3-D progressing wave.

Let the 3-D source potential be written as:

$$\Phi(x, y, z; x_0, y_0, z_0; t) = \mathrm{Re}\left[(\phi_1 + i\phi_2)e^{-i\omega t}\right] \qquad (2.43)$$

Which satisfies the continuity and boundary conditions as described below:

Continuity: $\qquad \nabla^2 \phi_i = 0, -\infty \le x \le \infty, z \le 0 \qquad (2.44)$

Free Surface: $\qquad \dfrac{\partial \phi_i}{\partial z} - v\phi_i = 0, z = 0 \text{ or on } S_F, v = \dfrac{\omega^2}{g} \qquad (2.45)$

Bottom: $\qquad \dfrac{\partial \phi_i}{\partial z} = 0, z = -\infty \text{ or on } S_B \qquad (2.46)$

Radiation: $\qquad \lim_{R \to \infty} \sqrt{R}\left(\dfrac{\partial \phi_1}{\partial R} + v\phi_2\right) = 0, \text{ on } S_\infty \qquad (2.47)$

where, $R = \sqrt{(x - x_0)^2 + (y - y_0)^2}$

Since the sum of 3-D simple source $1/r$ and 3-D simple sink $-1/r'$ does not satisfy the standing wave flow near the free surface, a third potential $\tilde{G}$ that is harmonic in the lower half domain is added:

$$\phi_1 = \frac{Q}{4\pi}\left(\frac{1}{r} - \frac{1}{r'}\right) + \tilde{G}(x, y, z; x_0, y_0; z_0) \qquad (2.48)$$

where,

$$r = \sqrt{(x - x_0)^2 + (y - y_0)^2 + (z - z_0)^2}$$
$$r' = \sqrt{(x - x_0)^2 + (y - y_0)^2 + (z + z_0)^2} \qquad (2.49)$$

19

2.6.1 The Free Surface Condition

Substituting ϕ_1 into the free surface condition given in eqn. (2.45) gives:

$$\frac{\partial \tilde{G}}{\partial z} - v\tilde{G} = \frac{Q}{2\pi} \frac{\partial}{\partial z_0} \frac{1}{\sqrt{(x-x_0)^2 + (y-y_0)^2 + z_0^2}}, \qquad z = 0 \qquad (2.50)$$

since,

$$\frac{\partial}{\partial z}\left(\frac{1}{r} - \frac{1}{r'}\right) = 2\frac{\partial}{\partial z_0} \frac{-1}{\sqrt{(x-x_0)^2 + (y-y_0)^2 + z_0^2}}, \qquad z = 0 \qquad (2.51)$$

and using the Hankel transform of the exponential function as given in Abramowitz and

Stegun (1972):

$$\int_0^\infty e^{kb} J_0(ka)dk = \frac{1}{\sqrt{(a^2 + b^2)}}, b < 0 \qquad (2.52)$$

We substitute $a = R = \sqrt{(x-x_0)^2 + (y-y_0)^2}$ and $b = z_0$ into eqn. (2.50) and use

eqn. (2.51) to write:

$$\frac{\partial \tilde{G}}{\partial z} - v\tilde{G} = \frac{Q}{2\pi} \frac{\partial}{\partial z_0} \int_0^\infty e^{kz_0} J_0(kR)dk = \frac{Q}{2\pi} \int_0^\infty k e^{kz_0} J_0(kR)dk, z = 0 \qquad (2.53)$$

The harmonic function $\tilde{G}$ may be assumed in the form:

$$\tilde{G} = \frac{Q}{2\pi} \int_0^\infty F(k) e^{k(z+z_0)} J_0(kR)dk \qquad (2.54)$$

with unknown $F(k)$. Substituting in eqn. (2.53) yields:

$$F(k) = \frac{k}{k-v} \qquad (2.55)$$

20

Hence, inserting $F(k)$ into eqn. (2.54), we determine the function $\tilde{G}$:

$$\tilde{G} = \frac{Q}{2\pi} PV \int_0^\infty \frac{k}{k-\nu} e^{k(z+z_0)} J_0(kR) \, dk \tag{2.56}$$

Substituting $\tilde{G}$ in the eqn. (2.48) we get:

$$\phi_1 = \frac{Q}{4\pi}\left(\frac{1}{r}-\frac{1}{r'}\right) + \frac{Q}{2\pi} PV \int_0^\infty \frac{k}{k-\nu} e^{k(z+z_0)} J_0(kR) \, dk \tag{2.57}$$

Since

$$\frac{k}{k-\nu} = 1 + \frac{\nu}{k-\nu} \tag{2.58}$$

We can write:

$$
\begin{aligned}
\phi_1 \quad &= \quad \frac{Q}{4\pi}\left(\frac{1}{r}-\frac{1}{r'}\right) + \frac{Q}{2\pi} PV \int_0^\infty \frac{k}{k-\nu} e^{k(z+z_0)} J_0(kR) \, dk \\[2mm]
&= \quad \frac{Q}{4\pi}\left(\frac{1}{r}-\frac{1}{r'}\right) + \frac{Q}{2\pi} PV \int_0^\infty \left(1 + \frac{\nu}{k-\nu}\right) e^{k(z+z_0)} J_0(kR) \, dk \\[2mm]
&= \quad \frac{Q}{4\pi}\left(\frac{1}{r}-\frac{1}{r'}\right) + \frac{Q}{2\pi} PV \int_0^\infty e^{k(z+z_0)} J_0(kR) \, dk + \frac{Q\nu}{2\pi} PV \int_0^\infty \frac{e^{k(z+z_0)}}{k-\nu} J_0(kR) \, dk \quad (2.59) \\[2mm]
&= \quad \frac{Q}{4\pi}\left(\frac{1}{r}-\frac{1}{r'}\right) + \frac{Q}{2\pi}\frac{1}{r'} + \frac{Q\nu}{2\pi} PV \int_0^\infty \frac{e^{k(z+z_0)}}{k-\nu} J_0(kR) \, dk \\[2mm]
&= \quad \frac{Q}{4\pi}\left(\frac{1}{r}+\frac{1}{r'}\right) + \frac{Q\nu}{2\pi} PV \int_0^\infty \frac{e^{k(z+z_0)}}{k-\nu} J_0(kR) \, dk
\end{aligned}
$$

2.6.2 Radiation Condition

The remaining condition to be satisfied by both ϕ_1 and ϕ_2 is the prescribed radiation condition:

21

$$\lim_{R \to \infty} \sqrt{R} \left(\frac{\partial \phi_1}{\partial R} + v\phi_2 \right) = 0, \, on \, S_\infty \tag{2.60}$$

Since, $(1/r + 1/r')$ of ϕ_1 vanish in the far field, the remaining task is to

investigate the asymptotic expression of the Cauchy PV integral.

We know, the first kind of Hankel function is defined as:

$$H_0^{(1)}(kR) = J_0^{(1)}(kR) + iY_0^{(1)}(kR) \tag{2.61}$$

Therefore, we consider the integral equation:

$$I = \mathrm{Re} \left[PV \int_0^\infty \frac{e^{k(z+z_0)}}{k-v} H_0^{(1)}(kR) dk \right] \tag{2.62}$$
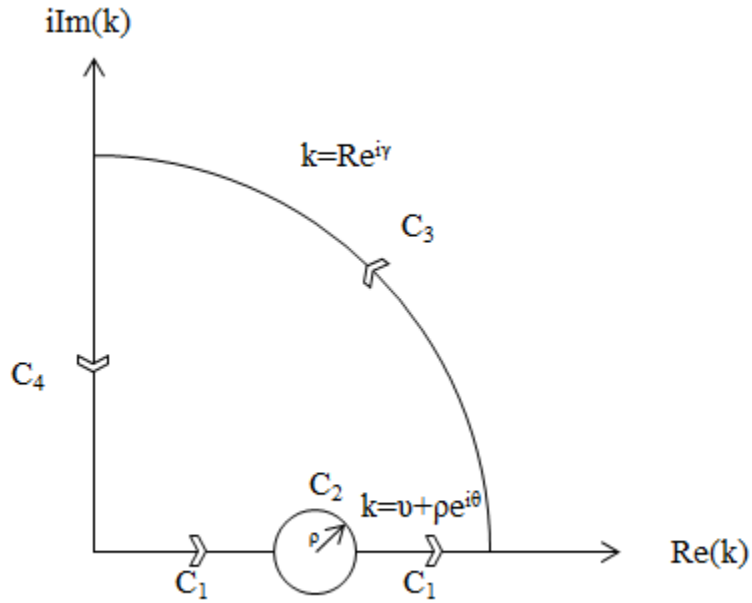

Fig. 4. K-plane

The closed contour integral along C_1, C_2, C_3 and C_4 in the complex k-domain vanishes according to Cauchy theorem as shown in Fig. 4. Further the integration along C_3 and C_4 vanish for the large radius $R \to \infty$, whereas the integral along $C_2 \left(k = \rho e^{i\theta} \right)$ yields a residue at $k = \nu$, i.e.,

$$\operatorname{Re} s \left(k = \nu \right) = -i\pi e^{\nu(z+z_0)} H_0^{(1)} \left(\nu R \right) |_{R \to \infty} \tag{2.63}$$

Substituting in eqn. (2.62) gives:

$$
\begin{aligned}
I &= \operatorname{Re} \left[PV \int_0^\infty \frac{e^{k(z+z_0)}}{k - \nu} H_0^{(1)} \left(kR \right) dk \right] \\
&= \operatorname{Re} \left[i\pi e^{\nu(z+z_0)} H_0^{(1)} \left(kR \right) |_{R \to \infty} \right] \\
&= -\pi e^{\nu(z+z_0)} Y_0 \left(kR \right) |_{R \to \infty}
\end{aligned}
\tag{2.64}
$$

Thus the asymptotic expression of ϕ_1 becomes:

$$
\begin{aligned}
\phi_1 |_{R \to \infty} &= -\frac{Q\nu}{2} e^{\nu(z+z_0)} Y_0 \left(\nu R \right) |_{R \to \infty} \\
&= -Q \sqrt{\frac{\nu}{2\pi R}} e^{\nu(z+z_0)} \sin \left(\nu R - \frac{\pi}{4} \right) + O \left(\frac{1}{R} \right)
\end{aligned}
\tag{2.65}
$$

According to the radiation condition, we can write the potential ϕ_2 as:

$$\phi_2 |_{R \to \infty} = -\frac{1}{\nu} \frac{\partial \phi_1}{\partial R} \tag{2.66}$$

$$\frac{\partial \phi_1}{\partial R} |_{R \to \infty} = -Q\nu \sqrt{\frac{\nu}{2\pi R}} e^{\nu(z+z_0)} \cos \left(\nu R - \frac{\pi}{4} \right) + O \left(\frac{1}{R} \right) \tag{2.67}$$

Hence,

$$\phi_2 |_{R \to \infty} = Q \sqrt{\frac{\nu}{2\pi R}} e^{\nu(z+z_0)} \cos \left(\nu R - \frac{\pi}{4} \right) + O \left(\frac{1}{R} \right) \tag{2.68}$$

23

Substituting ϕ_1 and ϕ_2 in eqn. (2.43) we get:

$$\Phi\mid_{R\to\infty} = \left(\phi_1\cos\omega t + \phi_2\sin\omega t\right)\mid_{R\to\infty}$$

$$= -Q\sqrt{\frac{v}{2\pi R}}e^{v(z+z_0)}\sin\left(vR-\omega t-\frac{\pi}{4}\right)+O\left(\frac{1}{R}\right) \tag{2.69}$$

This indicates progressive outgoing wave in the far-field. Thus the radiation condition has been satisfied.

Since the asymptotic expression of ϕ_2 is similar to cosine function, the ϕ_2 is expressed in terms of First Kind Bessel function $J_0(kR)$

$$\phi_2 = \frac{Qv}{2}e^{v(z+z_0)}J_0(vR) \tag{2.70}$$

2.6.3 Resultant 3-D Source Potential

The resultant 3-D source potential is given in the form:

$$\Phi = \left\{\frac{Q}{4\pi}\left(\frac{1}{r}+\frac{1}{r'}\right) + \frac{Qv}{2\pi}PV\int_0^{\infty}\frac{e^{k(z+z_0)}}{k-v}J_0(kR)\,dk\right\}\cos\omega t$$

$$+\frac{Qv}{2}e^{v(z+z_0)}J_0(vR)\sin\omega t \tag{2.71}$$

If we replace $\dfrac{Q}{4\pi}$ by unity, the resultant potential becomes:

$$\Phi = \left\{\left(\frac{1}{r}+\frac{1}{r'}\right) + 2v\,PV\int_0^{\infty}\frac{e^{k(z+z_0)}}{k-v}J_0(kR)\,dk\right\}\cos\omega t$$

$$+2\pi v\,e^{v(z+z_0)}J_0(vR)\sin\omega t \tag{2.72}$$

24

2.6.4 3-D Green's Function

The pulsating source potential also represents the Green's function if we omit the time factor.

$$\Phi = \text{Re}\left[G\left(P; P_0 \right) e^{-i\omega t} \right] \tag{2.73}$$

with,

$$
\begin{aligned}
G\left(P; P_0 \right) &= \frac{1}{r} + \frac{1}{r'} + 2\nu\, PV \int_0^\infty \frac{e^{k(z+z_0)}}{k-\nu} J_0\left(kR \right) dk \\
&\quad + i2\pi\nu e^{\nu(z+z_0)} J_0\left(\nu R \right)
\end{aligned}
\tag{2.74}
$$

According to Kim (2008) the Green's function is the reciprocating engine for determining velocity potentials at all points on the body surface at all frequencies. Wehausen and Laitone (1960) also presented a Green's function which considers the finite water depth and is used in many panel method codes which is useful for shallow water wave load predictions.

An efficient method of numerical computation of the infinite water Green's function is given by Telste and Noblesse (1986) which is described in next section.

2.7 Numerical Solution of the Green's Function and Its Gradient

Non dimensional coordinates $\vec{x}$ are defined in terms of some reference length L characterizing the size of the wave-radiating/ diffracting body; thus $\vec{x} = \vec{X} / L$ where $\vec{X}$ is dimensional. The mean sea is taken as the lower half-space $z \le 0, z_s \le 0$. The Greens function $G(\vec{x}, \vec{x}_s)$ is the "spatial component" of the velocity potential $Re[G(\vec{x}, \vec{x}_s)e^{-i\omega t}]$

corresponding to the flow at $\vec{x}(x, y, z)$ caused by a singularity at $\vec{x}_s(x_s, y_s, z_s)$. Here t is time, ω is the radian frequency of the waves.

For brevity, the following non dimensional variables are defined:

$$f = \frac{\omega^2 L}{g} \tag{2.75}$$

$$\rho = [(x - x_s)^2 + (y - y_s)^2]^{1/2} \tag{2.76}$$

$$r = [\rho^2 + (z - z_s)^2]^{1/2} \tag{2.77}$$

$$r' = [\rho^2 + (z + z_s)^2]^{1/2} \tag{2.78}$$

$$h = f\rho, v = f(z + z_s), d = (h^2 + v^2)^{1/2} = fr' \tag{2.79}$$

The Green function $G(\vec{x}, \vec{x}_s)$ and its gradients can be expressed in the form

$$G = \frac{1}{r} + \frac{1}{r'} + \tilde{G}_0(\vec{x}, \vec{x}_s, f) \tag{2.80}$$

$$\tilde{G}_0(\vec{x}, \vec{x}_s, f) = 2f\left[R_0(h, v) - i\pi J_0(h)e^v \right] \tag{2.81}$$

Telste and Noblesse (1986) gives the following equations for the derivatives of the frequency dependent portion of the Green function:

$$\frac{\partial \tilde{G}_0}{\partial \rho} = -2f^2\left[R_1(h, v) - i\pi J_1(h)e^v \right] \tag{2.82}$$

$$\frac{\partial \tilde{G}_0}{\partial x} = \frac{(x - x_s)}{\rho} \frac{\partial \tilde{G}_0}{\partial \rho} \tag{2.83}$$

$$\frac{\partial \tilde{G}_0}{\partial y} = \frac{(y - y_s)}{\rho} \frac{\partial \tilde{G}_0}{\partial \rho} \tag{2.84}$$

26

$$\frac{\partial \tilde{G}_0}{\partial z} = 2 f^2 \left[\frac{1}{d} + R_0(h,v) - i\pi J_0(h)e^v \right]$$ (2.85)

where $J_0(h)$ and $J_1(h)$ are the usual Bessel functions of the first kind, $R_0(h,v)$ and $R_1(h,v)$ are real functions to be defined.

2.8 Numerical Integration over a Panel

To evaluate the matrix α in Equation (2.15) and matrix β in Equation (2.18) also shown below, we need to integrate the Greens function and its derivatives over the panel surface.

$$\alpha_{ij} = \frac{1}{2\pi} \int_{\Delta S_j} \frac{\partial G(x, x_s)}{\partial n} dS$$ (2.86)

$$\beta_{ij} = \frac{1}{4\pi} \int_{\Delta S_j} G(\vec{x}_i, \vec{x}_s) dS$$ (2.87)

The Greens function is represented as:

$$G = \frac{1}{r} + \frac{1}{r'} + \tilde{G}_0(\vec{x}, \vec{x}_s, f)$$ (2.88)

Hence,

$$\alpha_{ij} = \frac{1}{2\pi} \int_{\Delta S_j} \frac{\partial}{\partial n}\left(\frac{1}{r}\right) dS + \frac{1}{2\pi} \int_{\Delta S_j} \frac{\partial}{\partial n}\left(\frac{1}{r'}\right) dS + \frac{1}{2\pi} \int_{\Delta S_j} \frac{\partial \tilde{G}_0}{\partial n} dS$$ (2.89)

$$\beta_{ij} = \frac{1}{4\pi} \int_{\Delta S_j} \frac{1}{r} dS + \frac{1}{4\pi} \int_{\Delta S_j} \frac{1}{r'} dS + \frac{1}{4\pi} \int_{\Delta S_j} \tilde{G}_0 dS$$ (2.90)

The frequency independent part of the Greens function is evaluated analytically using the method suggested by Hess and Smith (1964) to obtain α_{ij} and β_{ij}. To evaluate α_{ij}, the following equations are used:

$$\int_{\Delta S_j} \frac{\partial}{\partial n}\left(\frac{1}{r}\right) dS = \int_{\Delta S_j} \frac{\partial}{\partial x}\left(\frac{1}{r}\right) n_x dS + \int_{\Delta S_j} \frac{\partial}{\partial y}\left(\frac{1}{r}\right) n_y dS + \int_{\Delta S_j} \frac{\partial}{\partial z}\left(\frac{1}{r}\right) n_z dS \quad (2.91)$$

$$\int_{\Delta S_j} \frac{\partial}{\partial x}\left(\frac{1}{r}\right) dS = \frac{y_2 - y_1}{d_{12}} ln\left(\frac{r_1 + r_2 - d_{12}}{r_1 + r_2 + d_{12}}\right) + \frac{y_3 - y_2}{d_{23}} ln\left(\frac{r_2 + r_3 - d_{23}}{r_2 + r_3 + d_{23}}\right)$$
$$+ \frac{y_4 - y_3}{d_{34}} ln\left(\frac{r_3 + r_4 - d_{34}}{r_3 + r_4 + d_{34}}\right) + \frac{y_1 - y_4}{d_{41}} ln\left(\frac{r_4 + r_1 - d_{41}}{r_4 + r_1 + d_{41}}\right) \quad (2.92)$$

$$\int_{\Delta S_j} \frac{\partial}{\partial y}\left(\frac{1}{r}\right) dS = \frac{x_1 - x_2}{d_{12}} ln\left(\frac{r_1 + r_2 - d_{12}}{r_1 + r_2 + d_{12}}\right) + \frac{x_2 - x_3}{d_{23}} ln\left(\frac{r_2 + r_3 - d_{23}}{r_2 + r_3 + d_{23}}\right)$$
$$+ \frac{x_3 - x_4}{d_{34}} ln\left(\frac{r_3 + r_4 - d_{34}}{r_3 + r_4 + d_{34}}\right) + \frac{x_4 - x_1}{d_{41}} ln\left(\frac{r_4 + r_1 - d_{41}}{r_4 + r_1 + d_{41}}\right) \quad (2.93)$$

$$\int_{\Delta S_j} \frac{\partial}{\partial z}\left(\frac{1}{r}\right) dS = tan^{-1}\left(\frac{m_{12}e_1 - h_1}{zr_1}\right) - tan^{-1}\left(\frac{m_{12}e_2 - h_2}{zr_2}\right)$$
$$+ tan^{-1}\left(\frac{m_{23}e_2 - h_2}{zr_2}\right) - tan^{-1}\left(\frac{m_{23}e_3 - h_3}{zr_3}\right) \quad (2.94)$$
$$+ tan^{-1}\left(\frac{m_{34}e_3 - h_3}{zr_3}\right) - tan^{-1}\left(\frac{m_{34}e_4 - h_4}{zr_4}\right)$$
$$+ tan^{-1}\left(\frac{m_{41}e_4 - h_4}{zr_4}\right) - tan^{-1}\left(\frac{m_{41}e_4 - h_1}{zr_1}\right)$$

β_{ij} is evaluated using the analytical expressions given in Katz and Plotkin (2001):

$$\int_{\Delta S_j} \frac{1}{r} dS = \left[\frac{(x - x_1)(y_2 - y_1) - (y - y_1)(x_2 - x_1)}{d_{12}} \ln \frac{r_1 + r_2 + d_{12}}{r_1 + r_2 - d_{12}} \right.$$

$$\frac{(x - x_2)(y_3 - y_2) - (y - y_2)(x_3 - x_2)}{d_{23}} \ln \frac{r_2 + r_3 + d_{23}}{r_2 + r_3 - d_{23}}$$

$$\frac{(x - x_3)(y_4 - y_3) - (y - y_3)(x_4 - x_3)}{d_{34}} \ln \frac{r_3 + r_4 + d_{34}}{r_3 + r_4 - d_{34}}$$

$$\left. \frac{(x - x_4)(y_1 - y_4) - (y - y_4)(x_1 - x_4)}{d_{41}} \ln \frac{r_4 + r_1 + d_{41}}{r_4 + r_1 - d_{41}} \right]$$

$$- |z| \left[\tan^{-1} \left(\frac{m_{12} e_1 - h_1}{z r_1} \right) - \tan^{-1} \left(\frac{m_{12} e_2 - h_2}{z r_2} \right) \right.$$

$$+ \tan^{-1} \left(\frac{m_{23} e_2 - h_2}{z r_2} \right) - \tan^{-1} \left(\frac{m_{23} e_3 - h_3}{z r_3} \right)$$

$$+ \tan^{-1} \left(\frac{m_{34} e_3 - h_3}{z r_3} \right) - \tan^{-1} \left(\frac{m_{34} e_4 - h_4}{z r_4} \right)$$

$$\left. + \tan^{-1} \left(\frac{m_{41} e_4 - h_4}{z r_4} \right) - \tan^{-1} \left(\frac{m_{41} e_1 - h_1}{z r_1} \right) \right] \right] \tag{2.95}$$

where,

$$d_{12} = \sqrt{(x_2 - x_1)^2 + (y_2 - y_1)^2}$$

$$d_{23} = \sqrt{(x_3 - x_2)^2 + (y_3 - y_2)^2}$$

$$d_{34} = \sqrt{(x_4 - x_3)^2 + (y_4 - y_3)^2} \tag{2.96}$$

$$d_{41} = \sqrt{(x_1 - x_4)^2 + (y_1 - y_4)^2}$$

$$m_{12} = \frac{y_2 - y_1}{x_2 - x_1} \quad m_{23} = \frac{y_3 - y_2}{x_3 - x_2}$$

$$m_{34} = \frac{y_4 - y_3}{x_4 - x_3} \quad m_{41} = \frac{y_1 - y_4}{x_1 - x_4} \tag{2.97}$$

$$r_k = \sqrt{(x - x_k)^2 + (y - y_k)^2 + z^2}, k = 1, 2, 3, 4 \tag{2.98}$$

$$e_k = z^2 + (x - x_k)^2, k = 1, 2, 3, 4 \tag{2.99}$$

29

$$h_k = (y - y_k)(x - x_k), k = 1, 2, 3, 4 \tag{2.100}$$

The values of the terms which would be infinity while implementing the above equation numerically were set to 0. This is achieved by checking the denominator to be greater than a small error parameter entered through input file (e.g. ERROR 0.0000001).

The integration of frequency dependent term which is the wavy Green function ($\tilde{G}_0$) and its derivative ($\dfrac{\partial \tilde{G}_0}{\partial n}$) can be done is multiple ways. For higher accuracy a Gauss Quadrature method may be applied. However, these terms are regular throughout the fluid domain and oscillate approximately with wave length L . In practice L is generally large compared to the dimension of the immersed panel surface, so $\tilde{G}_0$ and $\dfrac{\partial \tilde{G}_0}{\partial n}$ vary slowly over S . Thus, a valid and convenient approximation to the integral is to evaluate the integrands at the centroid of the panel and multiply by ΔS_j .

2.9 Radiation Velocity Potentials

Radiation velocity potentials are obtained by solving the equation:

$$[\sigma] = 2[\alpha - I]^{-1}[v_n] \tag{2.101}$$

where $[v_n]$ is obtained by satisfying hull boundary condition for radiation

$$[v_n] = \frac{\partial \phi_k(x, y, z)}{\partial n} = i\omega n_k \tag{2.102}$$

where n_k is the generalized unit normal defined as

$$(n_1, n_2, n_3) = \vec{n} \tag{2.103}$$

30

$$(n_4, n_5, n_6) = \vec{r} \times \vec{n} \tag{2.104}$$

where

$\vec{n}$ = unit normal pointing outward of hull surface

$= n_1 \hat{i} + n_2 \hat{j} + n_3 \hat{k}$

$\vec{r}$ = is a vector from the origin to a point on the hull surface

$= x\hat{i} + y\hat{j} + z\hat{k}$

Radiation potential for each mode (i.e. surge, sway, heave, roll, pitch, yaw) is then calculated as

$$\phi_i = \sum_{j=1}^{N} \beta_{ij} \sigma_j \tag{2.105}$$

where σ_j is obtained by substituting v_n for that mode.

2.10   Incident and Diffracted Wave Potentials

The complex potential of a regular wave system for deep water is as follows:

$$\phi_I = \frac{iga}{\omega} exp\left[-ik\left(xcos\beta - ysin\beta\right)\right] exp\left(kz\right) \tag{2.106}$$

where a is the incident wave amplitude, we will use $a = 1$ for our calculations to obtain the RAOs. The above equation is based on the convention of the wave crest being at the xy origin at time $t = 0$. Fluid velocities are given by the following derivatives:

$$\frac{\partial \phi_I}{\partial x} = a\omega cos\beta \, exp\left[-ik\left(xcos\beta - ysin\beta\right)\right] exp\left(kz\right) \tag{2.107}$$

$$\frac{\partial \phi_I}{\partial y} = a\omega sin\beta \, exp\left[-ik\left(xcos\beta - ysin\beta\right)\right] exp\left(kz\right) \tag{2.108}$$

$$\frac{\partial \phi_I}{\partial z} = ia\omega \exp\left[-ik\left(x\cos\beta - y\sin\beta\right)\right]\exp\left(kz\right) \tag{2.109}$$

The diffraction potential ϕ_D is solved using

$$[\sigma] = 2[\alpha - I]^{-1}[v_n] \tag{2.110}$$

where $[v_n]$ is obtained by satisfying diffraction boundary condition:

$$\phi_i = \sum_{j=1}^{N} \beta_{ij}\sigma_j \tag{2.111}$$

where σ_j is calculated by substituting v_n obtained above.

2.11 Linearized Pressure Force on the Body

The total pressure in the fluid is given by Bernoulli's equation

$$p = -\rho\left(\frac{\partial \Phi}{\partial t} + \nabla\Phi.\nabla\Phi + gz\right) \tag{2.112}$$

where

$$\Phi = \phi e^{i\omega t} \tag{2.113}$$

The first term on the right side of Equation (2.112) is the linear component of the dynamic pressure, which is written in the complex form as $-i\rho\omega\phi$. The second term is the quadratic pressure, which contributes to the second-order forces. The third term is the hydrostatic pressure, which contributes to the restoring forces.

The linearized dynamic pressure on the immersed surface due to the six-degree of freedom motion of the body is given by:

$$p = -\rho\frac{\partial \Phi}{\partial t} \tag{2.114}$$

32

$$p_k = -\rho\omega\left[i\phi_k\right], k = 1, 2, ..., 6 \tag{2.115}$$

and the dynamic pressure due to wave interaction with the fixed hull is given as:

$$p_D = -\rho\omega\left[i(\phi_I + \phi_D)\right] \tag{2.116}$$

The total pressure is expressed as:

$$p = -\rho i\omega\left[\phi_I + \phi_D + \sum_{j=1}^{6}\eta_j\phi_j\right] \tag{2.117}$$

where η_j is the complex motion amplitude for the mode j. In our calculation we will set

$\eta_j = 1$.

The forces and moments caused by the dynamic fluid pressure acting on the immersed surface on the body are determined from the below expressions as given in Garrison (1978):

$$F_{ij}(t) = -\int_S P_j n_i dS \qquad i, j = 1, 2, ..., 6 \tag{2.118}$$

$$F_i(t) = -\int_S P_D n_i dS \qquad i = 1, 2, ..., 6 \tag{2.119}$$

where F_i denotes the ith component of wave excitation force or moment and F_{ij} denotes the ith component of force or moment arising from j^{th} component of body motion. The function n_i are generalized normal vectors $(n_1, n_2, n_3) = \vec{n}$ and $(n_3, n_4, n_5) = \vec{r} \times \vec{n}$ where $\vec{n}$ is the normal to the body surface and $\vec{r}$ is the position vector of the center of the body surface panel.

$$\begin{aligned}
n_1 &= n_x, n_2 = n_y, n_3 = n_z, n_4 = \left(\vec{r} \times \vec{n}\right)_x = yn_z - zn_y \\
n_5 &= \left(\vec{r} \times \vec{n}\right)_y = zn_x - xn_z, n_6 = \left(\vec{r} \times \vec{n}\right)_z = xn_y - yn_x
\end{aligned} \tag{2.120}$$

33

2.12   Added Mass and Damping Coefficients

As given in Ship Motion Lecture notes:

$$A_{jk} = -\frac{\rho}{\omega} \int_S n_j Im(\phi_k) dS \qquad (2.121)$$

$$B_{jk} = -\rho \int_S n_j Re(\phi_k) dS \qquad (2.122)$$

Non-dimensional values are:

$$\overline{A}_{ij} = \frac{A_{ij}}{\rho L^k} \qquad (2.123)$$

$$\overline{B}_{ij} = \frac{B_{ij}}{\rho L^k \omega} \qquad (2.124)$$

Here

$$
\begin{aligned}
&\text{k=3 for (i,j=1,2,3)}\\
&\text{k=4 for (i=1,2,3, j=4,5,6), or,(i=4,5,6, j=1,2,3)} \qquad (2.125)\\
&\text{k=5 for (i,j=4,5,6)}
\end{aligned}
$$

2.13   Exciting Forces

The exciting forces due to wave body interaction is calculated using two methods as explained in Lee (1995).

2.13.1 Total Exciting Forces from the Haskind Relations:

$$X_k = -i\omega\rho \int_S \left(n_k \phi_I - \phi_k \frac{\partial \phi_I}{\partial n} \right) dS \qquad (2.126)$$

2.13.2 Exciting Forces from Direct Integration of Hydrodynamic Pressure:

$$X_k = -i\omega\rho \int_S n_k \left(\phi_I + \phi_D\right) dS \qquad (2.127)$$

$$\overline{X}_i = \frac{X_i}{\rho g A L^m} \qquad (2.128)$$

where $m=2$ for $i=1,2,3$ and $m=3$ for $i=4,5,6$. A is the wave amplitude (1 in this case) and L is the characteristic length parameter $ULEN$.

2.14 Body Motion in Waves

The oscillatory motion of a freely floating body with harmonic excitation and without external constraints can be obtained by solving the equation of motion:

$$\sum_{j=1}^{6}\left[-\omega^2\left(M_{ij} + A_{ij}\right) + i\omega B_{ij} + C_{ij}\right]\xi_j = X_i \qquad (2.129)$$

where

$$m = \rho\nabla \qquad (2.130)$$

$$x_b = x_g \qquad y_b = y_g \qquad (2.131)$$

$$M = \begin{pmatrix} m & 0 & 0 & 0 & mz_g & -my_g \\ 0 & m & 0 & -mz_g & 0 & mx_g \\ 0 & 0 & m & my_g & -mx_g & 0 \\ 0 & -mz_g & my_g & I_{11} & I_{12} & I_{13} \\ mz_g & 0 & -mx_g & I_{21} & I_{22} & I_{23} \\ -my_g & mx_g & 0 & I_{31} & I_{32} & I_{33} \end{pmatrix} \qquad (2.132)$$

$$I_{ij} = \rho\nabla r_{ij}\left|r_{ij}\right| \qquad (2.133)$$

35

The array $XPRDCT(I,J)$ which is obtained from user input file contains the radius of gyration (r_{ij}) with the same units of length as the length scale $ULEN$ defined in the panel data file.

3 INCORPORATING EFFECT OF FORWARD SHIP SPEED

The effect of forward ship speed may be approximated for moderate vessel speeds by including encounter frequency. The method explained here follows the procedure outlined by McTaggart (2002). The setup up of the problem is similar to as explained in Section 2 with a few modified terms as shown below:

3.1 Modifications in Governing Equations

The total velocity potential in eqn. (2.2) may be modified as:

$$\Phi(x,y,z,t) = \mathrm{Re}\left\{\left[\phi_I(\vec{x},\beta,\omega_I) + \phi_D(\vec{x},\beta,\omega_I) + \sum_{j=1}^{6}\eta_j\phi_j(\vec{x},U,\omega_e)\right]e^{i\omega_e t}\right\} \qquad (3.1)$$

The wave encounter frequency ω_e is given by:

$$\omega_e = \left|\omega_I - k_I U \cos\beta_S\right| \qquad (3.2)$$

Wave number for radiated wave is given by:

$$k_e = \frac{\omega_e^{\;2}}{g} \qquad (3.3)$$

Neglecting second and higher order terms, the oscillatory pressure acting on the ship hull is given by:

$$p = -\rho\left(i\omega_e - U\frac{\partial}{\partial x}\right)\left[\phi_I + \phi_D + \sum_{j=1}^{6}\eta_j\phi_j\right] - \rho g\zeta_3 \qquad (3.4)$$

37

The last term of the above equation denotes the oscillatory pressure due to hydrostatic pressure, with ζ_3 being the oscillatory vertical displacement:

$$\zeta_3 = \eta_3 + y\eta_4 - x\eta_5 \qquad (3.5)$$

The oscillatory motion of the ship can be solved as follows:

$$\left\{ -\omega_e^2 \left([M] + [A] \right) + i\omega_e [B] + [C] \right\} \{\eta\} = \{F^I + F^D\}$$

where $[M]$ is the ship mass matrix, $[A]$ is the added mass matrix, $[B]$ is the radiation damping, $[C]$ is the hydrostatic stiffness matrix, $\{F^I\}$ is the incident wave force vector, and $\{F^D\}$ is the wave diffraction force vector. The added mass and damping matrix terms are given by:

$$A_{jk} = -\frac{\rho}{\omega_e} \int_S \left[\operatorname{Im}(\phi_k) - \frac{U}{\omega_e} \operatorname{Re}\left(\frac{\partial \phi_k}{\partial x} \right) \right] n_j \, dS \qquad (3.6)$$

$$B_{jk} = -\rho \int_S \left[\operatorname{Re}(\phi_k) - \frac{U}{\omega_e} \operatorname{Im}\left(\frac{\partial \phi_k}{\partial x} \right) \right] n_j \, dS \qquad (3.7)$$

The wave excitation forces on the ship are given by:

$$F_j^I = \rho \omega_e \int_S \left(i\phi_I - \frac{U}{\omega_e} \frac{\partial \phi_I}{\partial x} \right) n_j \, dS \qquad (3.8)$$

$$F_j^D = \rho \omega_e \int_S \left(i\phi_I - \frac{U}{\omega_e} \frac{\partial \phi_D}{\partial x} \right) n_j \, dS \qquad (3.9)$$

The solution of velocity potential using source distribution remains same except the radiation boundary condition in eqn. (2.11) which is modified as:

$$\frac{\partial \phi_k(\vec{x})}{\partial n} = i\omega_e n_k \tag{3.10}$$

3.2 Radiation Velocity Potential for Non-Zero Forward Speed

The velocity potentials for non-zero forward speed may be calculated efficiently from velocity potentials for zero forward speed. Beck and Loken (1989), Papanikolaou and Schellin (1992) and Salvesen, Tuck and Faltinsen (1970) used this method as well for velocity potential calculation. Once the velocity potential for zero speed is found, velocity potential at non-zero speed are given by:

$$
\begin{aligned}
\phi_1\left(U, \omega_e\right) &= \phi_1\left(0, \omega_e\right) \\
\phi_2\left(U, \omega_e\right) &= \phi_2\left(0, \omega_e\right) \\
\phi_3\left(U, \omega_e\right) &= \phi_3\left(0, \omega_e\right) \\
\phi_4\left(U, \omega_e\right) &= \phi_4\left(0, \omega_e\right) \\
\phi_5\left(U, \omega_e\right) &= \phi_5\left(0, \omega_e\right) + \frac{U}{i\omega_e}\phi_3\left(0, \omega_e\right) \\
\phi_6\left(U, \omega_e\right) &= \phi_6\left(0, \omega_e\right) + \frac{U}{i\omega_e}\phi_2\left(0, \omega_e\right)
\end{aligned}
\tag{3.11}
$$

Similarly, the x derivatives of the forward speed potentials can be evaluated using the x derivatives of the zero speed potentials.

As mentioned before, the speed correction term used in above equations are approximate and are based on the assumption of U/ω_e being small. Care should be taken when using the above model for practical purposes. An upper limit for U/ω_e equal to $L/2$ is suggested by McTaggart (2002).

More accurate but computationally intensive methods using frequency domain Green's function which incorporates forward ship effect has been also developed. One of such implementation is presented in Inglis and Price (1981). Many such algorithms exist among which the Green's function developed by Ba and Guilbaud (1995) is considered most efficient and most commonly used.

The selection of method for incorporating forward speed effect in the presented code here is under consideration and has not been implemented yet. The results presented in this thesis are evaluated for zero speed case only.

4   IRREGULAR FREQUENCY REMOVAL

4.1 Definition of the Irregular Frequencies

The integral equation formulated using unknown source strengths in eqn. (2.9) is solved to obtain the potential at the centroid of body surface panels from which we calculate the flow velocity and pressure to obtain the wave force on the floating body. The Fredholm determinant of this integral equation vanishes at the irregular frequencies. It is shown by Ohmatsu (1975) that the irregular frequencies corresponds to the eigenfrequencies of the interior homogeneous Dirichlet problem.

It is not possible to analytically determine the irregular frequencies for an arbitrary shaped body. However, for simple structures such as a truncated cylinder or a box barge it is possible to solve the Laplace equation with Dirichlet boundary condition to determine the location of the irregular frequencies. Example calculation for analytically determining the irregular frequencies is shown in Zhu (1994).

4.1.1   Irregular Frequency of Truncated Circular Cylinder

The irregular frequencies may be calculated analytically for truncated circular cylinder. Considering a cylinder of radius R and draft T, the velocity potential $\phi_-(x)$ is may be represented as:

$$\phi_-(x) = \begin{Bmatrix} \sinh kz \\ \cosh kz \end{Bmatrix} \begin{Bmatrix} \cos m\theta \\ \sin m\theta \end{Bmatrix} J_m(kr) \qquad (4.1)$$

where $m = 0, 1, 2, ...,$ and J_m is the Bessel function of order m.

Since $\phi_-(x)$ satisfies the homogeneous Dirichlet condition on the cylinder bottom, the above equation becomes

$$\phi_-(x) = \sinh k(z+T) \begin{Bmatrix} \cos m\theta \\ \sin m\theta \end{Bmatrix} J_m(kr) \qquad (4.2)$$

On applying the homogeneous Dirichlet condition on the surface of the cylinder, $J_m(kR) = 0$ defines a set of k's. These values of k corresponds to the irregular frequencies.

The infinite depth wavenumber K is calculated using the relation obtained by applying the free surface condition:

$$K = k \coth kT \qquad (4.3)$$

The values calculated for a truncated floating cylinder of radius R=1 and draft T=1 using Fig. 5 is shown in Table 1.
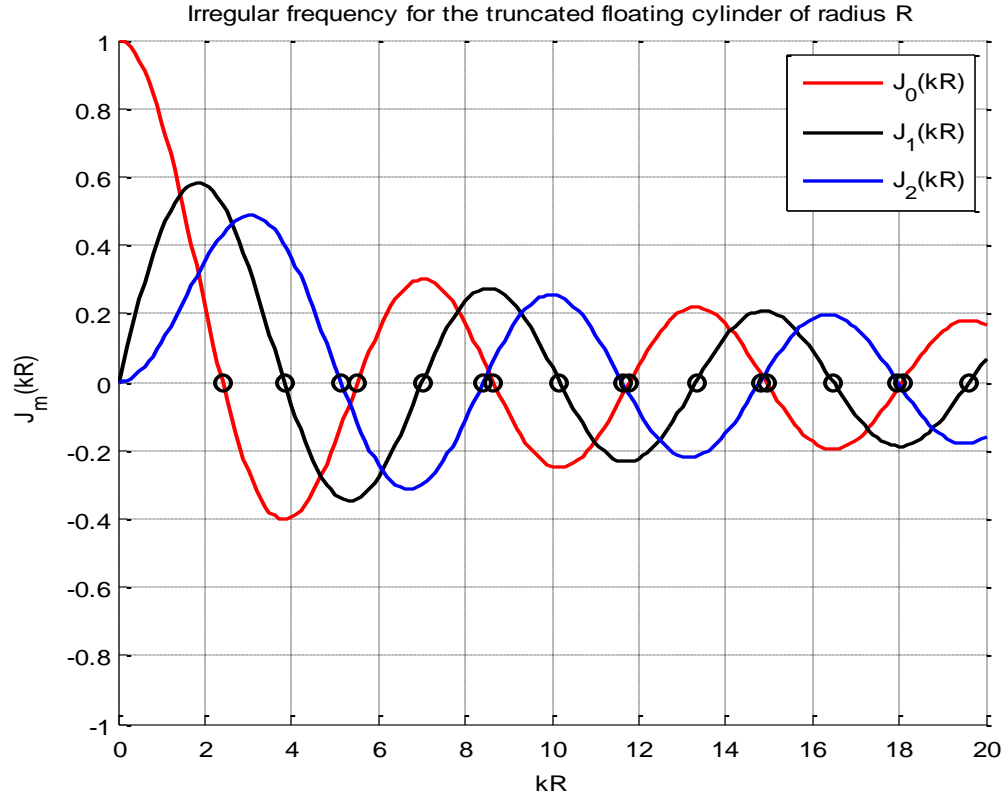
Fig. 5. Irregular frequency of the truncated floating cylinder of radius R

Table 1: List of irregular frequencies

k	K	ω	ω√(L/g)
2.4048	2.4443	4.8966	1.5634
3.8317	3.8353	6.1336	1.9584
5.1356	5.136	7.0978	2.2663
5.5201	5.5203	7.3586	2.3495
7.0156	7.0156	8.2956	2.6487
8.4172	8.4172	9.0866	2.9012
8.6537	8.6537	9.2133	2.9417
10.1735	10.1735	9.9896	3.1896
11.6198	11.6198	10.6762	3.4088
11.7915	11.7915	10.7547	3.4339
13.3237	13.3237	11.4321	3.6502
14.796	14.796	12.0472	3.8466
14.9309	14.9309	12.102	3.8641
16.4706	16.4706	12.7107	4.0584
17.9598	17.9598	13.2729	4.2379
18.0711	18.0711	13.3139	4.251
19.6159	19.6159	13.8713	4.429
21.117	21.117	14.3923	4.5953
21.2116	21.2116	14.4245	4.6056

The effect of irregular frequency is shown in Fig. 6, Fig. 7, Fig. 8 and Fig. 9 in the numerically calculated added mass and damping plots.
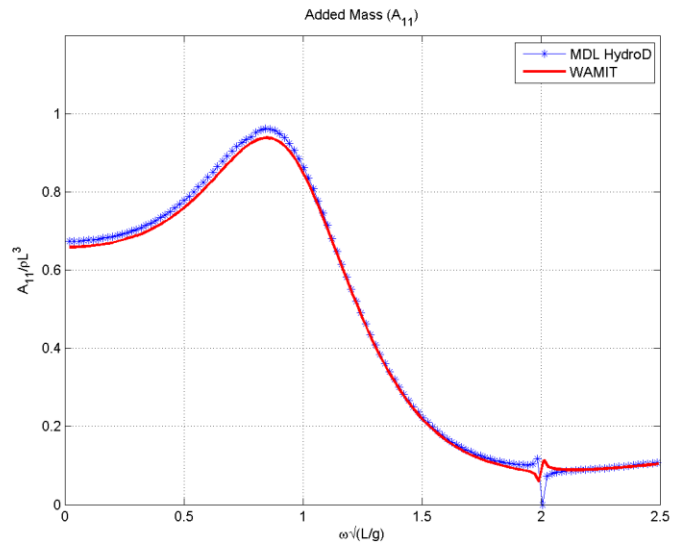
Fig. 6. Irregular frequency at non dimensional frequency 1.96 shown in numerically calculated surge added mass (A_{11})
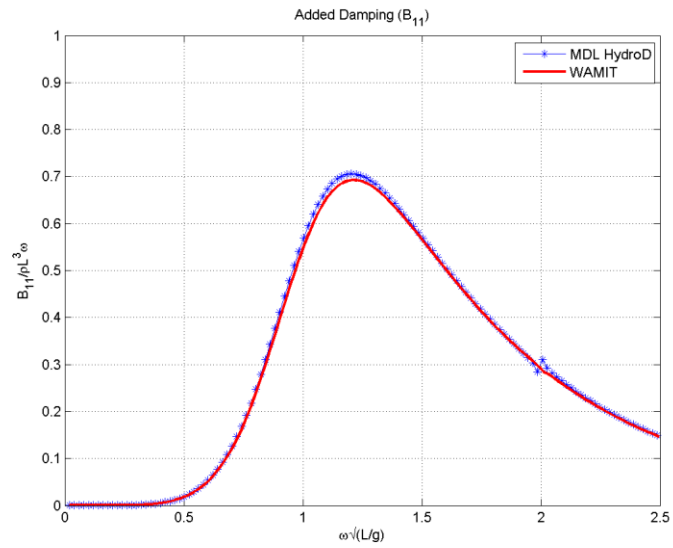
Fig. 7. Irregular frequency at non dimensional frequency 1.96 shown in numerically calculated surge damping (B_{11})
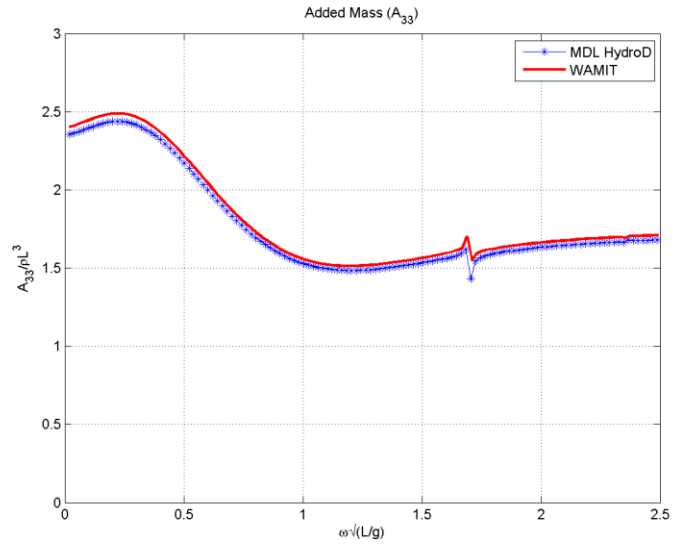
Fig. 8. Irregular frequency at non dimensional frequency 1.56 and 2.27 shown in numerically calculated heave added mass (A_{33})
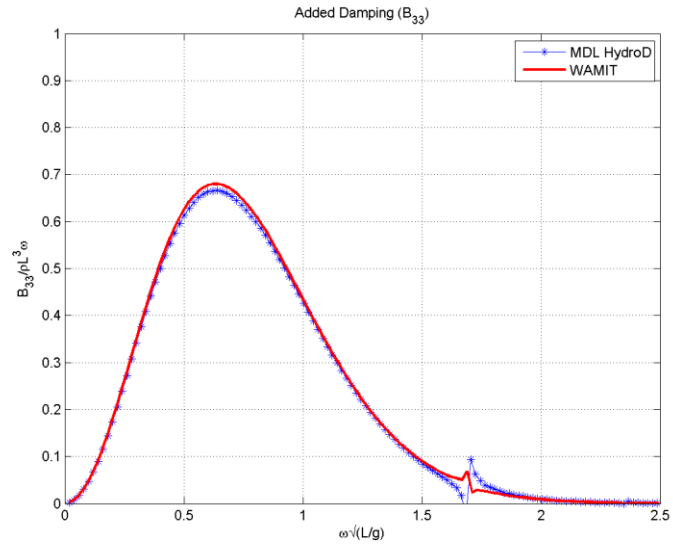
Fig. 9. Irregular frequency at non dimensional frequency 1.56 and 2.27 shown in numerically calculated heave damping (B_{33})

46

4.1.2 Irregular Frequency of Box Barge

The irregular frequency of a box barge of length L, breadth B and draft T may also be found analytically. Considering $\phi_-(x)$ satisfying homogeneous Dirichlet condition on the bottom:

$$\phi_-(x) = \sin k\,(z+T)\begin{Bmatrix}\cos k_1 x\\ \sin k_1 x\end{Bmatrix}\begin{Bmatrix}\cos k_2 y\\ \sin k_2 y\end{Bmatrix} \tag{4.4}$$

$$k = \left(k_1^{\,2} + k_2^{\,2}\right)^{1/2} \tag{4.5}$$

To satisfy the homogeneous Dirichlet boundary condition on the sides $x = \pm L/2$ and $y = \pm B/2$, the value of k_1 and k_2 must be:

$$k_1 = \frac{2}{L}\begin{Bmatrix} n\pi \\ n\pi + \dfrac{\pi}{2}\end{Bmatrix} \tag{4.6}$$

$$k_2 = \frac{2}{B}\begin{Bmatrix} m\pi \\ m\pi + \dfrac{\pi}{2}\end{Bmatrix} \tag{4.7}$$

where $m, n = 0,1,\cdots$ .The above two equations and eqn. (4.5) gives a discrete set of irregular frequencies.

The calculation for a box barge of L=80m, B=20m, T=10m is shown in Table 2 and Table 3 with non dimensionalizing length equal to 40m. The irregular frequency of box barge is shown in Fig. 10, Fig. 11, Fig. 12, and Fig. 13.

Table 2: Values of k_1 and k_2

n	k1		m	k2	
0	0	0.03927	0	0	0.15708
1	0.07854	0.11781	1	0.314159	0.471239
2	0.15708	0.19635	2	0.628319	0.785398
3	0.235619	0.274889	3	0.942478	1.099557

Table 3: Nondimensional irregular frequencies

k1	k2	k	K	ω	ω√(L/g)
0.03927	0	0.03927	0.10508834	1.015294	2.050252
0.03927	0.15708	0.161914	0.17513694	1.3107	2.646786
0.03927	0.314159	0.316604	0.31773218	1.765408	3.565009
0.03927	0.471239	0.472872	0.47294619	2.153875	4.349465
0.03927	0.628319	0.629545	0.6295488	2.485017	5.018162
0.03927	0.785398	0.786379	0.78637953	2.77735	5.608492
0.03927	0.942478	0.943296	0.94329558	3.041855	6.142623
0.03927	1.099557	1.100258	1.10025845	3.285201	6.634029
0.07854	0	0.07854	0.1197629	1.083866	2.188725
0.07854	0.15708	0.17562	0.18641818	1.352255	2.730701
0.07854	0.314159	0.323828	0.3248263	1.785008	3.604588
0.07854	0.471239	0.477739	0.47780676	2.164914	4.371758
0.07854	0.628319	0.633208	0.63321225	2.492236	5.032742
0.07854	0.785398	0.789315	0.78931561	2.78253	5.618952
0.07854	0.942478	0.945745	0.94574464	3.045801	6.150592
0.07854	1.099557	1.102359	1.10235885	3.288335	6.640358
0.11781	0.15708	0.19635	0.20424235	1.415427	2.858268
0.11781	0.314159	0.335522	0.33634065	1.81637	3.667919
0.11781	0.471239	0.485742	0.4858006	2.182949	4.408177
0.11781	0.628319	0.639268	0.63927137	2.504132	5.056763
0.11781	0.785398	0.794185	0.79418494	2.7911	5.636257
0.11781	0.942478	0.949812	0.94981237	3.052344	6.163805
0.11781	1.099557	1.105851	1.10585066	3.293539	6.650867

Table 3: Continued

0.15708	0.15708	0.222144	0.22743205	1.493621	3.01617
0.15708	0.314159	0.351241	0.35186617	1.857819	3.751619
0.15708	0.471239	0.496729	0.49677757	2.207474	4.457702
0.15708	0.628319	0.647656	0.64765899	2.520506	5.089829
0.15708	0.785398	0.800952	0.80095229	2.802966	5.66022
0.15708	0.942478	0.955478	0.95547811	3.061434	6.182162
0.15708	1.099557	1.110721	1.11072074	3.300783	6.665495
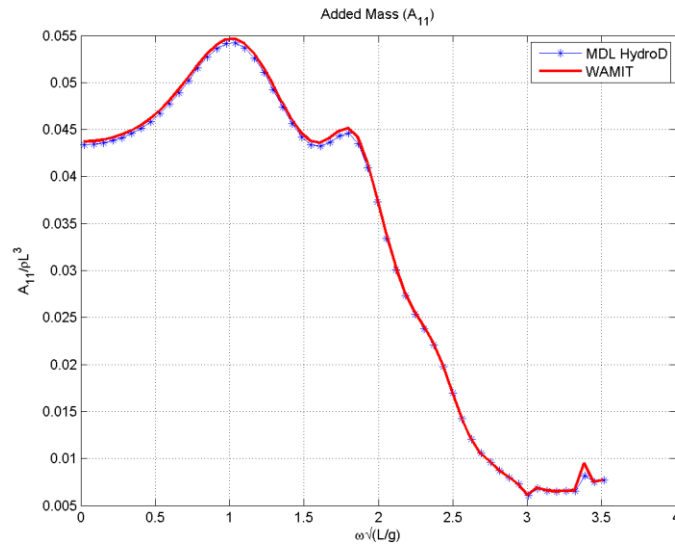
Fig. 10. Irregular frequency at non dimensional frequency 3.02 shown in surge added mass (A_{11}) of a box barge
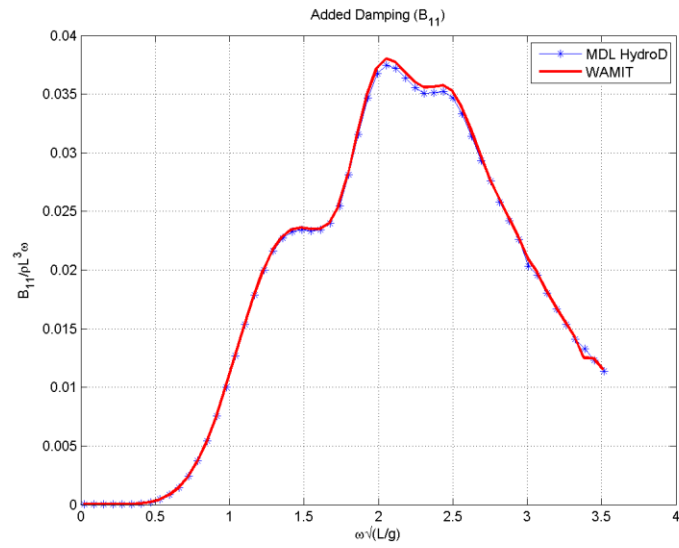
Fig. 11. Irregular frequency at non dimensional frequency 3.02 shown in surge damping (B_{11}) of a box barge
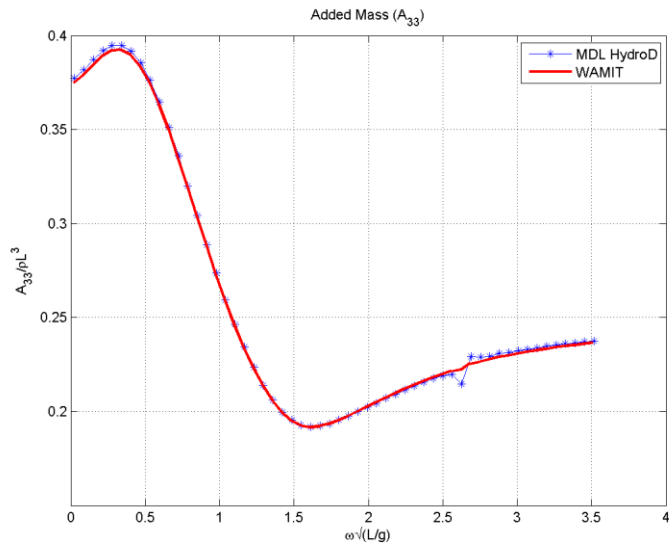
Fig. 12. Irregular frequency at non dimensional frequency 2.64 shown in heave added mass (A_{33}) of a box barge

50
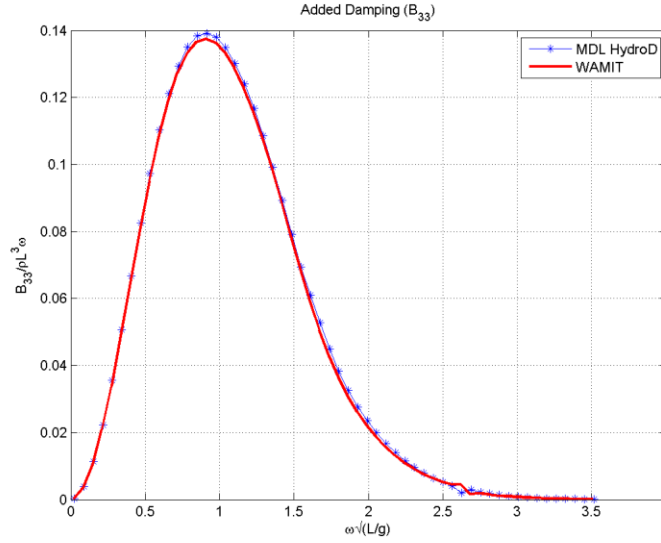
Fig. 13. Irregular frequency at non dimensional frequency 2.64 shown in heave damping (B_{33}) of a box barge

4.2 Removal of Irregular Frequencies

Many methods exist for irregular frequencies removal. A survey of such different methods may be found in Lau and Hearn (1989). Zhu (1994) presented two methods to remove irregular frequencies including the results of their numerical implementation. The first method is developed using a modified Green's function where it is argued that a source point placed at specific known locations at the free surface inside the body unless it's at the nodal point can remove the irregular frequencies. This method is tested for structures with two planes of symmetry and found to be effective. However, for arbitrary shaped bodies it is not possible to find the location of nodal points. This makes this method impractical for our purpose.

51

The second method is called "Extended Boundary Condition Method". Since, the irregular frequencies corresponds to the eigenfrequencies of the interior Dirichlet problem as shown by Ohmatsu (1975), a rigid lid can be placed on the interior free surface of the body to suppress the internal sloshing modes. This method has been developed by Ohmatsu (1975) and Kleinman (1982).

The numerical implementation of the second method is discussed in detail by Zhu (1994) including a method to generate the free surface lid automatically. It was found that the irregular frequency removal requires the number of panels on the lid to exceed a certain number below which the irregular frequencies are not completely removed. The additional panels on the lid increase the size of the linear equations to be solved which requires additional computational time. It was found that the number of panels required at the free surface lid reasonably small and the increase in computation time is acceptable. This method is found to be more efficient compared to other methods and will be implemented in MDL HydroD. However at this time the results presented in this report does not include irregular frequency removal.

5   MEAN DRIFT FORCES AND MOMENTS

The boundary element method described in previous sections shows wave force and moment calculation of an arbitrarily shaped floating body using linear wave theory. The higher order terms were neglected in the previous calculations. The nonlinear terms, in some cases can be of significant importance. For example, the second order drift force and moment terms can be used to calculate the mean drift force and moment in an irregular sea. Although, these forces are small in magnitude compared to the linear wave forces, they may cause large excursions of a freely floating body, since without mooring the restoring force in horizontal plane is zero.

An exact expression for the horizontal drift force and moment is presented in Newman (1967) which is modified by Faltinsen and Michelsen (1975) for finite depth and given as:

$$\overline{F_x} = -\int\int_\infty \Big[p\cos\theta + \rho V_r \left(V_r \cos\theta - V_\theta \sin\theta \right) \Big] r\, d\theta\, dz$$

$$\overline{F_y} = -\int\int_\infty \Big[p\sin\theta + \rho V_r \left(V_r \sin\theta + V_\theta \cos\theta \right) \Big] r\, d\theta\, dz \qquad (5.1)$$

$$\overline{M_z} = -\int\int_\infty V_r V_\theta r^2\, d\theta\, dz$$

where the bars denote time average and the integration is over the surface S_∞ of a vertical circular cylinder of large radius r, that is extending from the free surface down to $z = -h$. The x and y component of the drift force is represented as F_x & F_y

53

correspondingly and M_z is the drift moment about z axis. The cylindrical polar coordinate system (r, θ, z) is used with $x = r \cos \theta$ and $y = \sin \theta$. V_r and V_θ are the radial and tangential velocity components, respectively, and p is the dynamic pressure.

The eqn. (5.1) is approximated and only the second order terms with respect to wave amplitude are kept. To do this, velocity potential of only first order with respect to wave amplitude is required.

$$\phi \sim \frac{g \zeta_a}{\omega} \frac{\cosh k (z + h)}{\cosh kh} e^{i(kx \cos \beta + ky \sin \beta - \omega t)}$$
$$+ F(\theta) e^{i\phi(\theta)} \cosh (k(z + h)) \sqrt{\frac{1}{r}} e^{i(kr - \omega t)} \tag{5.2}$$

Here $F(\theta)$ is real and $F(\theta) e^{i\phi(\theta)}$ is given by:

$$F(\theta) e^{i\phi(\theta)} = \frac{2\pi (v^2 - k^2)}{k^2 h - v^2 h + v} \sqrt{\frac{2}{\pi k}} e^{-i3\pi/4}$$
$$\times \iint_S Q(\xi, \eta, \zeta) \cosh [k(\zeta + h)] e^{-ik\xi \cos \theta - ik\eta \sin \theta} ds \tag{5.3}$$

Further,

$$Q(\xi, \eta, \zeta) = Q_7 + \sum_1^6 Q_i (-i\omega) \overline{\eta_i} \tag{5.4}$$

Here $\overline{\eta_i}$ is defined by

$$\eta_i = \overline{\eta_i} e^{-i\omega t} \tag{5.5}$$

where, $\eta_i, i = 1 \cdots 6$ are the six modes of motion.

Using Bernoulli's equation we may write,

$$\overline{\int_{-h}^{\zeta} p\,dz} = \overline{\frac{\rho g}{2}\zeta^2} - \overline{\frac{\rho}{2}\int_{-h}^{0}|V|^2\,dz} \tag{5.6}$$

Here ζ is the free-surface elevation and V the fluid velocity vector which has

the components (V_r, V_θ, V_z). It is found that

$$\overline{\frac{\rho g}{2}\zeta^2} = \frac{\rho g}{2}\{\frac{\zeta_a^2}{2} + \zeta_a F(\theta)\frac{\omega}{g}\cos(kh)r^{-\frac{1}{2}}$$
$$\times \cos\left(kr\left(1 - \cos\theta\cos\beta - \sin\theta\sin\beta + \phi(\theta)\right)\right) \tag{5.7}$$
$$+ \frac{1}{2}\frac{\omega^2}{g^2}F^2(\theta)\cosh^2 kh\, r^{-1}\}$$

$$\overline{\frac{\rho}{2}\int_{-h}^{0}V_r^2\,dz} = \frac{\rho}{2}\left[\frac{1}{k}\frac{\sinh 2kh}{4} + \frac{h}{2}\right]$$
$$\times\{\frac{1}{2}\frac{\omega^2\zeta_a^2\cos^2(\beta-\theta)}{\sinh^2 kh} + \frac{1}{8}F^2(\theta)r^{-3} + \frac{1}{2}F^2(\theta)k^2 r^{-1}$$
$$+ \frac{1}{2}\omega\zeta_a\frac{\cos(\beta-\theta)}{\sinh kh}F(\theta)r^{-\frac{3}{2}}$$
$$\times \sin\left(kr\left(\cos(\beta-\theta)-1\right) - \phi(\theta)\right)$$
$$+ \omega\zeta_a\frac{\cos(\beta-\theta)}{\sinh kh}F(\theta)kr^{-\frac{1}{2}}$$
$$\times \cos\left[kr\left(\cos(\beta-\theta)-1\right) - \phi(\theta)\right]\} \tag{5.8}$$

$$\overline{\frac{\rho}{2}\int_{-h}^{0}V_{\theta}^{2}dz} = \frac{\rho}{2}\left[\frac{1}{k}\frac{\sinh 2kh}{4}+\frac{h}{2}\right]\{\frac{1}{2}\frac{\omega^{2}\zeta_{a}^{2}\sin^{2}(\theta-\beta)}{\sinh^{2}kh}$$

$$+\frac{1}{2}r^{-3}\left(F^{'}(\theta)\right)^{2}+\frac{1}{2}r^{-3}\left(F(\theta)\phi^{'}(\theta)\right)^{2}+\frac{\omega\zeta_{a}}{\sinh kh}$$

$$\times\sin(\theta-\beta)r^{-\frac{3}{2}}F^{'}(\theta)\sin\left[kr(\cos(\theta-\beta)-1)-\phi(\theta)\right] \qquad (5.9)$$

$$-\frac{\omega\zeta_{a}}{\sinh kh}\sin(\theta-\beta)r^{-\frac{3}{2}}F(\theta)\phi^{'}(\theta)$$

$$\times\cos\left[kr(\cos(\theta-\beta)-1)-\phi(\theta)\right]\}$$

$$\overline{\frac{\rho}{2}\int_{-h}^{0}V_{r}V_{\theta}dz} = \rho\left[\frac{1}{k}\frac{\sin 2kh}{4}+\frac{h}{2}\right]\{\frac{1}{2}\frac{\omega^{2}\zeta_{a}^{2}}{\sinh^{2}kh}$$

$$\times\cos(\theta-\beta)\sin(\theta-\beta)-\frac{1}{2}\frac{\omega\zeta_{a}}{\sinh kh}\cos(\theta-\beta)$$

$$\times r^{-\frac{3}{2}}F^{'}(\theta)\sin\left[kr(\cos(\theta-\beta)-1)-\phi(\theta)\right]$$

$$+\frac{1}{2}\frac{\omega\zeta_{a}}{\sinh kh}\cos(\theta-\beta)r^{-\frac{3}{2}}F(\theta)\phi^{'}(\theta)$$

$$\times\cos\left[kr(\cos(\theta-\beta)-1)-\phi(\theta)\right]$$

$$-\frac{1}{4}\frac{\omega\zeta_{a}}{\sinh kh}r^{-\frac{3}{2}}F(\theta)\sin(\theta-\beta)$$

$$\times\sin\left[(kr(\theta-\beta)-1)-\phi(\theta)\right]-\frac{1}{4}r^{-3}F(\theta)F^{'}(\theta)$$

$$+\frac{1}{2}kr^{-2}F^{2}(\theta)\phi^{'}(\theta)-\frac{1}{2}\frac{\omega\zeta_{a}}{\sinh kh}r^{-\frac{1}{2}}F(\theta)k\sin(\theta-\beta)$$

$$\times\cos\left[kr(\cos(\theta-\beta)-1)-\phi(\theta)\right]\} \qquad (5.10)$$

Here $F^{'}(\theta)$ and $\phi^{'}(\theta)$ mean $dF/d\theta$ and $d\phi/d\theta$, respectively. By applying

the method of stationary phase it has been calculated for large r:

$$\int_0^{2\pi} g(\theta) \cos\left[kr(\cos(\theta - \beta) - 1) - \phi(\theta) \right] d\theta$$

$$\sim \left(\frac{2\pi}{rk} \right)^{\frac{1}{2}} \{ g(\beta) \cos\left(\phi(\beta) + \frac{\pi}{4} \right) \tag{5.11}$$

$$+ g(\beta + \pi) \cos\left(-\phi(\beta + \pi) + \frac{\pi}{4} - 2kr \right) \}$$

where $g(\theta)$ is some arbitrary function. By using eqn. (5.6) to eqn. (5.11) the drift forces and moment may be written as:

$$\left\{ \frac{\overline{F}_x}{\overline{F}_y} \right\} = -\frac{\rho}{2} \frac{\omega \zeta_a}{\sinh kh} \sqrt{\left(\frac{2\pi}{k} \right)} \left(\frac{1}{4} \sinh 2kh + \frac{kh}{2} \right)$$

$$\times 2F(\beta) \cos\left(\phi(\beta) + \frac{\pi}{4} \right) \left\{ \begin{array}{c} \cos\beta \\ \sin\beta \end{array} \right\} \tag{5.12}$$

$$-\frac{\rho}{2} k \left(\frac{1}{4} \sinh 2kh + \frac{kh}{2} \right) \int_0^{2\pi} F^2(\theta) \left\{ \begin{array}{c} \cos\theta \\ \sin\theta \end{array} \right\} d\theta$$

$$\overline{M}_z = \left[\frac{1}{k} \frac{\sinh 2kh}{4} + \frac{h}{2} \right] \{ -\frac{\omega \zeta_a}{\sinh kh} \sqrt{\left(\frac{2\pi}{k} \right)}$$

$$\times F'(\beta) \sin\left(\phi(\beta) + \frac{\pi}{4} \right) - \frac{\omega \zeta_a}{\sinh kh} \sqrt{\left(\frac{2\pi}{k} \right)}$$

$$\times \phi'(\beta) F(\beta) \cos\left(\phi(\beta) + \frac{\pi}{4} \right) - \frac{k}{2} \tag{5.13}$$

$$\times \int_0^{2\pi} F^2(\theta) \phi'(\theta) d\theta \}$$

where $\phi'(\beta)$ means $d\phi / d\theta$ evaluated at $\theta = \beta$.

Numerical implementation of the above expressions to calculate the mean drift force for arbitrary shaped floating body required more study and will be considered as a future effort.

6   RESULTS AND DISCUSSION

A number of cases have been analyzed to both verify and demonstrate the capability of the developed numerical code. Since the Green's function is comprised of a Rankine source, image source and frequency dependent wavy part, we can verify the numerical implementation in stages. The panel setup and integration of the Rankine source over panel can be verified by analyzing deeply submerged bodies where the effect of the free surface is not present. Hence, the image source and the wavy part of the Green's function will not have any effect for such cases. Added mass is calculated for a deeply submerged sphere and a cube and compared with the analytical results given by Sarpkaya and Isaacson (1981).

6.1 Sphere

The theoretical value of added mass of sphere (Fig. 14) is given by $\frac{2}{3}\pi\rho r^3$. The ρ and r are the density of water and the radius of sphere respectively. The comparison results are shown in Table 4.
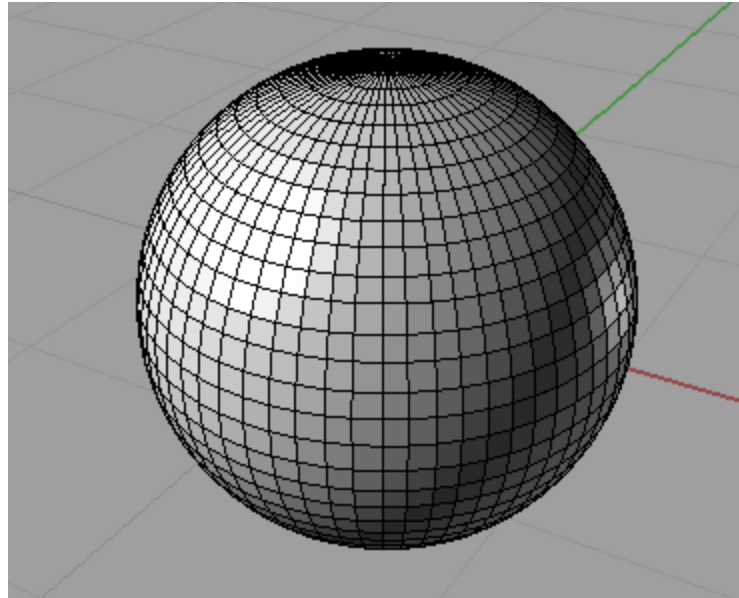
Fig. 14. Deeply submerged sphere

Table 4: Added mass of deeply submerged sphere

	$\rho = 1025\,kg\,/\,m^3$			$r = 1\,m$		
Panel No	Theoretical Added Mass			Numerical Added Mass		
	Surge	Sway	Heave	Surge	Sway	Heave
128	2146.75	2146.75	2146.75	2303.17	2303.17	2215.74
2048				2206.77	2206.77	2192.41

6.2 Cube
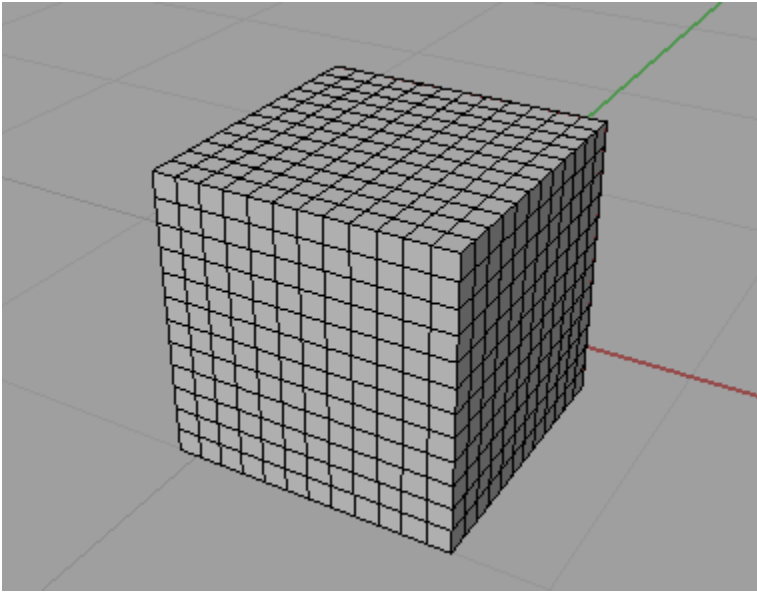
Fig. 15. Deeply submerged cube

The theoretical value of the added mass of a deeply submerged cube (Fig. 15) is given by $0.7\rho a^3$. The ρ and r are the density of water and the length of cube respectively. The comparison result is shown in Table 5.

Table 5: Added mass of deeply submerged cube

	$\rho = 1025\,kg\,/\,m^3$			$a = 1\,m$		
Panel	Theoretical Added Mass			Numerical Added Mass		
No	Surge	Sway	Heave	Surge	Sway	Heave
864	717.50	717.50	717.50	665.37	665.37	665.34

As shown above, the analytical results and numerical results for added mass calculation agree with each other. The next step of verification is performed for the frequency dependent added mass calculation for a hemisphere with free surface. The results were found to compare well with the WAMIT results.

6.3 Floating Hemisphere

The simple floating hemisphere (Fig. 16) of dimension given in Table 6 is analyzed and the comparison results are presented in Fig. 17 and Fig. 18.
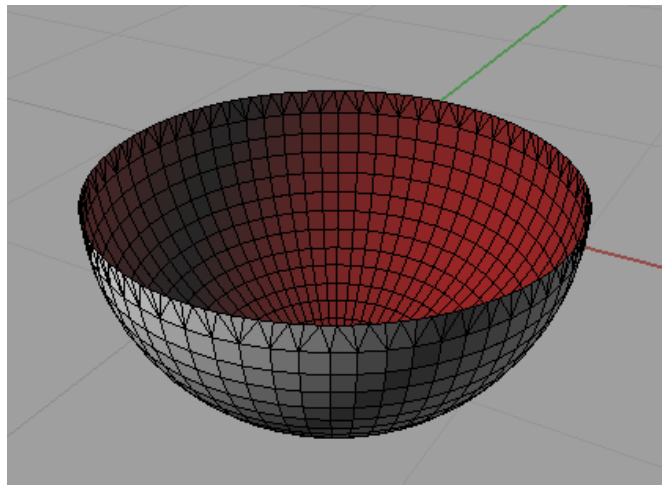
Fig. 16. Floating hemisphere

Table 6: Floating hemisphere

Parameter	Value
Radius	1 m
Number of Panels	1152
Water Depth	Infinite
Non dimensionalizing length (L)	1m
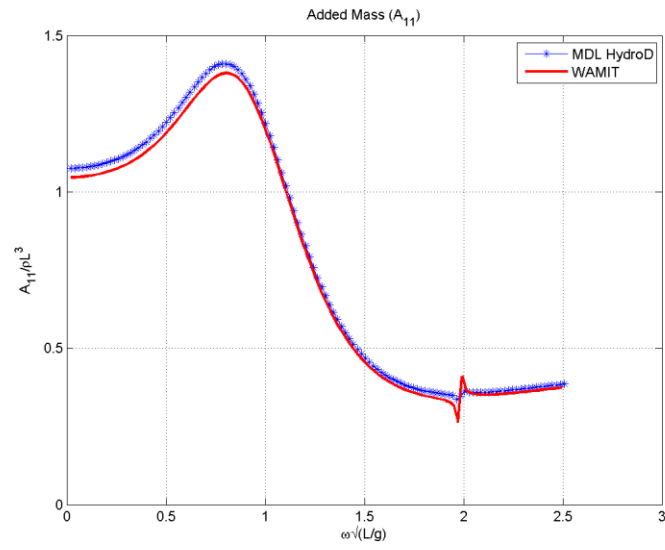
Fig. 17. Comparison of surge added mass of a floating hemisphere
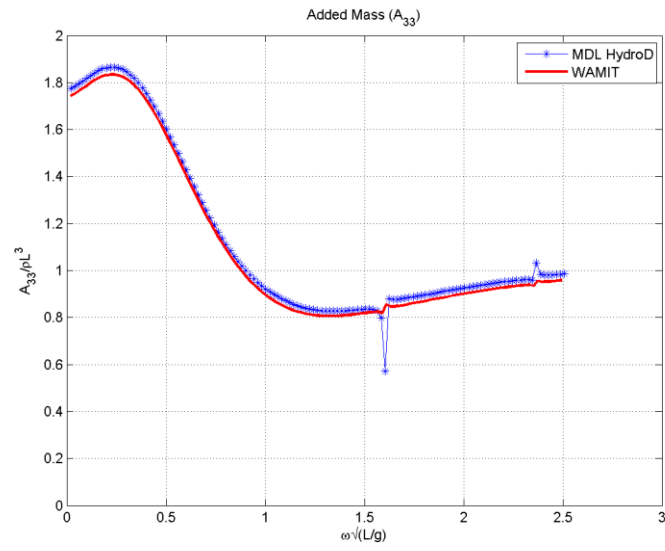
Fig. 18. Comparison of heave added mass of a floating hemisphere

Once the effect of free surface is incorporated successfully, a number of structures ranging from simple structures such as a truncated cylinder to complex structures such as TLP is analyzed and compared with WAMIT results. See APPENDIX III for more detailed results.

The results are shown to break down at some certain frequencies. These frequencies are called irregular frequencies which can be removed using numerical techniques as described in earlier sections.

The developed program is used to analyze the motion characteristics of a US Navy Large Medium Speed Roll-on/roll-off vessel the USN Bob Hope. The Response Amplitude Operator calculated from MDL HydroD and WAMIT were compared and shown below.

6.4 USN LMSR Ship (Bob Hope)

The US Navy Large Medium Speed Roll on-Roll off vessel Bob Hope (Fig. 19) is also analyzed and compared with WAMIT results. Vessel parameters are given in Table 7.

6.4.1 Geometry and Panel Details
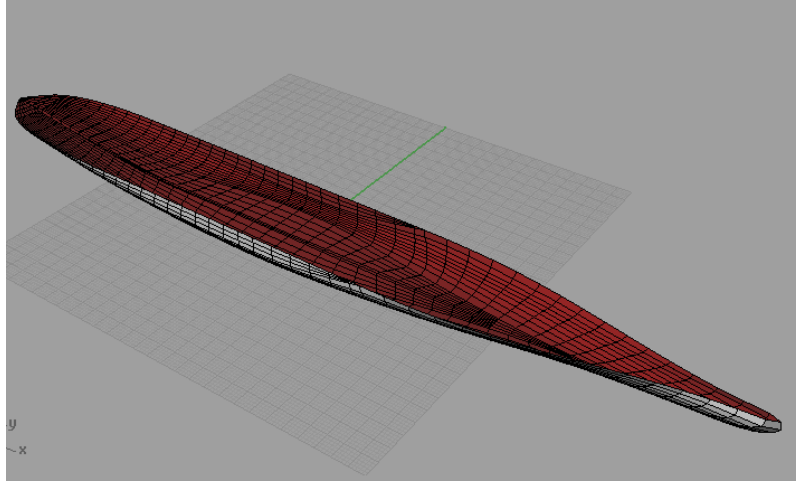
Fig. 19. Panel model of Bob Hope

Table 7: USN LMSR Bob Hope dimension and panel details

Parameter	Value
Length Between Perpendicular, L_{pp}	269.45 m
Breadth molded on waterline, B	32.258m
Draft, T	8.795 m
Number of Panels	1416
Water Depth	Infinite
Non dimensionalizing length	135 m

6.4.2 Hydrostatics

The hydrostatic result comparison is listed in Table 8.

Table 8: Hydrostatics result comparison

Parameter	MDLHydroD	WAMIT
Volume	VOLX = 49017.17 VOLY= 48950.77 VOLZ = 49029.09	VOLX = 49012.4 VOLY= 48951.0 VOLZ = 49033.7
Center of Buoyancy	Xb= -9.4776773 Yb= 0.00000 Zb= -3.897359	Xb= -9.485846 Yb= 0.00000 Zb= -3.898955
Hydrostatic Stiffness Terms	C33 = 0.3918698 C35 = 4.2208418E-02 C44 = 6.0625182E-04 C55 = 0.1000643	C33 = 0.39187 C35 = 4.2221E-02 C44 = 6.0621E-04 C55 = 0.10002

6.4.3 RAO

The vessel RAO comparison is shown in Fig. 20, Fig. 21, and Fig. 22.
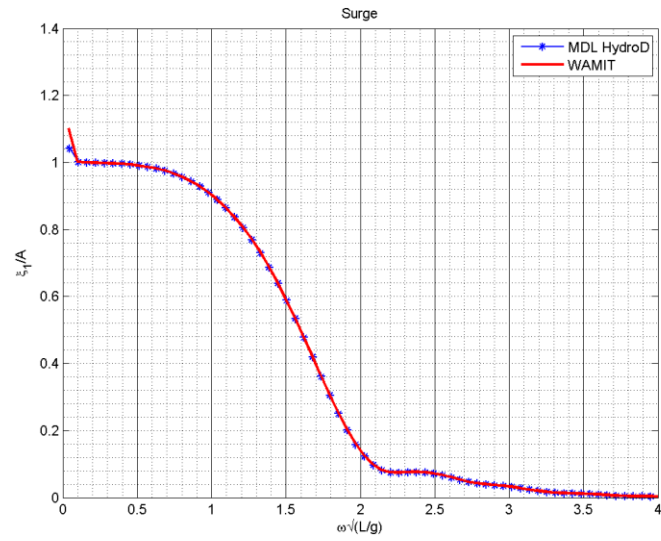
Fig. 20. Surge RAO of USN LMSR Bob Hope
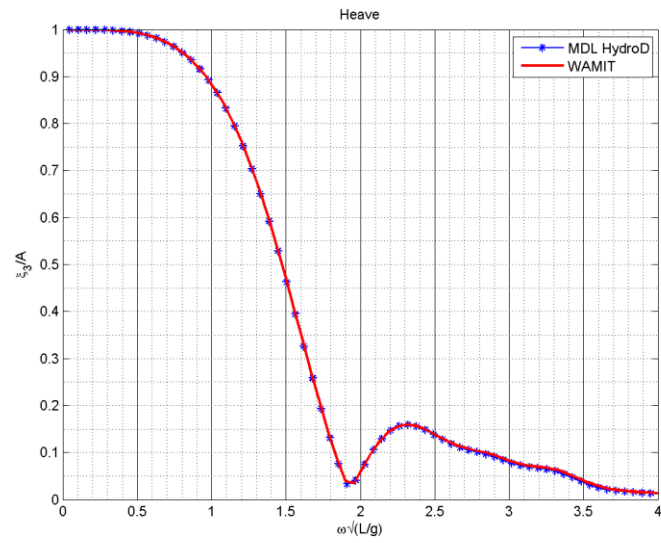
Fig. 21. Heave RAO of USN LMSR Bob Hope
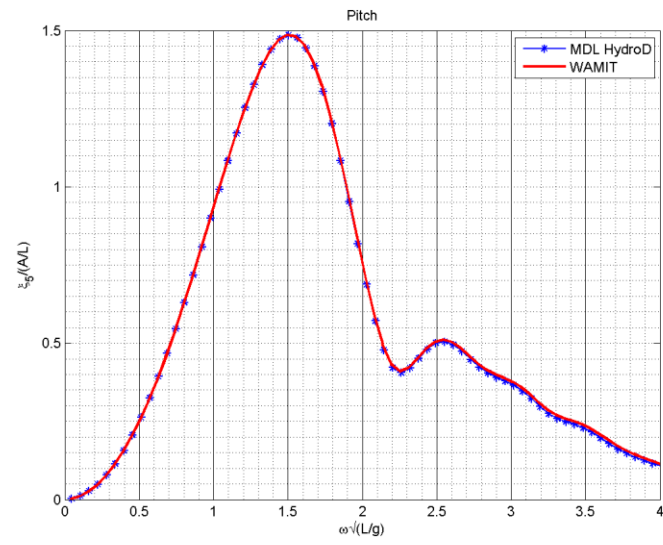
Fig. 22. Pitch RAO of USN LMSR Bob Hope

7   CONCLUSIONS

The objective of the present work has been to develop a computer software system to predict hydrodynamic coefficients, wave loads and motion of floating bodies in deep water. From a survey of available theoretical formulations and numerical codes, the zero speed infinite depth Green function based method has been selected as a starting point and an efficient analysis tool has been developed.

The current implementation includes hydrostatics, frequency domain added mass, radiation wave damping, wave excitation calculated using diffraction potential and using the Haskind relation, Froude Krylov forces and vessel response amplitude operator. A module has also developed to obtain the time domain coefficients from frequency domain.

A number of models have been tested to verify and validate the numerical implementation. The results were compared with analytical results and the industry standard seakeeping application WAMIT and found to show good agreement.

Further development of the program to include irregular frequency removal, mean drift calculation and forward speed effect are ongoing.

REFERENCES

Abramowitz, M. and I. A. Stegun,1972. Handbook of Mathematical Functions: With Formulas, Graphs, and Mathematical Tables.Vol. 55. Dover Publications, New York.

Ba, M. and M. Guilbaud,1995. A Fast Method of Evaluation for the Translating and Pulsating Green's Function. Ship Technology Research. 42(2), 68-80.

Beck, R. F. and S. Liapis,1987. Transient Motions of Floating Bodies at Zero Forward Speed. Journal of Ship Research. 31(3), 164-176.

Beck, R. F. and A. E. Loken,1989. Three-Dimensional Effects in Ship Relative-Motion Problems. Journal of Ship Sesearch. 33(4), 261-268.

Bingham, H. B.,1998. Computing the Green Function for Linear Wave-Body Interaction. 13th International Workshop on Water Waves and Floating Bodies, 5-8.

Borgarino, B., A. Babarit, P. Ferrant, J. Spinneken, C. Swan, et al.,2011. Extension of Free-Surface Green's Function Multipole Expansion for Infinite Water Depth Case. International Journal of Offshore and Polar Engineering. 21(3), 161-168.

Faltinsen, O. M.,1990. Wave Loads on Offshore Structures. Annual Review of Fluid Mechanics. 22(1), 35-56.

Faltinsen, O. M. and F. C. Michelsen,1975. Motions of Large Structures in Waves at Zero Froude Number. Symposium on the Dynamics of Marine Vehicles and Structures in Waves. London, 3-18.

Filkovic, D.,2008. Theory and Implementation of Structured 3d Panel Method. M.S. Thesis, University of Zagreb, Croatia.

Garrison, C. J.,1978. Hydrodynamic Loading of Large Offshore Structures: Three-Dimensional Source Distribution Methods. Numerical Methods in Offshore Engineering. O. Zienkiewicz, Lewis, R. and Stagg, K. (Eds.). John Wiley & Sons, Chichester, England,pp. 87-139.

Garrison, C. J.,1984. Interaction of Oblique Waves with an Infinite Cylinder. Applied Ocean Research. 6(1), 4-15.

Hess, J. L. and A. M. Smith,1964. Calculation of Non-Lifting Potential Flow About Arbitrary Three-Dimensional Bodies. Journal of Ship Research. 8(3), 22-44.

Hess, J. L. and D. C. Wilcox,1969. Progress in the Solution of the Problem of a Three-Dimensional Body Oscillating in the Presence of a Free Surface. Report No. DAC 67647. McDonnell Douglas Corp, Long Beach, California.

Hong, S. Y., B. W. Nam, J. H. Kim, Y. S. Kim, S. W. Hong, et al.,2011. Second-Order Motion Characteristics of a Semi-Submersible Platform in Waves. International Journal of Ocean System Engineering. 1(3), 155-164.

Inglis, R. B. and W. G. Price,1981. Calculation of the Velocity Potential of a Translating, Pulsating Source. Transactions, Royal Institution of Naval Architects. 23, 163–175.

Islam, M. N., M. R. Islam and M. S. Baree,2009. Computation of Ship Responses in Waves Using Panel Method. Journal of Naval Architecture and Marine Engineering. 1(1), 35-46.

John, F.,1950. On the Motion of Floating Bodies II. Simple Harmonic Motions. Communications on Pure and Applied Mathematics. 3(1), 45-101.

Katz, J. and A. Plotkin,2001. Low-Speed Aerodynamics.Vol. 13. Cambridge University Press, United Kingdom.

Kim, C. H.,2008. Nonlinear Waves and Offshore Structures.Vol. 27. World Scientific Publishing Co, Singapore.

Kleinman, R. E.,1982. On the Mathematical Theory of the Motion of Floating Bodies: An Update. Research and Development Report, DTNSRDC-82/074. Ship Performance Department, David W. Taylor Naval Ship Research and Development Centre, Bethesda, Maryland.

Kouh, J. and J. Suen,2001. A 3d Potential-Based and Desingularized High Order Panel Method. Ocean Engineering. 28(11), 1499-1516.

Lau, S. M. and G. E. Hearn,1989. Suppression of Irregular Frequency Effects in Fluid–Structure Interaction Problems Using a Combined Boundary Integral Equation Method. International Journal for Numerical Methods in Fluids. 9(7), 763-782.

Lee, C. H.,1995. Wamit Theory Manual. Report No. 95-2. Department of Ocean Engineering, Massachusetts Institute of Technology, Cambridge.

Lee, C. H. and J. N. Newman,2005. Computation of Wave Effects Using the Panel Method. Numerical Models in Fluid Structure Interaction, MIT press, Cambridge,Massachusetts. 42,pp. 211-251.

Liapis, S. J.,1986. Time-Domain Analysis of Ship Motions. PhD Dissertation, University of Michigan, Ann Arbor.

Lin, W. M., Y. S. Shin, J. S. Chung, S. Zhang and N. Salvesen,1997. Nonlinear Predictions of Ship Motions and Wave Loads for Structural Analysis. 16th International Conference on Offshore Mechanics and Arctic Engineering, American Society of Mechanical Engineers. Yokohama, 243-251.

Lin, Z. and S. Liao,2011. Calculation of Added Mass Coefficients of 3d Complicated Underwater Bodies by FMBEM. Communications in Nonlinear Science and Numerical Simulation. 16(1), 187-194.

Liu, C. F., B. Teng, Y. Gou and L. Sun,2011. A 3d Time-Domain Method for Predicting the Wave-Induced Forces and Motions of a Floating Body. Ocean Engineering. 38(17-18), 2142–2150.

McNeel, R. and Associates,2003. Rhinoceros User Guide: Nurbs Modeling for Windows Version 4.0. McNeel North America, Seattle.

McTaggart, K. A.,1997. Shipmo7: An Updated Strip Theory Program for Predicting Ship Motions and Sea Loads in Waves. Report No. TM 96/243. Defence Research Establishment Atlantic, Dartmouth, Nova Scotia.

McTaggart, K. A.,2002. Three Dimensional Ship Hydrodynamic Coefficients Using the Zero Forward Speed Green Function. Report No. TM 2002-059. Defence Research Development Canada, Ottawa.

McTaggart, K. A.,2003. Hydrodynamic Forces and Motions in the Time Domain for an Unappended Ship Hull. Report No. TM 2003-104. Defence Research Development Canada, Ottawa.

Mei, C. C.,1978. Numerical Methods in Water-Wave Diffraction and Radiation. Annual Review of Fluid Mechanics. 10(1), 393-416.

Nakos, D. E., D. Kring and P. D. Sclavounos,1994. Rankine Panel Methods for Transient Free-Surface Flows. 6th International Conference on Numerical Ship Hydrodynamics, National Academy Press. University of Iowa, Iowa City, 613-632.

Newman, J. N.,1967. The Drift Force and Moment on Ships in Waves. Journal of Ship Research. 11(1), 51-60.

Newman, J. N.,1984. Approximations for the Bessel and Struve Functions. Mathematics of Computation. 43(168), 551-556.

Newman, J. N.,1986. Distributions of Sources and Normal Dipoles over a Quadrilateral Panel. Journal of Engineering Mathematics. 20(2), 113-126.

Newman, J. N.,1992. Panel Methods in Marine Hydrodynamics. 11th Australasian Fluid Mechanics Conference. University of Tasmania, Hobart, Australia, 123-129.

Newman, J. N. and P. D. Sclavounos,1988. The Computation of Wave Loads on Large Offshore Structures. Conference on the Behaviour of Offshore Structures. Trondheim. 2, 605-622.

Ohkusu, M. and H. Iwashita,1989. Evaluation of the Green Function for Ship Motions at Forward Speed and Application to Radiation and Diffraction Problems. 4th Int Workshop on Water Waves and Floating Bodies, 195-199.

Ohmatsu, S.,1975. On the Irregular Frequencies in the Theory of Oscillating Bodies in a Free Surface. Ship Research Institute. 48, 1-13.

Papanikolaou, A. D. and T. E. Schellin,1992. A Three-Dimensional Panel Method for Motions and Loads of Ships with Forward Speed. Ship Technology Research. 39(4), 145-155.

Planchard, D. C. and M. P. Planchard,2010. Solidworks 2010 Tutorial.Vol. 1. SDC Publications, Mission, Kansas.

Ponizy, B., M. Guilbaud and M. Ba,1998. Numerical Computations and Integrations of the Wave Resistance Green's Function. Theoretical and Computational Fluid Dynamics. 12(3), 179-194.

Ponizy, B. and F. Noblesse,1994. Numerical Evaluation of Free-Surface Green Functions. Journal of Ship Research. 38(3), 193-202.

Rahman, M.,1984. Wave Diffraction by Large Offshore Structures: An Exact Second-Order Theory. Applied Ocean Research. 6(2), 90-100.

Rahman, M.,1998. Nonlinear Hydrodynamic Loading on Offshore Structures. Theoretical and Computational Fluid Dynamics. 10(1), 323-347.

Salvesen, N., E. O. Tuck and O. M. Faltinsen,1970. Ship Motions and Sea Loads. Transactions of the Society of Naval Architects and Marine Engineers. 78, 250-287.

Sarpkaya, T. and M. Isaacson,1981. Mechanics of Wave Forces on Offshore Structures.Vol. 96. Van Nostrand Reinhold Company, New York.

Sclavounos, P. D. and C. H. Lee,1985. Topics on Boundary-Element Solutions of Wave Radiation-Diffraction Problems. 4th International Conference on Numerical Ship Hydrodynamics. Washington, DC 1-10.

Telste, J. G. and F. Noblesse,1986. Numerical Evaluation of the Green Function of Water-Wave Radiation and Diffraction. Journal of Ship Research. 30(2), 69-84.

Webster, W. C.,1975. The Flow About Arbitrary, Three-Dimensional Smooth Bodies. Journal of Ship Research. 19(4), 206-218.

Wehausen, J. V.,1971. The Motion of Floating Bodies. Annual Review of Fluid Mechanics. 3(1), 237-268.

Wehausen, J. V. and E. V. Laitone,1960. Surface Waves. Encyclopedia of Physics. 9, 446-815.

Willis, D. J., J. Peraire and J. K. White,2006. A Quadratic Basis Function, Quadratic Geometry, High Order Panel Method. Report No. AIAA-2006-1253. The 44th AIAA Aerospace Sciences Meeting, Reno, Nevada.

Yang, C. and R. Lohner,2004. Comparison of Classical and Simple Free-Surface Green Functions. International Journal of Offshore and Polar Engineering. 14(4), 257-264.

Zhu, X.,1994. Irregular Frequency Removal from the Boundary Integral Equation for the Wave-Body Problem. M.S. Thesis, Massachusetts Institute of Technology, Cambridge.

Zhu, X.,1997. A Higher-Order Panel Method for Third-Harmonic Diffraction Problems. PhD Dissertation, Massachusetts Institute of Technology, Cambridge.

APPENDIX I

PROGRAMMING DETAILS

1   Language

The numerical implementation of velocity potential and hydrodynamic force calculation is done using Fortran 90 language. Fortran 90 is extensively used in computationally intensive areas of scientific computing and it is one of the most popular languages in high-performance computing. This program is developed with the intension of future development of larger applications which will use this as a sub module and benefits from its faster response time.

2   Compiler and IDE

The program is developed and tested in both Windows and UNIX environment. In Windows, Microsoft Visual Studio 2008 is used as IDE and Intel Visual Fortran with Intel Math Kernel Library which comes in a bundle as Intel Composer XE is used. The program is also tested in UNIX (Macintosh machine) using Netbeans as IDE, gfortran as Fortran compiler and inbuilt library (vecLib) provided by Apple Inc.

3   Deploying Source Code

This section describes the method of deploying the source code and compiling it with required library files. The program is compiled and tested in both Windows and UNIX platform. Here, deploying in Windows platform is explained in detail.

Many Integrated Development Environments (IDEs) are available in Microsoft Windows platform for example Netbeans, MS Visual Studio and FORTRAN compilers like gfortran and Intel Visual Fortran etc. Deploying the source code using Microsoft Visual Studio 2008 along with Intel Composer XE 2011 Fortran compiler which includes Intel Math Kernel Library (MKL) is described below.

Create a new project from menu *File > New > Project*. The window shown in Fig. 23 will be opened. Click on *Intel® Visual Fortran* from left menu and select *Empty Project* from Templates. Name the project "*MDLHydroD*" and select a location as shown in Fig. 23. Click OK to save the project.
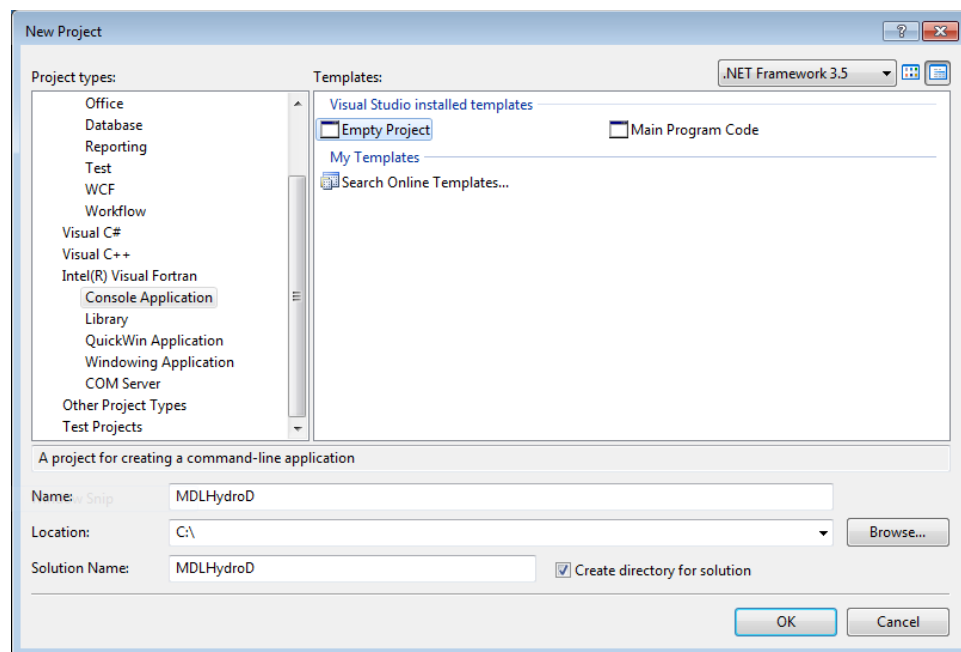
Fig. 23. New project window

Open the directory where the project is saved and go inside *MDLHydroD* directory. Create a new directory called "*Source*" and save all source files here as shown in Fig. 24.
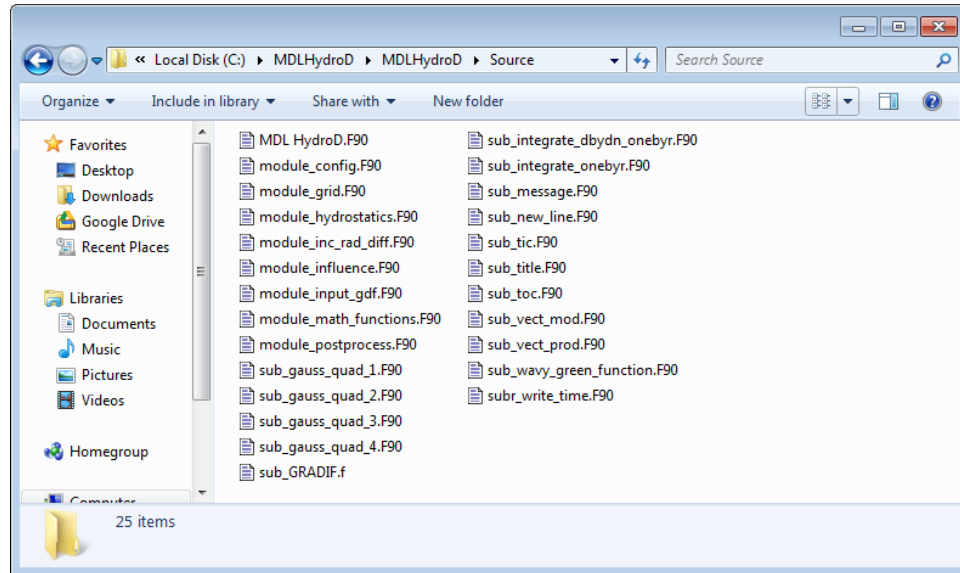
Fig. 24. Source directory

Now from menu *Project>Add Existing Item* select all the source files and add them to the project. The source files will be displayed under *Source Files* in *Solution Explorer* view as shown in Fig. 25.
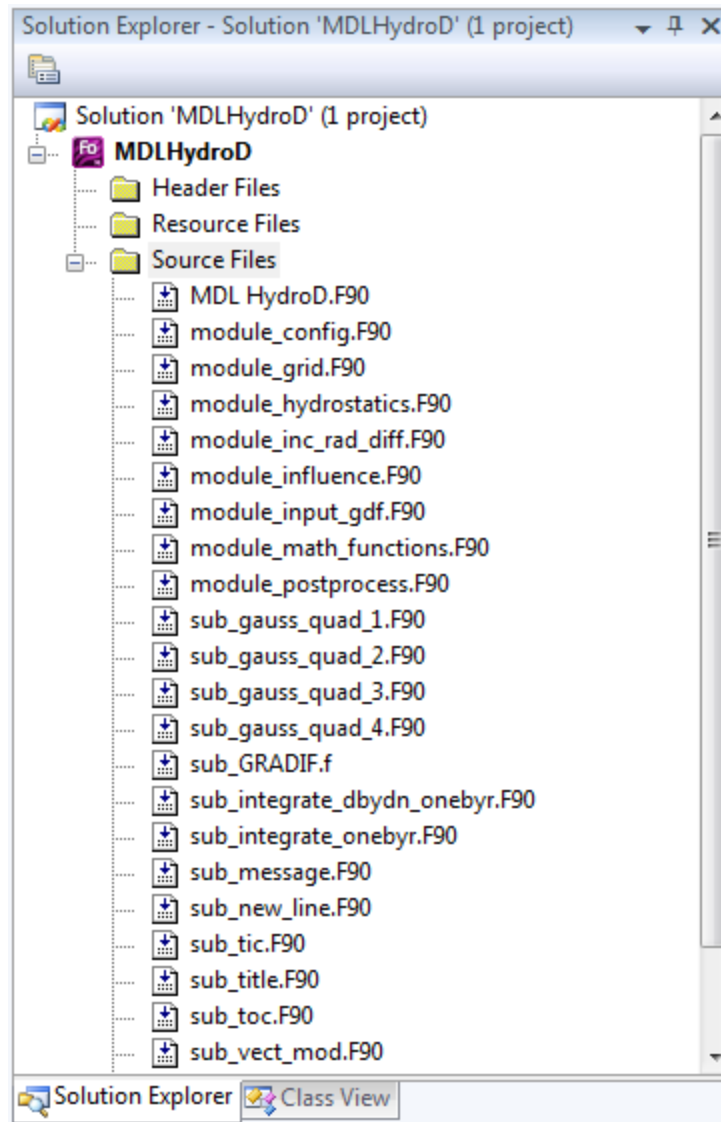
Fig. 25. Solution Explorer

Now to setup the compiler options and libraries, open project properties from menu *Project>MDLHydroD Properties*. Then click on *Configuration Properties>Fortran>General* in the left menu. In *Additional Include Libraries* add the location of Intel Math Kernel Libraries (MKL). The path looks like "*C:\Program Files (x86)\Intel\Composer XE 2011 SP1\mkl\include*"
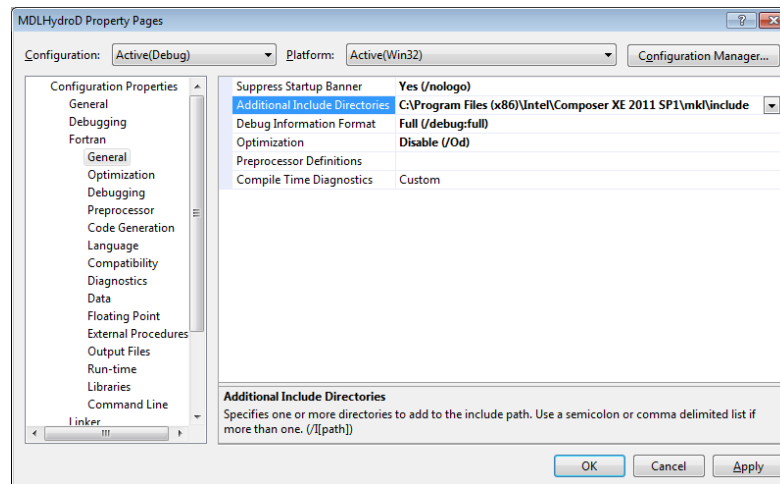
Fig. 26. Configuration Properties - Fortran – General

Next under *Fortran>Preprocessor*, select *Preprocess Source Files – Yes*, and add the same "*include*" directory location if not added automatically.
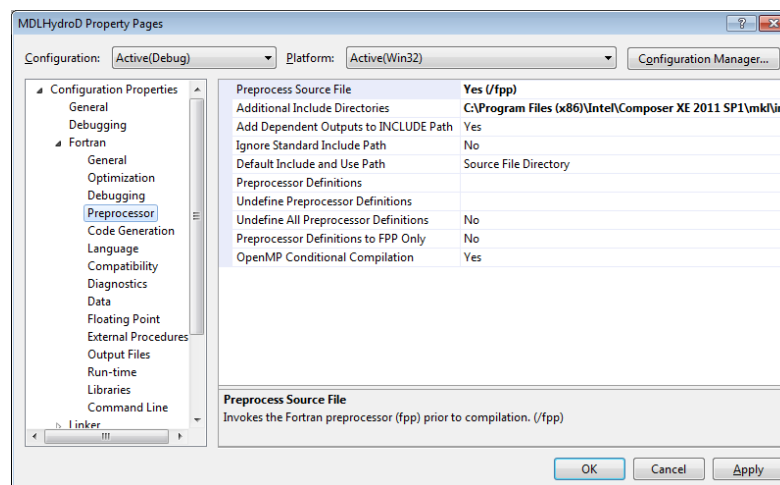
Fig. 27. Configuration Properties - Fortran - Processor

Next open "Configuration Properties>Linker>General" and add the MKL library location ("C:\Program Files (x86)\Intel\Composer XE 2011 SP1\mkl\lib\ia32") in Additional Library Directories.
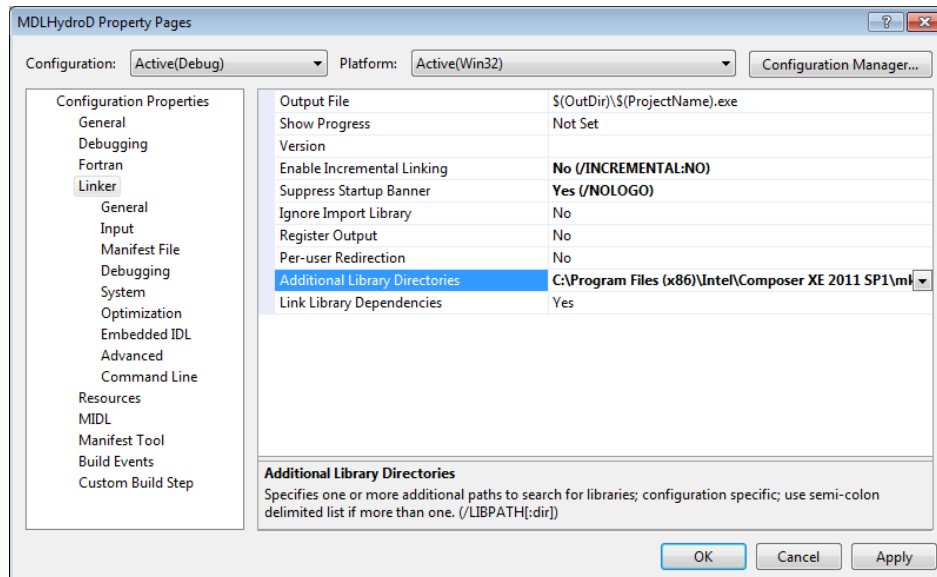
Fig. 28. Configuration Properties - Linker – General

Then open Linker>Input and in the Additional Dependencies add following libraries: "mkl_intel_c.lib mkl_intel_thread.lib mkl_core.lib libiomp5md.lib". Click OK to save setting and close the properties window.
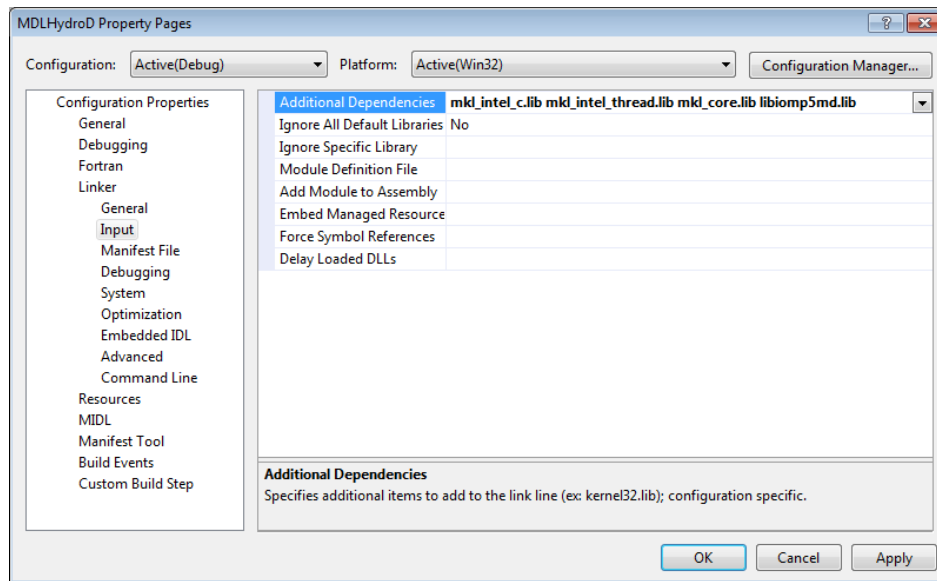
Fig. 29. Configuration Properties - Linker – Input

Once done, click on menu option *Build>Build Solution* to compile the source files. Now click on *Debug>Start Debugging* to test the program.
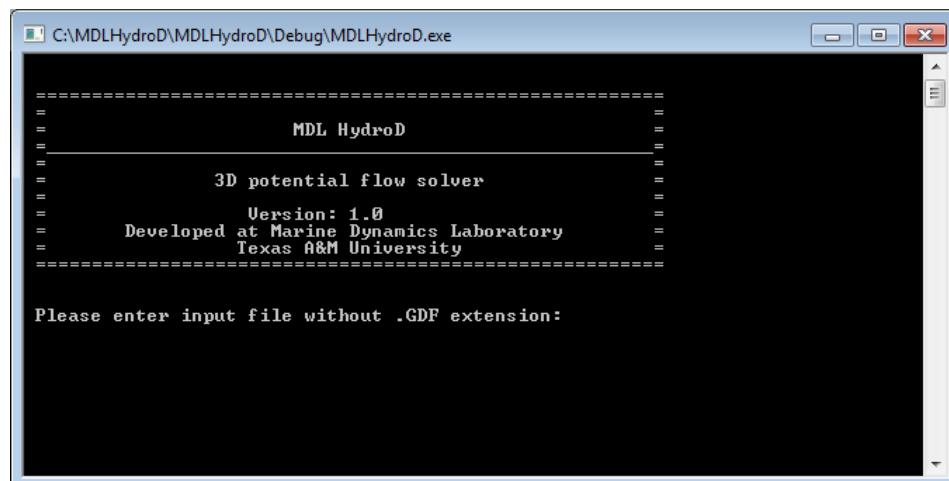
Fig. 30. Running MDLHydroD

APPENDIX II

RUNNING MDLHYDROD

The program MDL HydroD is developed using FORTRAN and the source is compiled in both UNIX and WINDOWS machine. The executable file and the input files needs to be placed under the same directory. The WINDOWS user needs to open a command prompt ($Start > All\ Programs > Accessories > Command\ Prompt$) and use cd command to enter the directory where the executable and input files are saved. Then type mdlhydrod.exe and press enter to execute the program.

1 Input Files

Two input files are required, one specifying the geometry of the body to be analyzed and another specifying configurations such as frequency, wave heading angle, radius of gyration, location of body coordinate system origin etc. These two files structure is explained in detail below.

2 The Geometric Data File

The wave load is calculated for submerged part of the body under mean waterline. The Geometric Data File (*.GDF) is a standard body geometry description file which is similar to format used by WAMIT and can be created easily from CAD software Rhinoceros. The GDF file contains a description of discretized surface, body length scale, gravity, symmetry indices, total number of panels specified, and for each panel the Cartesian coordinates x, y, z of its four vertices. A triangular panel can be

describes by defining two coincident vertices. A panel is described by four lines each containing 3 real numbers for x, y, z coordinate of the vertices separated by a space. The vertices must be arranged in anticlockwise fashion when looked from the fluid region. The coordinate system x, y, z in which the panels are defined is referred to as the *body coordinate system*. The body coordinate system must be a right-handed Cartesian system with $z - axis$ vertical and positive upwards.

The name of the GDF file can be any legal filename with maximum 100 characters followed by '.gdf' extension.

The data in the GDF file can be input in the following form:

```
Header
ULEN UGRAV
ISX ISY
NSPAN
X1(1) Y1(1) Z1(1)
X2(1) Y2(1) Z2(1)
X3(1) Y3(1) Z3(1)
X4(1) Y4(1) Z4(1)
X1(2) Y1(2) Z1(2)
X2(2) Y2(2) Z2(2)
X3(2) Y3(2) Z3(2)
X4(2) Y4(2) Z4(2)
…
```
Input data must be in the order as shown above, with at least one blank space separating data on the same line.

The definitions of each line in this file are as follows:

'Header' denotes one line description of the file, must be less than 100 characters.

ULEN is the dimensional length characterizing the body dimension. This quantity is used as length parameter L for obtaining non-dimensional output.

GRAV is the acceleration of gravity $9.80665 m/s^2$.

ISX, ISY are geometry symmetry indices. Currently MDL HydroD doesn't support symmetry indices, hence only ISX=0, ISY=0 should be used.

NPAN is equal to the number of panels with coordinates defined in this file.

X1(1), Y1(1), Z1(1) are the (x, y, z) of vertex 1of the first panel. X2(1), Y2(1), Z2(1) are the (x, y, z) coordinate of second vertex of the first panel and so on.

The origin of the body coordinate system is used to define the forces, moments and body motions.

3   Configuration File

The configuration file is used to define physical parameters, result parameters, geometry parameters, and solver parameters. This file can be created using any text editor (e.g. Notepad in Windows or Textedit in Macintosh). The file name must be same as the geometry definition file (*.GDF) with extension '*.cfg'. For example if the geometry file is named 'Ship.gdf' then the configuration file must be named 'Ship.cfg'.

The data in the CFG file can be input in following form:

```
#Water density [kg/m^3]
DENSITY 1025

#Number of frequencies (NFRQ) and frequencies in Hz
NFRQ -80
0.01 0.01

#Vertical Center of Gravity in body coordinate system
VCG -61.7
```

#Location of Body Coordinate System
XBODY 1
0 0 0 0

#Radiation of gyration
XPRDCT 1
70.54 0 0
0 70.54 0
0 0 61.85

#beta (deg)
NBETA 1
0

#SOLVER PARAMETERS
#error
ERROR 0.0000001

#collocation point depth
COLLDIST 0.0000001

The data blocks can be written in any order and empty lines or comments can be entered anywhere. Any line starting with # is considered as a comment. The definition of each entry in this file are as follows:

DENSITY is used to define water density in kg/m^3.

NFRQ denotes number of wave frequencies for which hydrodynamic analysis needs to be done. If NFRQ>0 the the frequencies must be defined in the next line separated by a space. If NFRQ<0 then the next line must be start of frequency and increment in frequency separated by space. The program will generate |NFRQ| frequency values starting from the defined value with defined increment.

VCG is the dimensional z coordinate of the center of gravityof the body relative to origin of the body coordinate system.

XBODY are the dimensional x, y, z coordinates of the origin of the body fixed coordinate system relative to the global coordinate system and the angle in degrees of the $x - axis$ of the body coordinate system relative to the $X - axis$ of the global coordinate system, defined as positive in the counterclockwise sense about the vertical axis.

XPRDCT is the 3×3 matrix of the body radii of gyration about the body-fixed axes, where $I, J = 1, 2, 3$ correspond to (x, y, z) respectively. These values are used to calculate the body inertia matrix m_{ij} for $i, j = 4, 5, 6$ according to the equation $m_{ij} = m \times XPRDCT (i - 3, j - 3) \times |XPRDCT (i - 3, j - 3)|$. The body mass m is evaluated from the displaced mass of fluid. The remaining elements of m_{ij} are evaluated assuming the body is freely floating in equilibrium, based on the calculated values of the displaced volume and center of buoyancy and on the specified value of VCG. In practical cases the matrix XPRDCT is symmetric. Zeros may be specified if the body motions are not evaluated.

NBETA is the number of wave headings, must be an integer.

BETA is an array of length NBETA defined as the wave headings in degrees. If NBETA is defined less than zero then the BETA should be defined as starting value and increment value. The array will be generated by the program with NBETA number of elements.

ERROR is a solver parameter which is used to determine the accuracy requirement. Default value is 0.0000001

COLLDIST is the distance by which the source is pushed below the panel surface. Default value is 0.0000001.

4   Output Files

Once the program is executed it will create a new directory named "out" and store all output files inside this directory. The format of output files are described below.

4.1 Hydrostatics

The hydrostatics results are output in '*_hydrostatics.csv' file. Following values are output:

Table 9: Hydrostatics

VOLX, VOLY,VOLZ
Center of buoyancy relative to waterline
Longitudinal center of buoyancy
Water plane area
Longitudinal center of floatation
Water plane moment about x-axis
Water plane moment about y-axis
Hydrostatic stiffness terms (C33, C35, C44, C53,C55)

4.2 Added Mass and Damping

Non-dimensional added mass and damping are output in '*_AM_AD.csv' file. Added mass and damping are non-dimensionalized as follows:

$$\bar{A}_{ij} = \frac{A_{ij}}{\rho L^k} \tag{6.1}$$

$$\bar{B}_{ij} = \frac{B_{ij}}{\rho L^k \omega} \tag{6.2}$$

Here

$$k=3 \text{ for } (i,j=1,2,3)$$
$$k=4 \text{ for } (i=1,2,3, j=4,5,6), \text{ or},(i=4,5,6, j=1,2,3) \qquad (6.3)$$
$$k=5 \text{ for } (i,j=4,5,6)$$

The results are tabulated as:

Table 10: Added mass and damping

FRQ	I	J	A(I,J)	B(I,J)

4.3 Radiation Pressure

Radiation pressure at each panel center is exported in output file '*_RadiationPressure.csv' file. The results are tabulated as:

Table 11: Radiation pressure

FRQ	Panel No	Re(p1)	Im(p1)	Re(p2)	Im(p2)	…

Here … denotes the remaining components for modes 3,4,5 and 6

4.4 Pressure on Fixed Hull

The diffraction pressure on the panels are exported in output file '*_PressureOnFixdHull.csv'. The results are tabulated as:

Table 12: Pressure on fixed hull

FRQ	BETA	Panel No	Mod(pD)	Pha(pD)	Re(pD)	Im(pD)

4.5 Force

Exciting forces are calculated using Haskind relation, direct pressure integration of hydrodynamic pressure and using Froude Krylov method. The forces are non-dimensionalized as:

$$\bar{X}_i = \frac{X_i}{\rho g A L^m} \tag{6.4}$$

where $m=2$ for $i=1,2,3$ and $m=3$ for $i=4,5,6$. A is the wave amplitude (1 in this case) and L is the characteristic length parameter $ULEN$.

Three separate output files are written named '*_ForceHaskind.csv', '*_ForceDiffractionPotential.csv' and '*_ForceFroudeKrylov.csv'. Format used in exporting the result are as follows:

Table 13: Force

FRQ	BETA	Mode	Mod(F)	Pha(F)	Re(F)	Im(F)

4.6 Response Amplitude Operator

The response of the vessel due to waves of unit amplitude is output in the file '*_RAO.csv'. Format of the output file is:

Table 14: Response amplitude operator

FRQ	BETA	I	Mod(Xi)	Pha(Xi)	Re(Xi)	Im(Xi)

4.7 Log File

The program writes all runtime information and error messages in the '*.log' file. The user should check this file for any errors during runtime before using the result output files.

5 Post Processing

The output files contain large number of data and it's quite difficult to interpret the results from these files. MATLAB scripts are written to generate plots of the results obtained from MDL HydroD and also comparison plots with WAMIT output files. Following scripts are packaged under Matlab Post Processing directory:

- plotAddedMassDamping.m

- plotForce.m

- getRAOdata.m

- plotRAO.m

- plotAddedMassDampingWAMIT.m

- plotForceWAMIT.m

- getRAOdataWAMIT.m

- plotRAO_WAMIT.m

- allplots.m

The user needs to copy appropriate output files from MDL HydroD and WAMIT (if comparison is required) to the 'Matlab Post Processing' directory. Only the 'allplots.m' file needs to be updated for different cases. Once this file is run, it will

generate plots and save them in a separate folder for each individual and WAMIT

comparison cases.

APPENDIX III

VERIFICATION AND VALIDATION

The numerical implementation of the three dimensional method is verified for various test cases which include different floating and deeply submerged structures. The results obtained were compared with WAMIT (Wave Analysis Massachusetts Institute of Technology) version 7.03 results for identical setup. WAMIT is a well proven application most widely used across industry for hydrodynamic load prediction in the frequency domain and also based on the theory of three dimensional panel methods.

The following quantities are compared for each structure:

- Hydrostatics

- Added Mass

- Damping

- Force calculated using Haskind relation

- Force calculated using direct integration of diffraction pressure

- Froude Krylov Force

- Response Amplitude Operator

1   Floating Hemisphere

1.1 Geometry and Panel Details
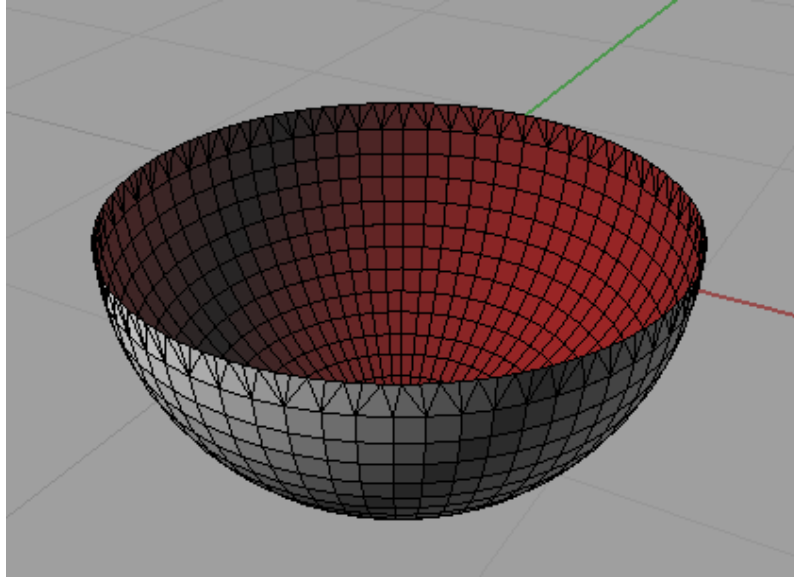
Fig. 31. Floating hemisphere

Table 15: Hemisphere dimension

Parameter	Value
Radius	1 m
Number of Panels	1152
Water Depth	Infinite
Non dimensionalizing length (L)	1m

1.2 Hydrostatics

Parameter	MDLHydroD	WAMIT
Volume	VOLX = 2.086208 VOLY= 2.086209 VOLZ = 2.086216	VOLX = 2.08621 VOLY= 2.08621 VOLZ = 2.08621
Center of Buoyancy	Xb= 0.00000 Yb= 0.00000 Zb= -0.3744191	Xb= 0.00000 Yb= 0.00000 Zb= -0.374416
Hydrostatic Stiffness Terms	C33 = 3.140320 C35 = 4.2791362E-07 C44 = 2.3961067E-03 C55 = 2.3962855E-03	C33 = 3.1403 C35 = 4.2011E-07 C44 = 2.4248E-03 C55 = 2.4252E-03
Water plane moment about x-axis	0.7835154 m^4	---
Water plane moment about y-axis	0.7835152 m^4	---

1.3 Added Mass and Damping
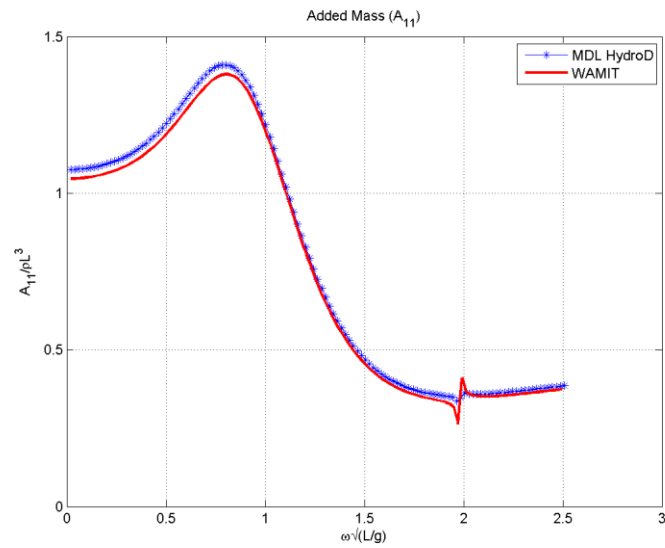
Fig. 32. Floating hemisphere surge added mass A_{11}
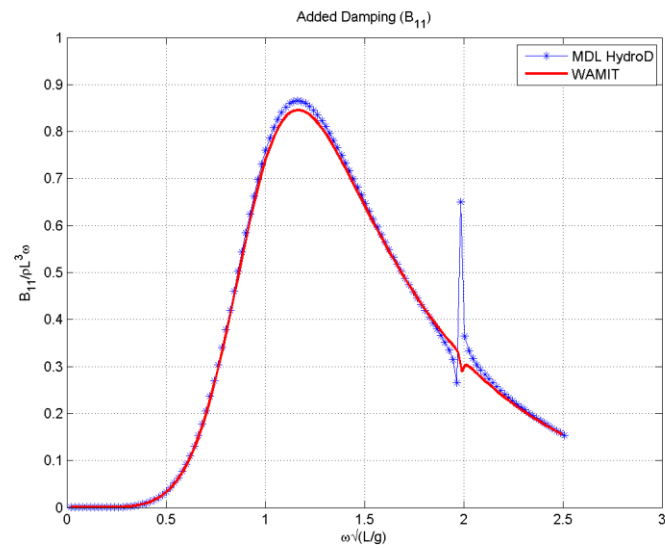
Fig. 33. Floating hemisphere surge damping B_{11}
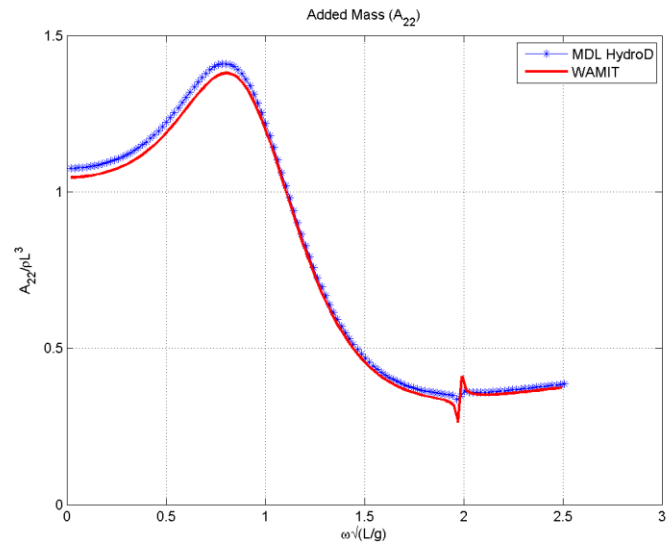
Fig. 34. Floating hemisphere sway added mass A_{22}
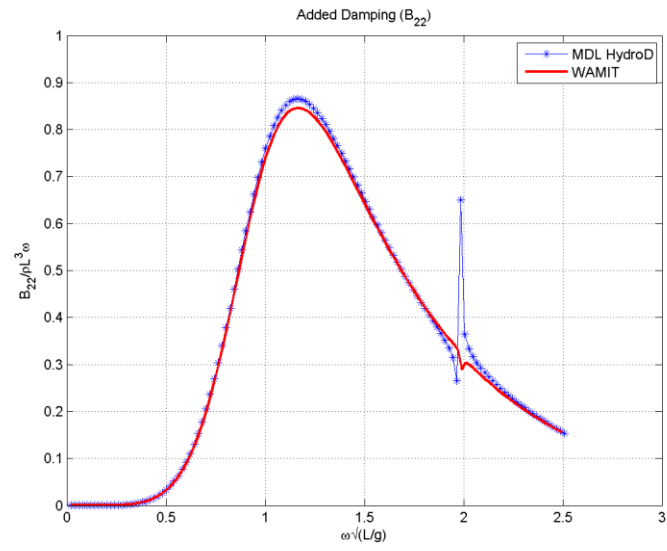
Fig. 35. Floating hemisphere sway damping B_{22}
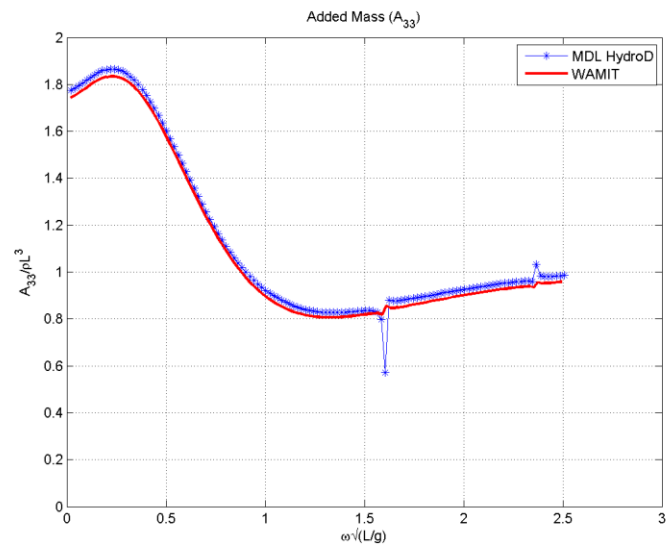
Fig. 36. Floating hemisphere heave added mass A_{33}
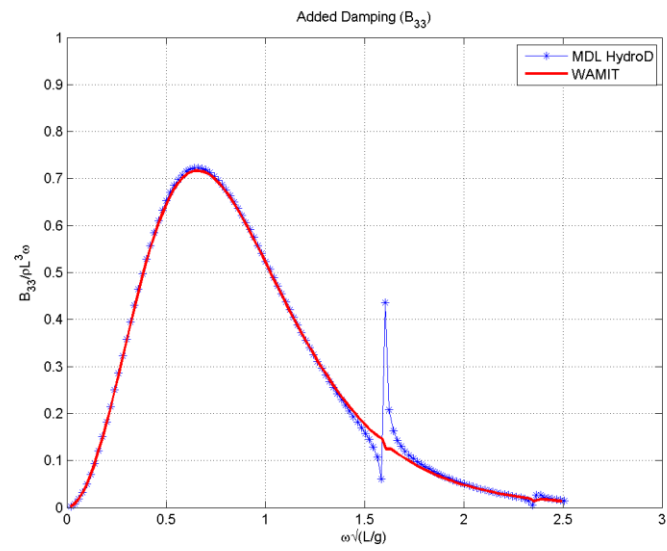
Fig. 37. Floating hemisphere heave damping B_{33}

1.4 Forces
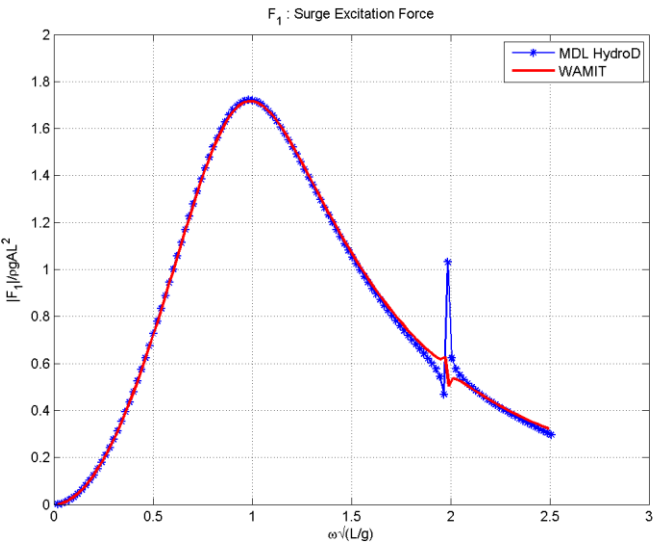
Fig. 38. Floating hemisphere surge excitation force
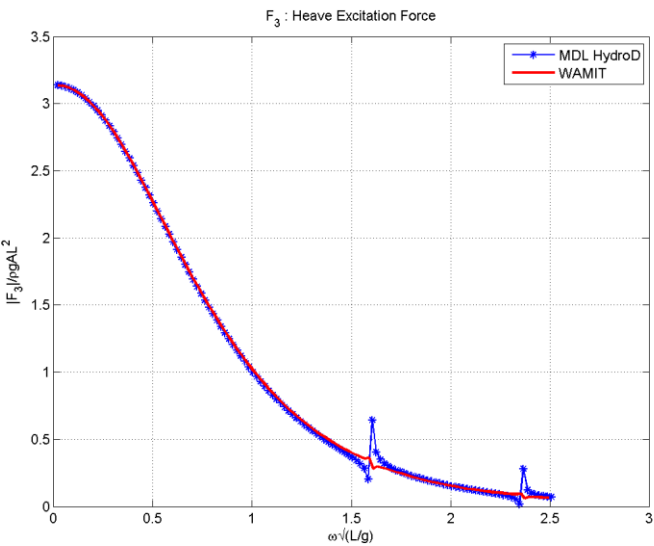
Fig. 39. Floating hemisphere heave excitation force

100

1.5 RAO
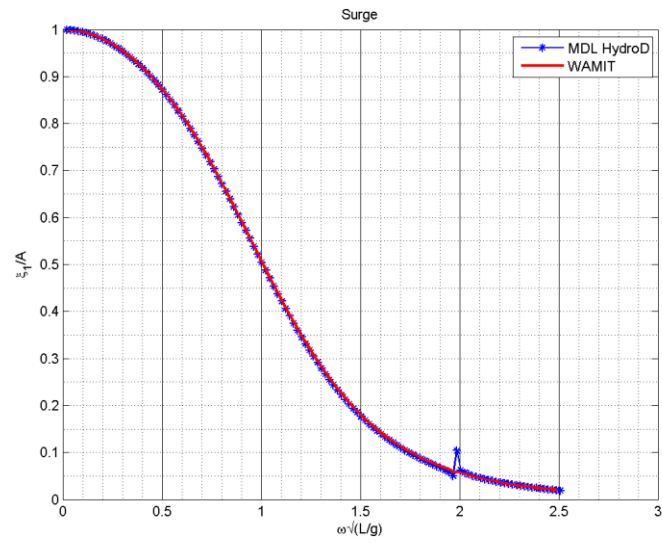
Fig. 40. Surge RAO of floating hemisphere
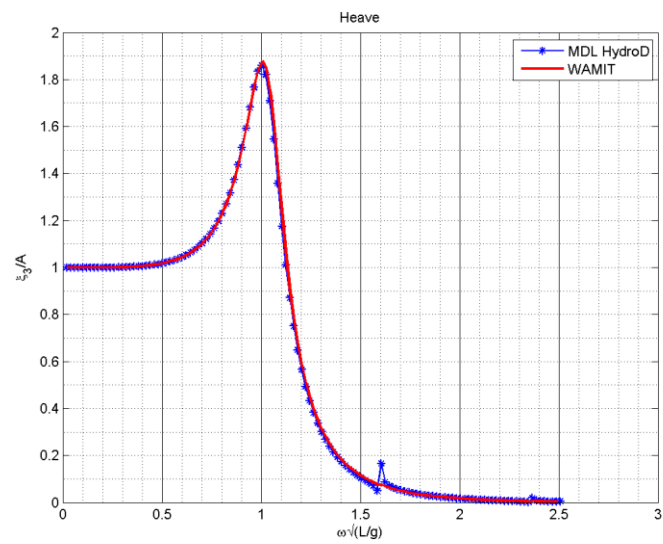
Fig. 41. Heave RAO of floating hemisphere

2 Floating cylinder

2.1 Geometry and Panel Details
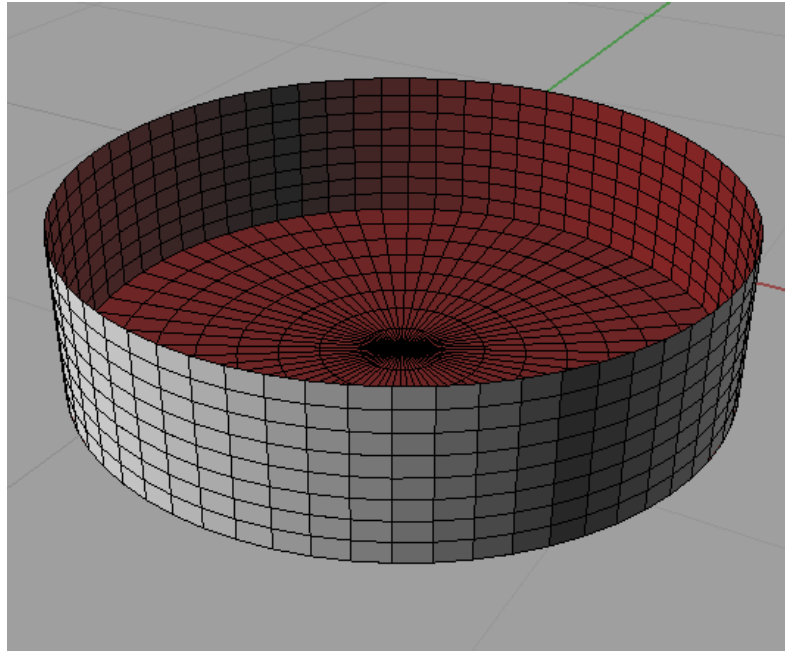
Fig. 42. Floating cylinder

Table 16: Cylinder dimension

Parameter	Value
Radius	1 m
Height	0.5 m
Number of Panels	1024
Water Depth	Infinite
Non dimensionalizing length (L)	1 m

2.2 Hydrostatics

Parameter	MDLHydroD	WAMIT
Volume	VOLX = 1.568274 VOLY= 1.568273 VOLZ = 1.568273	VOLX = 1.56827 VOLY= 1.56827 VOLZ = 1.56827
Center of Buoyancy	Xb= 0.00000 Yb= 0.00000 Zb= -0.2500000	Xb= 0.00000 Yb= 0.00000 Zb= -0.250000
Hydrostatic Stiffness Terms	C33 = 3.136547 C35 = -1.2520468E-07 C44 = 0.3881322 C55 = 0.3881319	C33 = 3.1365 C35 = 1.6461E-07 C44 = 0.38816 C55 = 0.38816
Water plane moment about x-axis	$0.7802002 \ m^4$	---
Water plane moment about y-axis	$0.7802005 \ m^4$	---

2.3 Added Mass and Damping
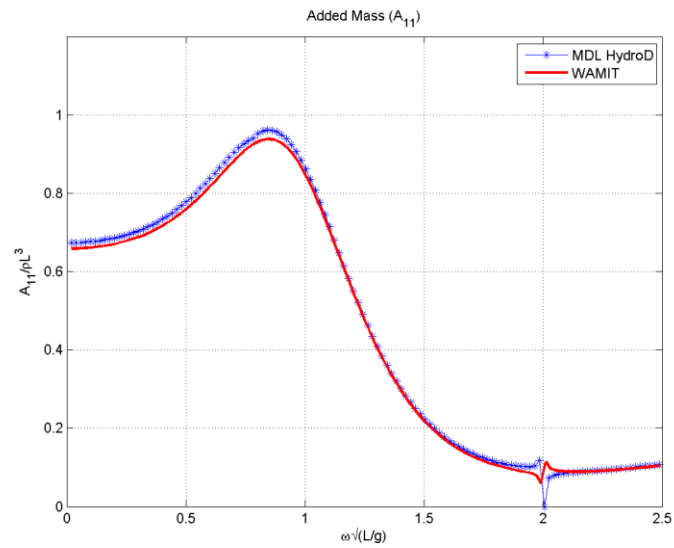
Fig. 43. Floating cylinder surge added mass A_{11}
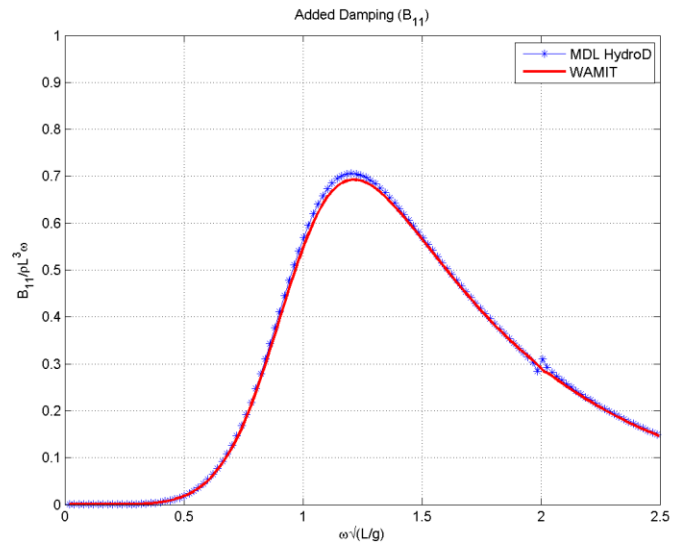
Fig. 44. Floating cylinder surge damping B_{11}
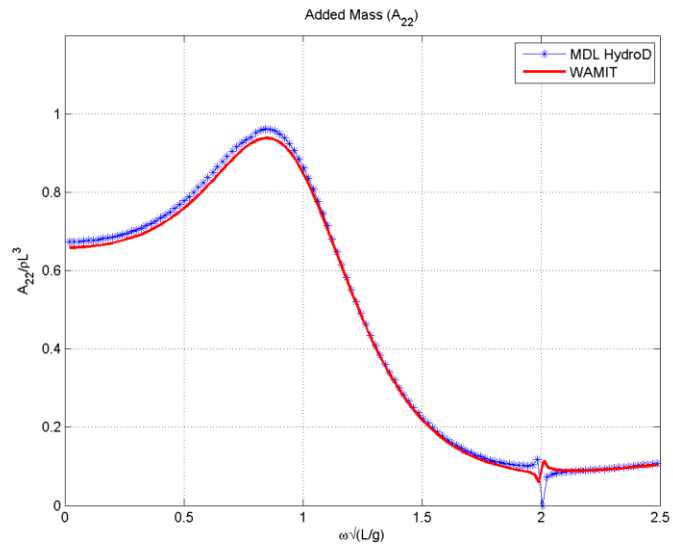
Fig. 45. Floating cylinder sway added mass A_{22}
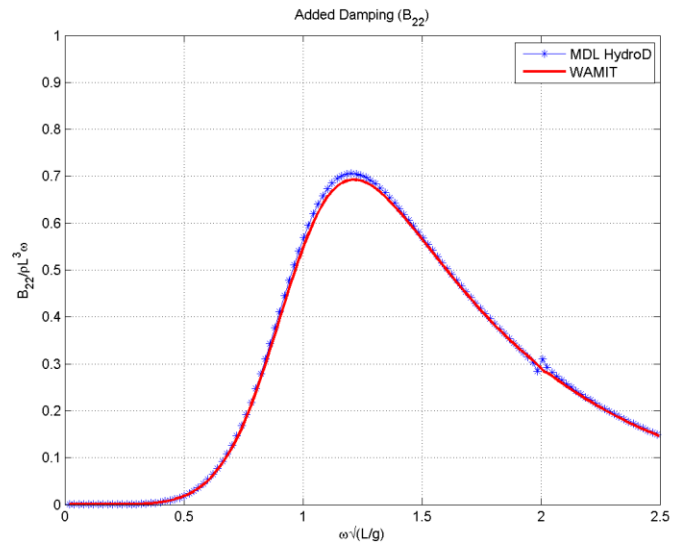
Fig. 46. Floating cylinder sway damping B_{22}
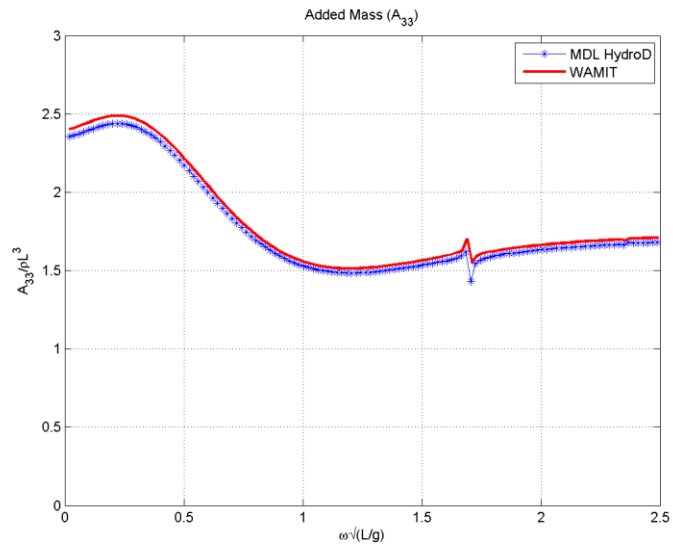
Fig. 47. Floating cylinder heave added mass A_{33}
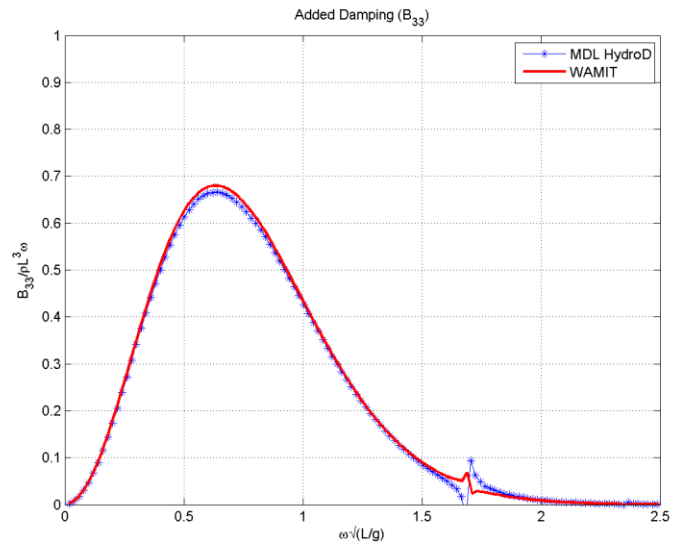
Fig. 48. Floating cylinder heave damping B_{33}
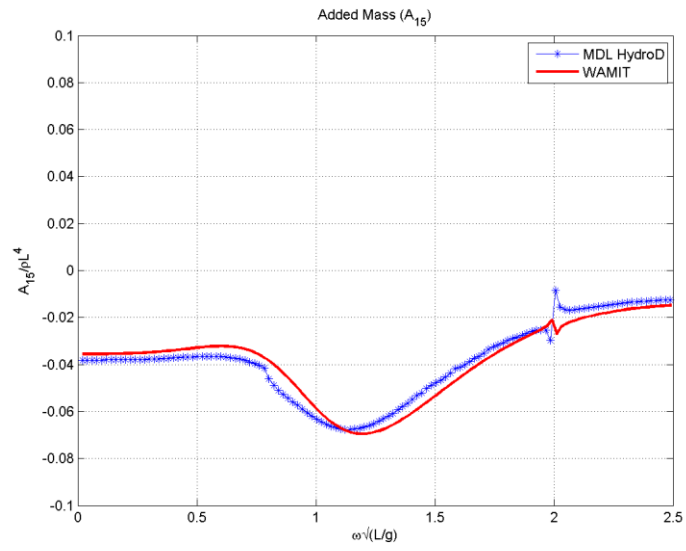
Fig. 49. Floating cylinder added mass A_{15}
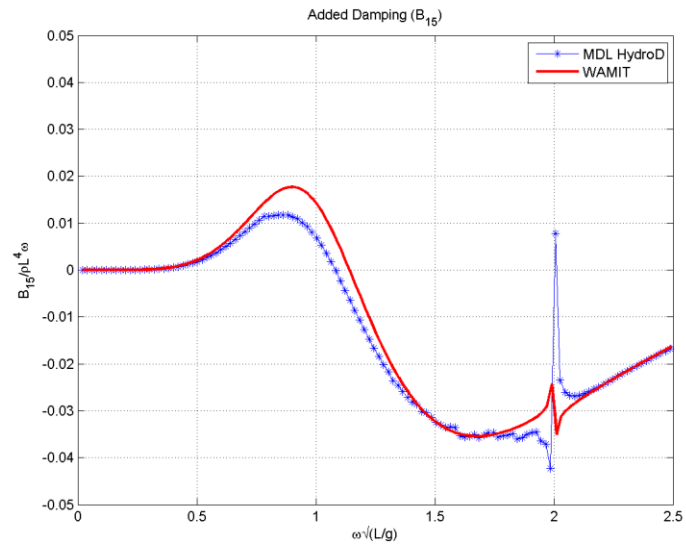
Fig. 50. Floating cylinder damping B_{15}
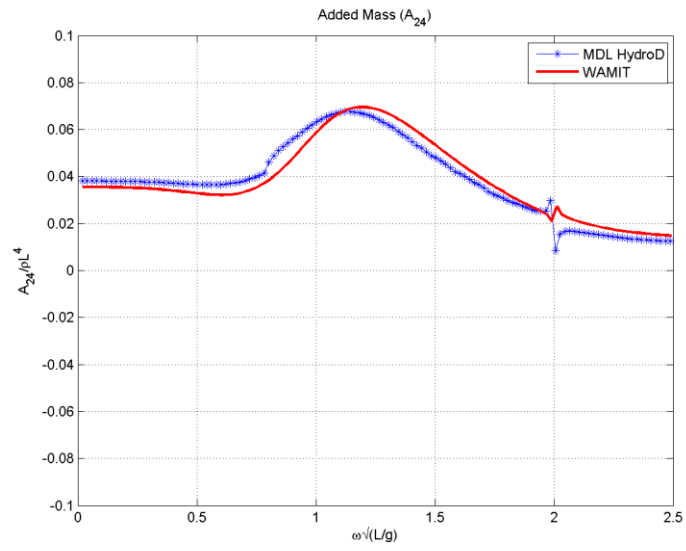
Fig. 51. Floating cylinder added mass A_{24}
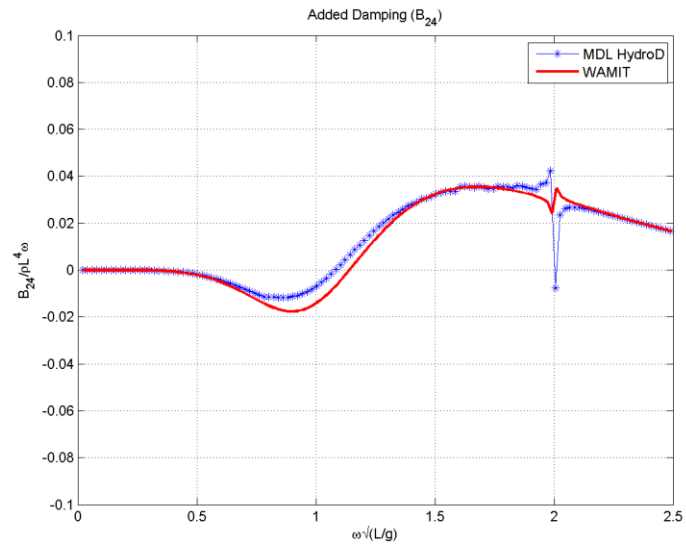
Fig. 52. Floating cylinder damping B_{15}
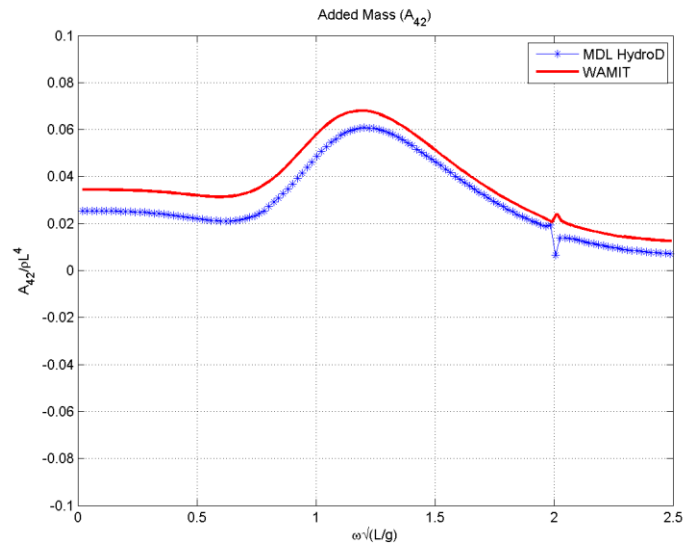
Fig. 53. Floating cylinder added mass A_{42}
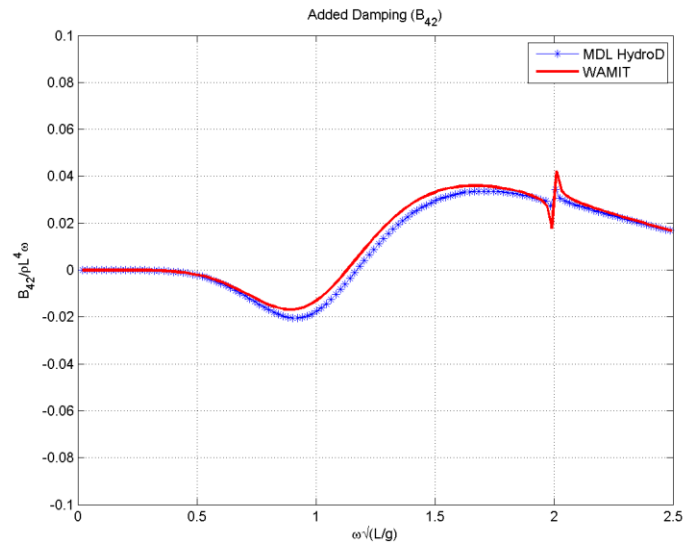
Fig. 54. Floating cylinder damping B_{42}
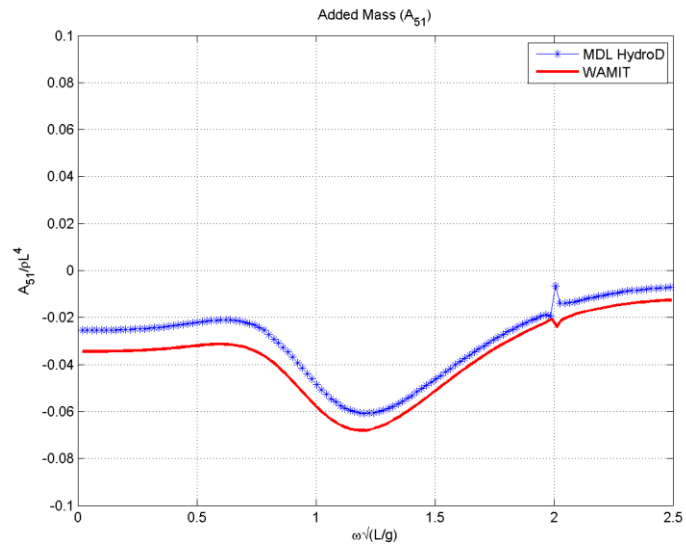
Fig. 55. Floating cylinder added mass A_{51}

109
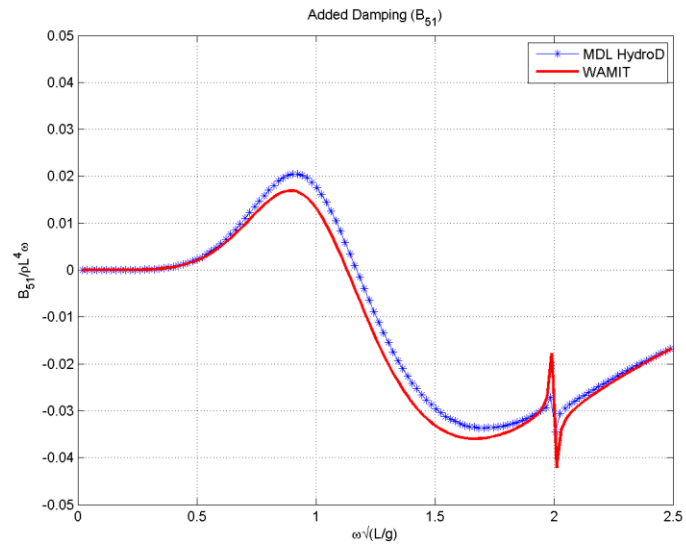
Fig. 56. Floating cylinder damping B_{51}
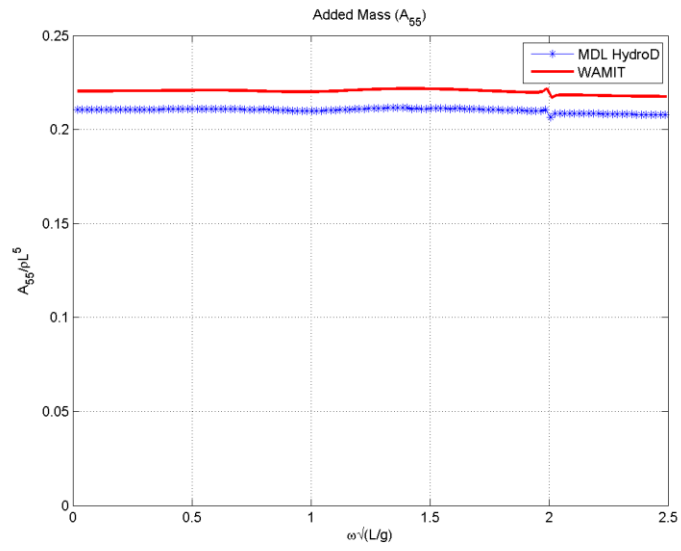
Fig. 57. Floating cylinder added mass A_{55}

2.4 Forces
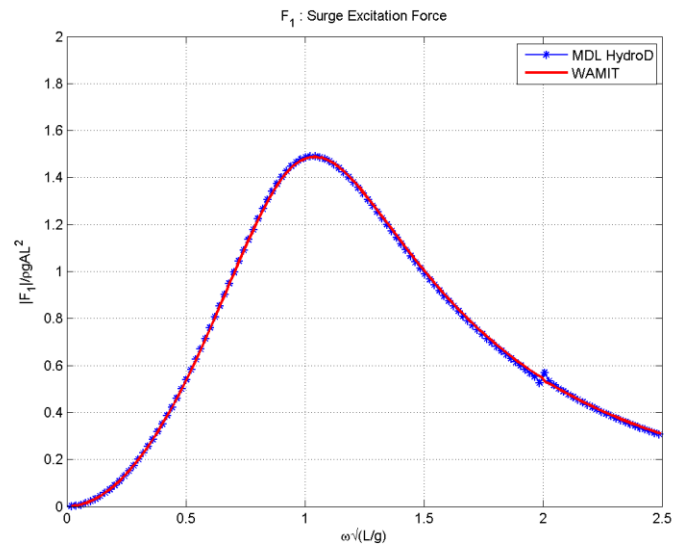
Fig. 58. Floating cylinder surge excitation force
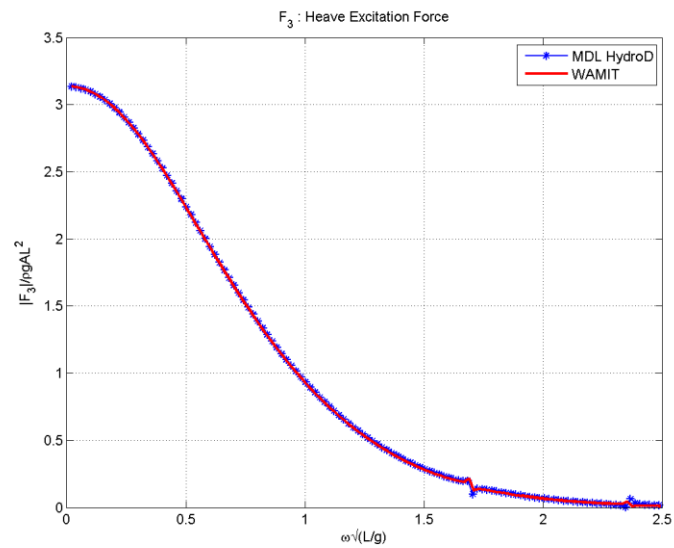
Fig. 59. Floating cylinder heave excitation force
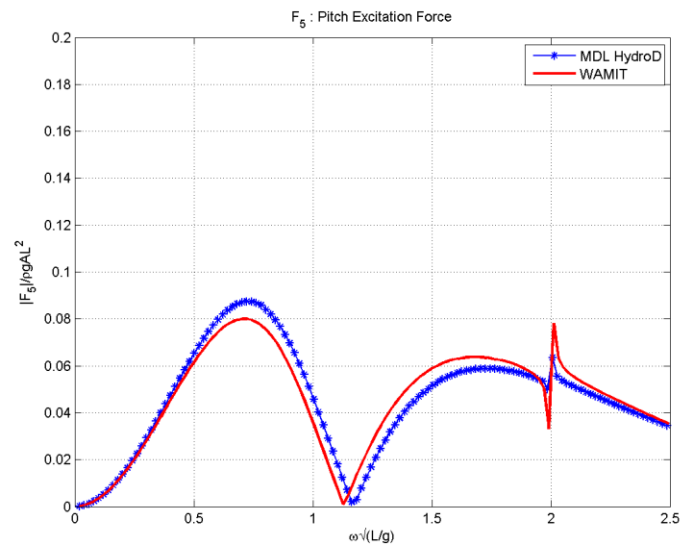
Fig. 60. Floating cylinder pitch excitation force

2.5 RAO
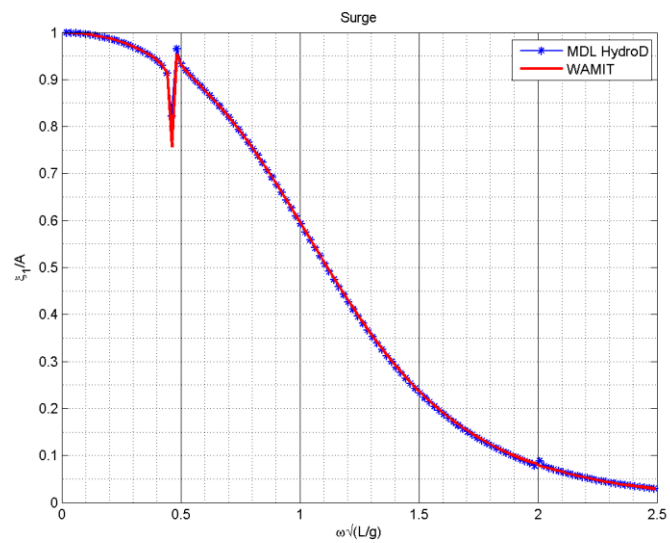
Fig. 61. Floating cylinder surge RAO
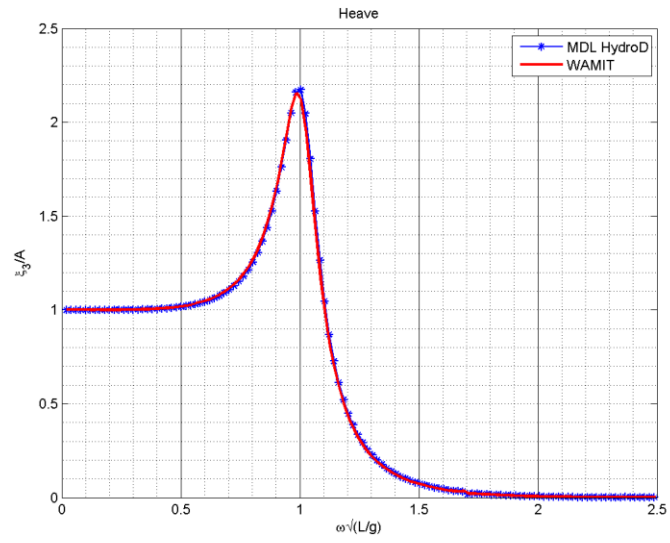
Fig. 62. Floating cylinder heave RAO
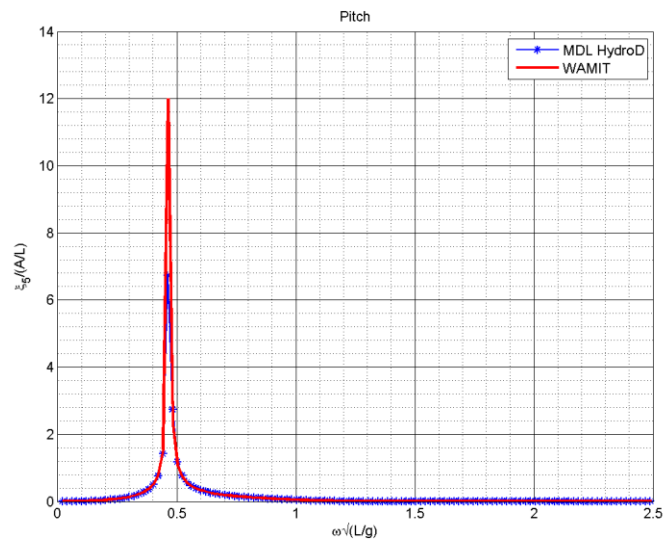
Fig. 63. Floating cylinder pitch RAO

3   Box Barge

3.1 Geometry and Panel Details
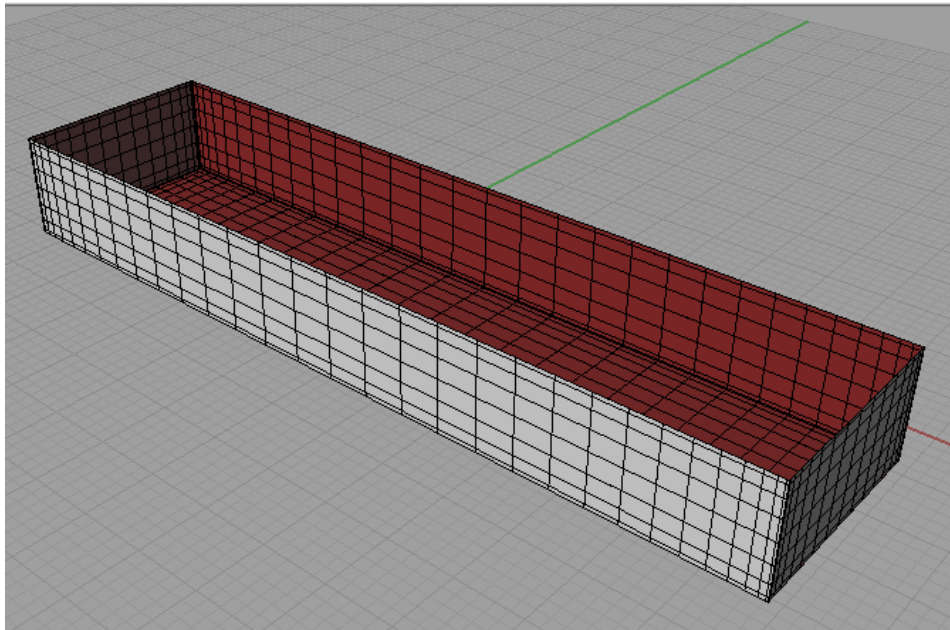
Fig. 64. Box barge panel model

Table 17: Box barge dimension

Parameter	Value
Length	80 m
Breadth	20 m
Draft	10 m
Number of Panels	1280
Water Depth	Infinite
Non dimensionalizing length	40 m

3.2 Hydrostatics

Parameter	MDLHydroD	WAMIT
Volume	VOLX = 16000.01 VOLY= 15999.99 VOLZ = 16000.00	VOLX = 16000.0 VOLY= 16000.0 VOLZ = 16000.0
Center of Buoyancy	Xb= 0.00000 Yb= 0.00000 Zb= -5.000000	Xb= 0.00000 Yb= 0.00000 Zb= -5.000000
Hydrostatic Stiffness Terms	C33 = 1.000000 C35 = 3.7509952E-08 C44 = -2.9299891E-02 C55 = 0.2827983	C33 = 1.0000 C35 = -0.20827E-08 C44 = -2.9300E-02 C55 = 0.28280
Water plane moment about x-axis	851963.8 m^4	---
Water plane moment about y-axis	52992.30 m^4	---

3.3 Added Mass and Damping
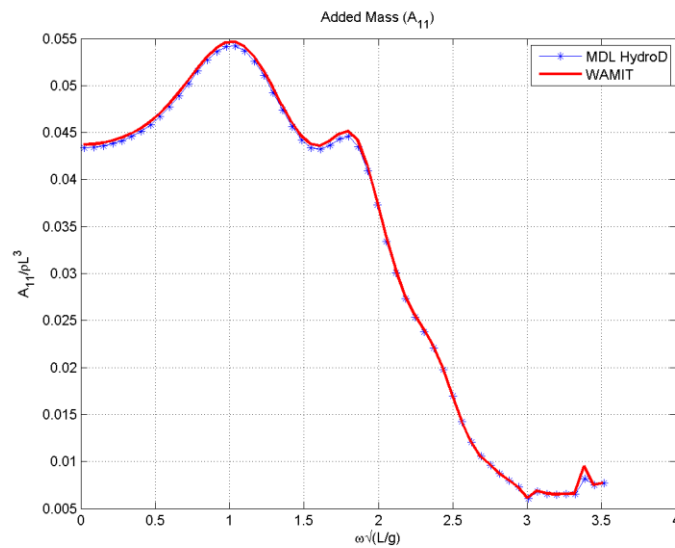
Fig. 65. Box barge added mass A_{11}
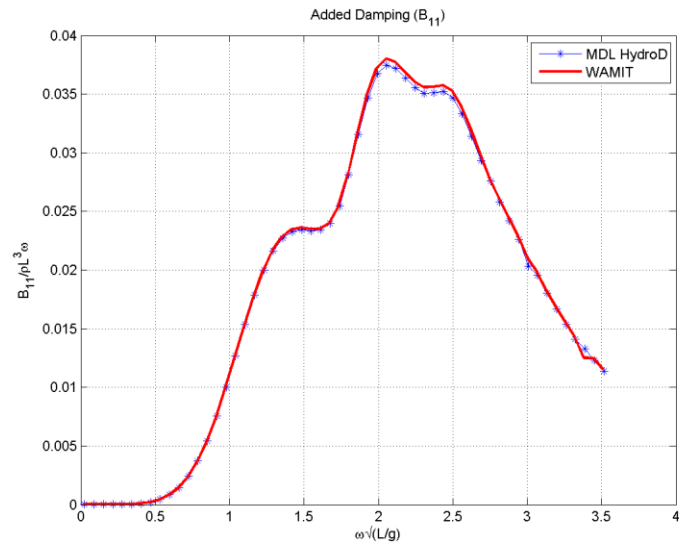
Fig. 66. Box barge damping B_{11}
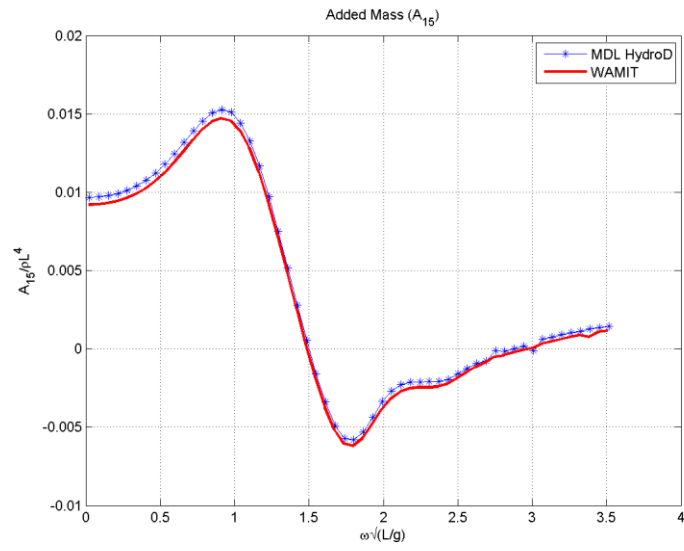
Fig. 67. Box barge added mass A_{15}
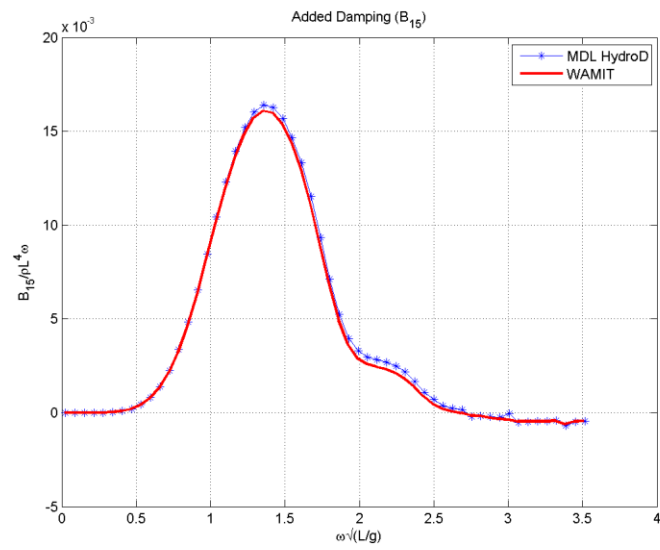
Fig. 68. Box barge damping B_{15}
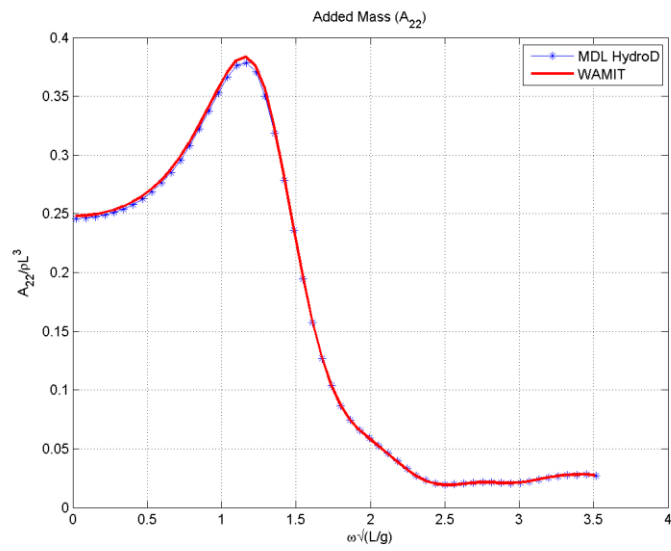
Fig. 69. Box barge added mass A_{22}
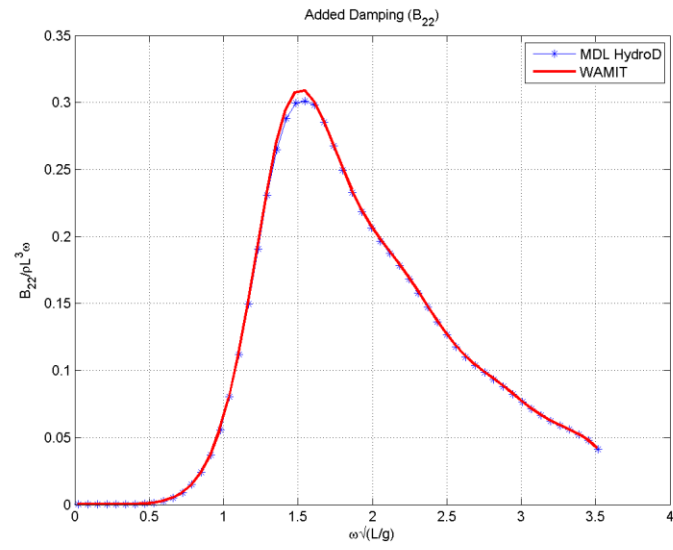
Fig. 70. Box barge damping B_{22}
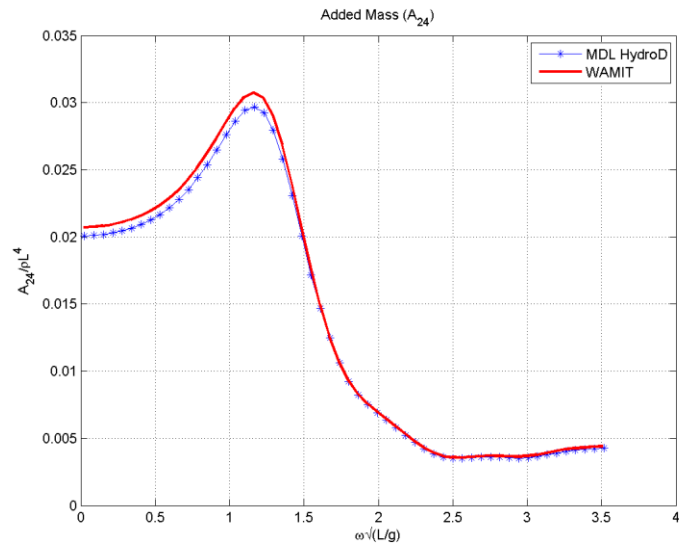
Fig. 71. Box barge added mass A_{24}

118
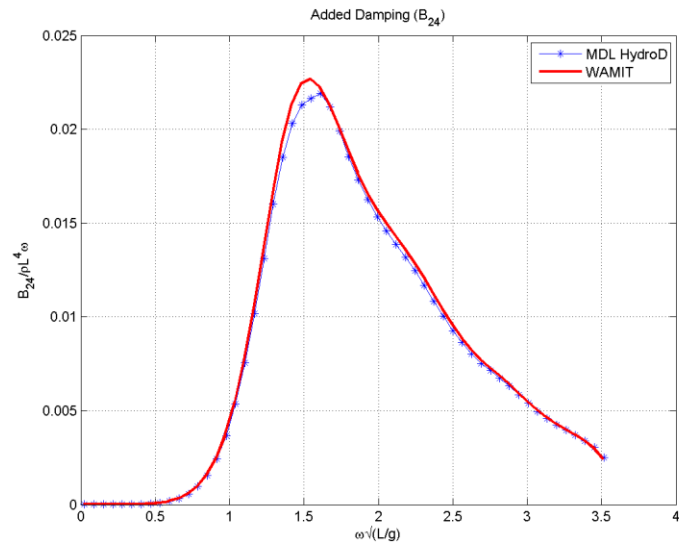
Fig. 72. Box barge damping B_{24}
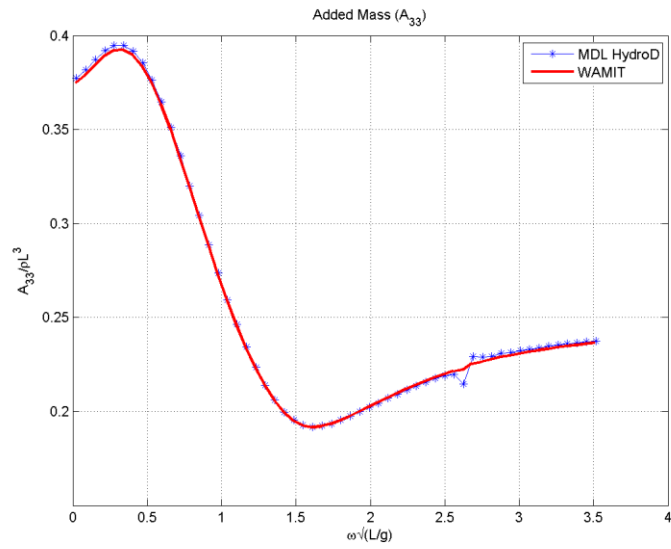
Fig. 73. Box barge added mass A_{33}
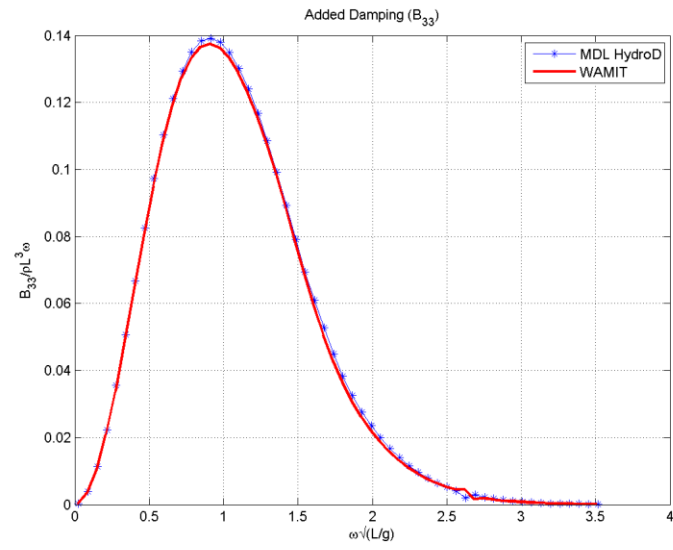
Fig. 74. Box barge damping B_{33}
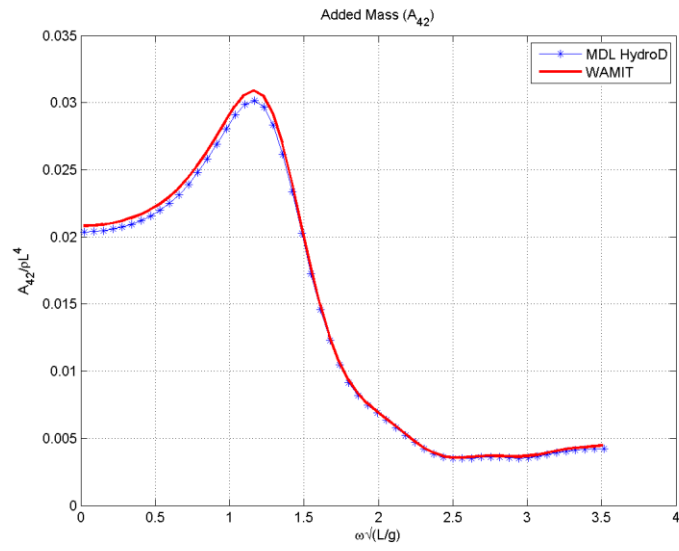
Fig. 75. Box barge added mass A_{42}
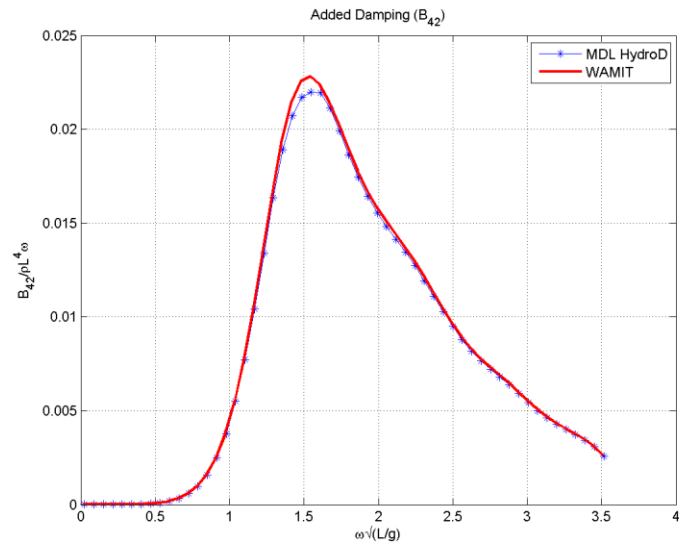
Fig. 76. Box barge damping B_{42}
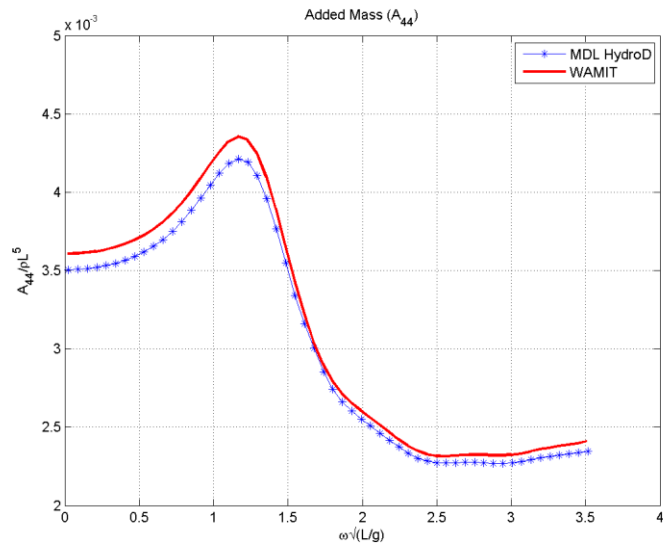
Fig. 77. Box barge added mass A_{44}
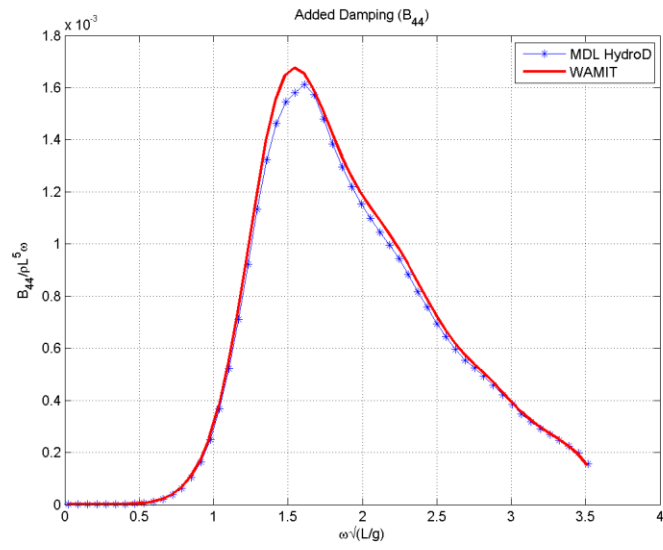
Fig. 78. Box barge damping B_{44}
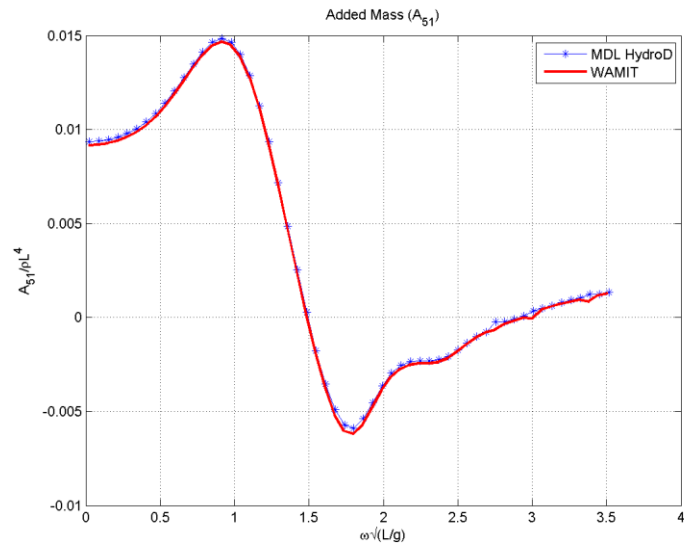
Fig. 79. Box barge added mass A_{51}
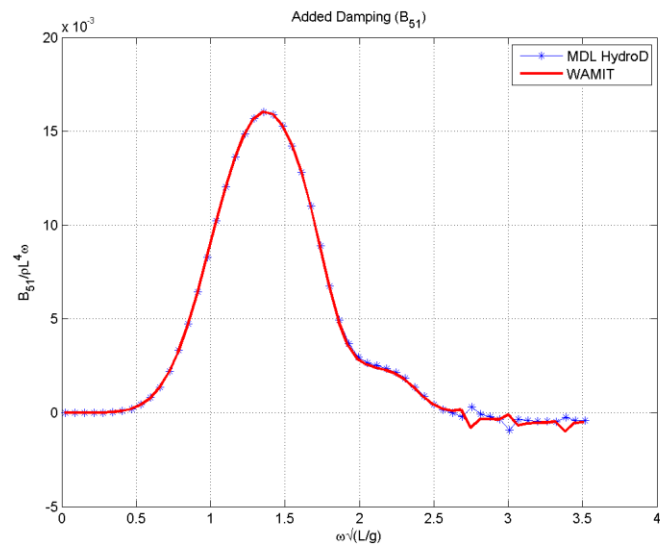
Fig. 80. Box barge damping B_{51}
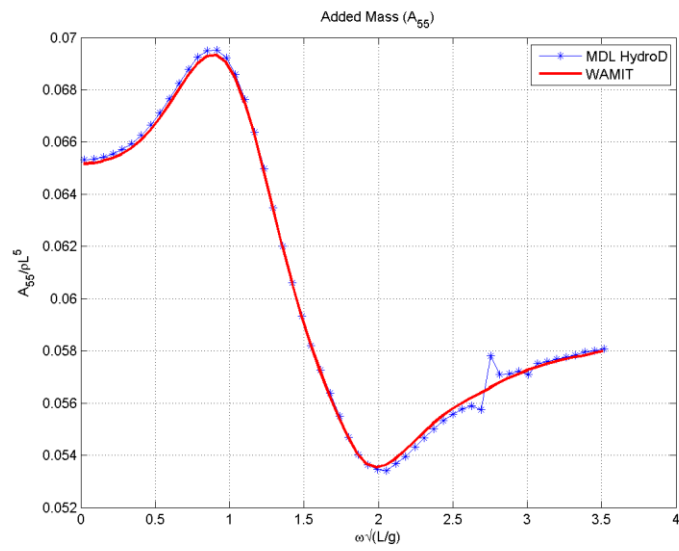
Fig. 81. Box barge added mass A_{55}
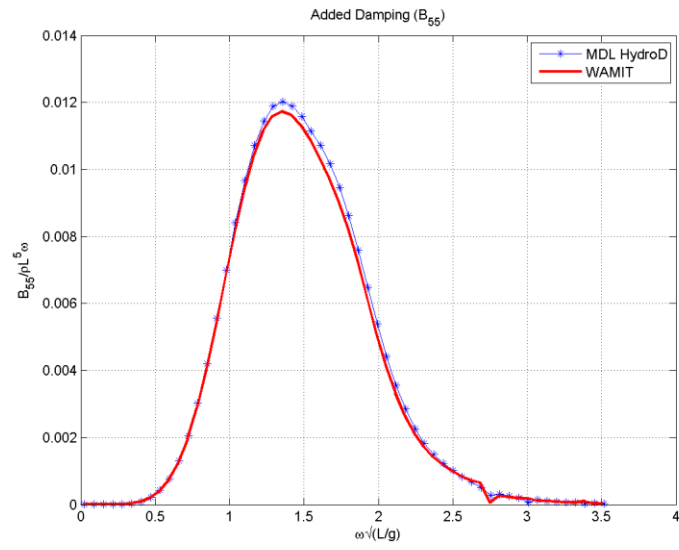
Fig. 82. Box barge damping B_{55}
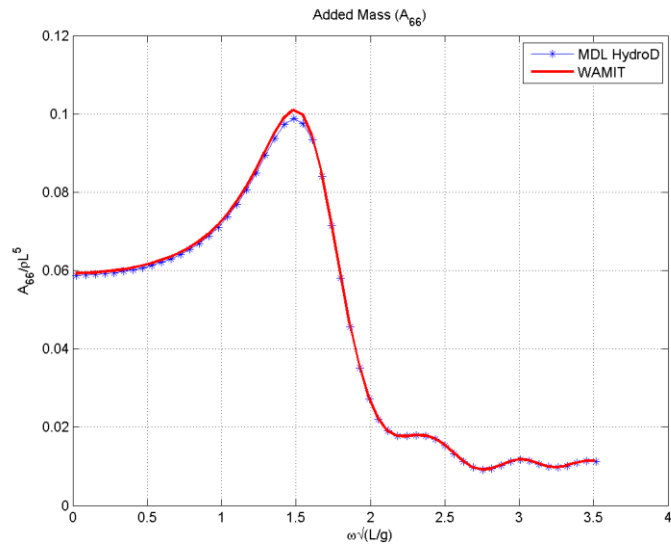
Fig. 83. Box barge added mass A_{66}
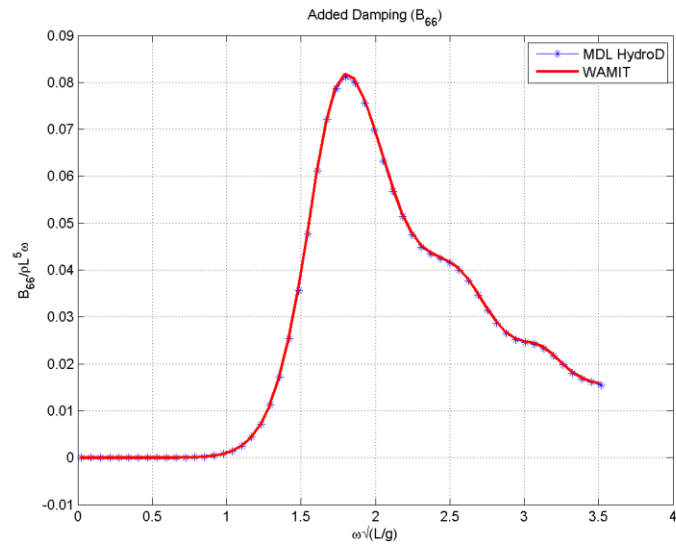
Fig. 84. Box barge damping B_{66}

3.4 Forces
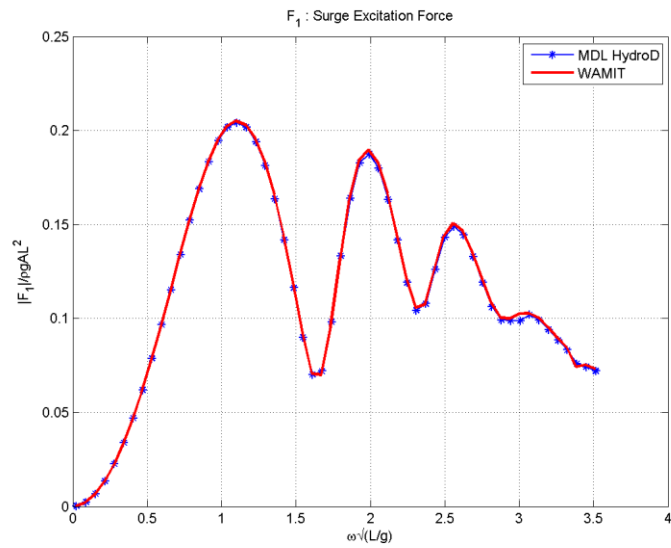
Fig. 85. Box barge surge excitation force
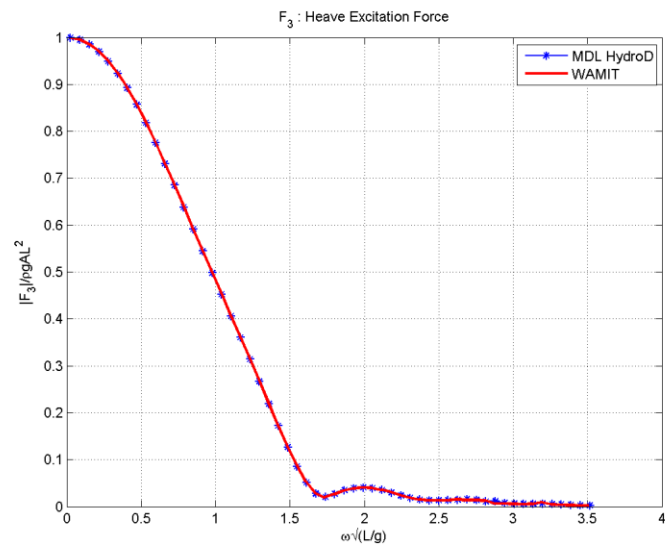
Fig. 86. Box barge heave excitation force
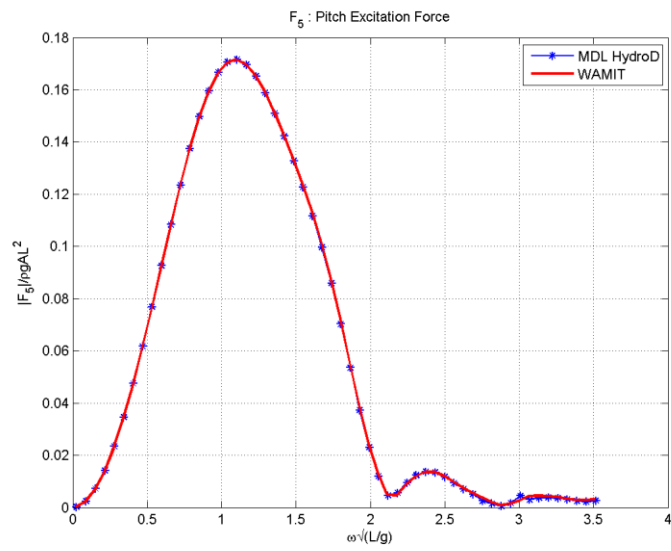
Fig. 87. Box barge pitch excitation force

3.5 RAO
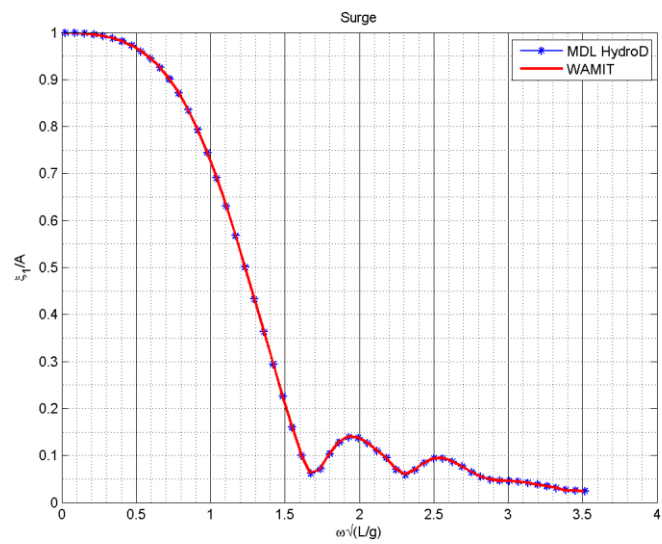
Fig. 88. Box barge surge RAO
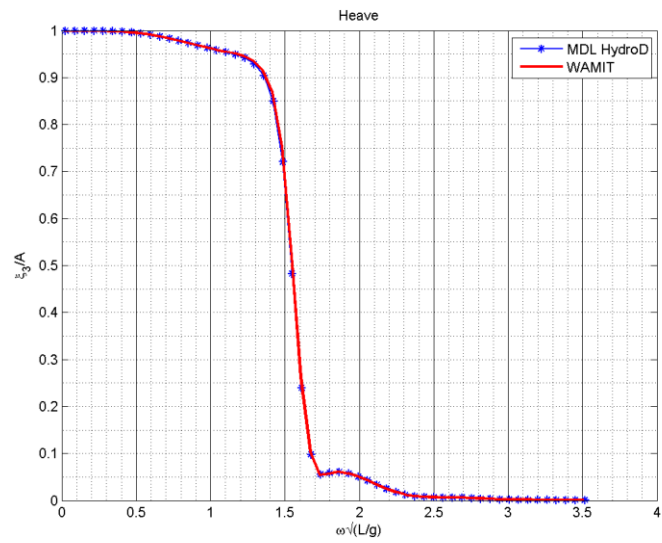
Fig. 89. Box barge heave RAO
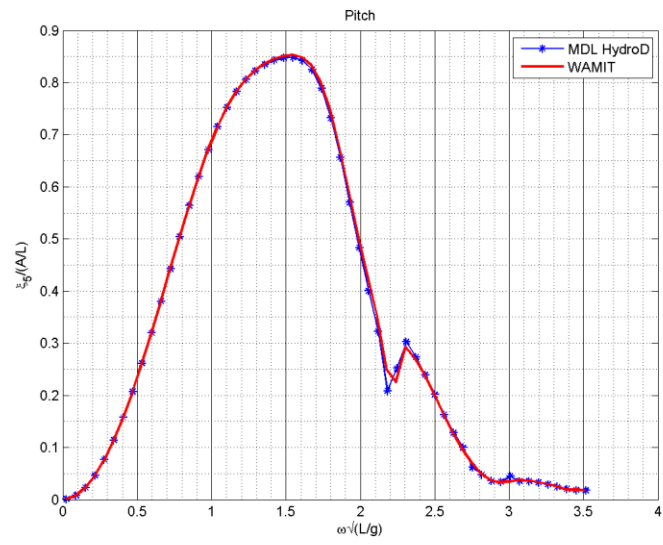
Fig. 90. Box barge pitch RAO

4 DWSC Spar

The Deep Water Stable Craneship (DWSC) spar is a specialized hull to be used to transfer cargo from LMSR to T-Craft.

4.1 Geometry and Panel Details
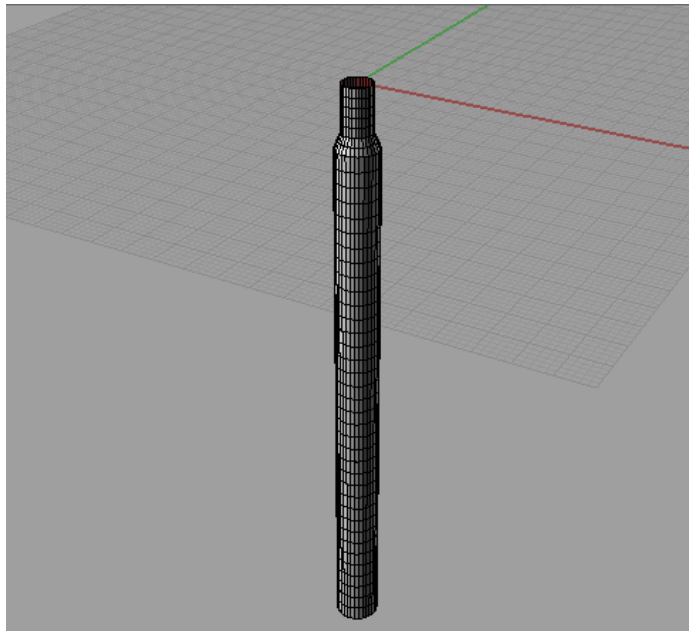
Fig. 91. DWSC Spar panel model

Table 18: Spar dimension

Parameter	Value
Diameter (U)	6.0 m
Diameter (L)	8.5 m
Length	129.6 m
Draft	118.0 m
Number of Panels	1536
Water Depth	Infinite
Non dimensionalizing length (L)	6.0 m

4.2 Hydrostatics

Parameter	MDLHydroD	WAMIT
Volume	VOLX = 6353.422 VOLY= 6353.422 VOLZ = 6353.520	VOLX = 6353.48 VOLY= 6353.48 VOLZ = 6353.46
Center of Buoyancy	Xb= 0.00000 Yb= 0.00000 Zb= -61.52966	Xb= 0.00000 Yb= 0.00000 Zb= -61.529995
Hydrostatic Stiffness Terms	C33 = 0.7803620 C35 = -2.4283374E-08 C44 = 0.8828591 C55 = 0.8828591	C33 = 0.78036 C35 = -0.12106E-07 C44 = 0.88083 C55 = 0.88083
Water plane moment about x-axis	61.93528 m^4	---
Water plane moment about y-axis	61.93533 m^4	---

4.3 Added Mass and Damping
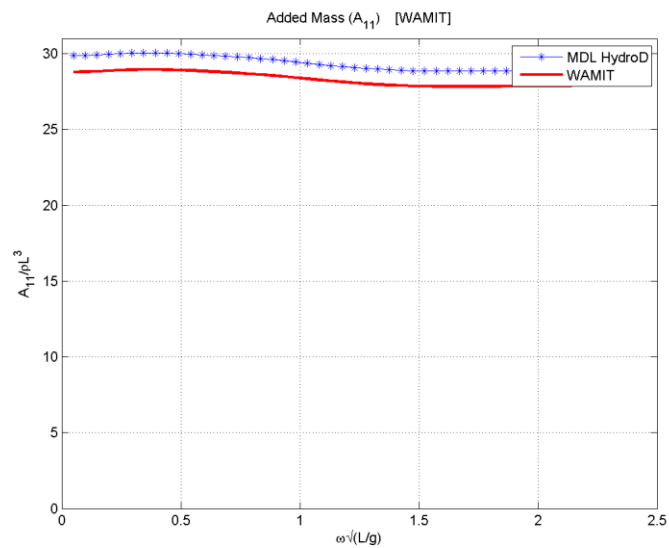
Fig. 92. Spar added mass A_{11}

130
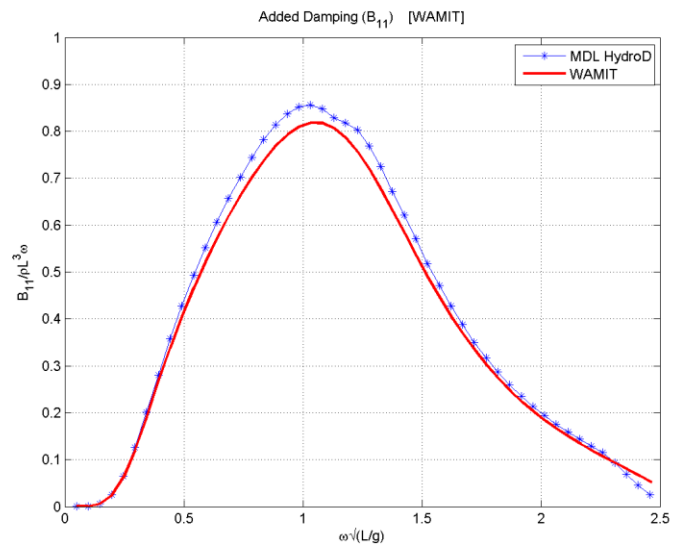
Fig. 93. Spar damping B_{11}
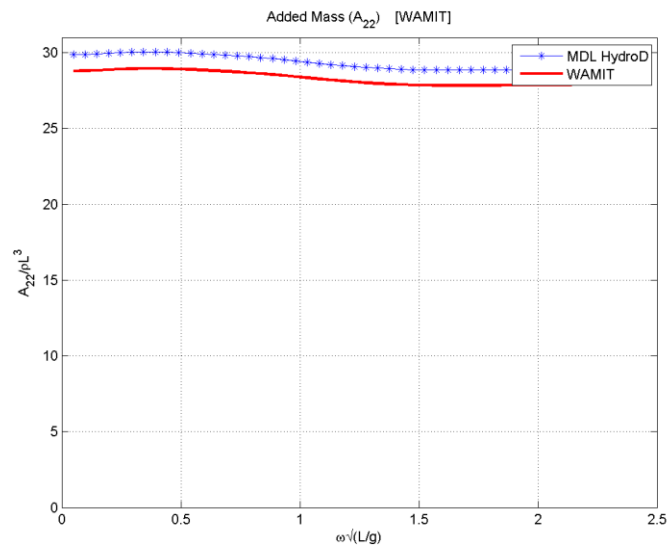
Fig. 94. Spar added mass A_{22}

131
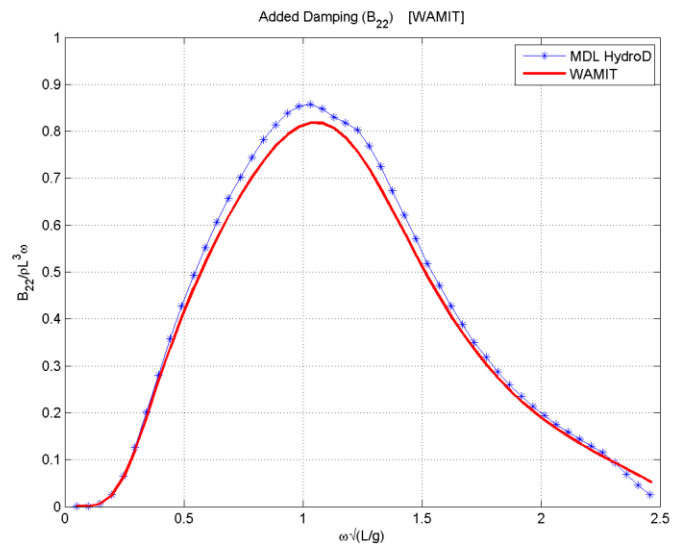
Fig. 95. Spar damping B_{22}
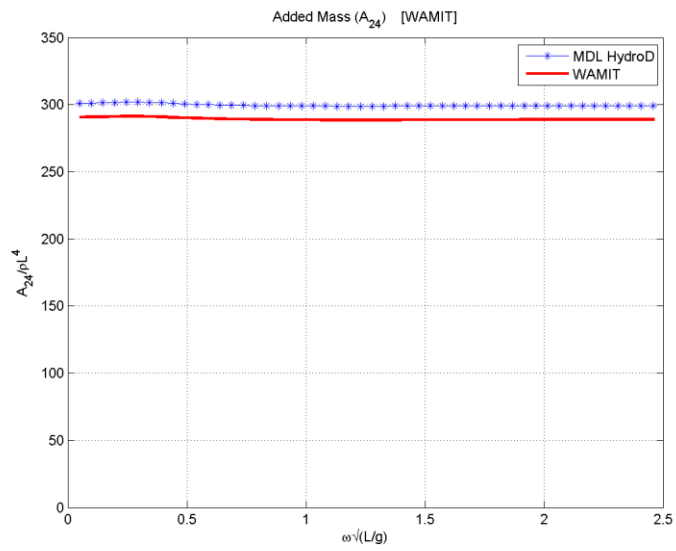
Fig. 96. Spar added mass A_{24}

132
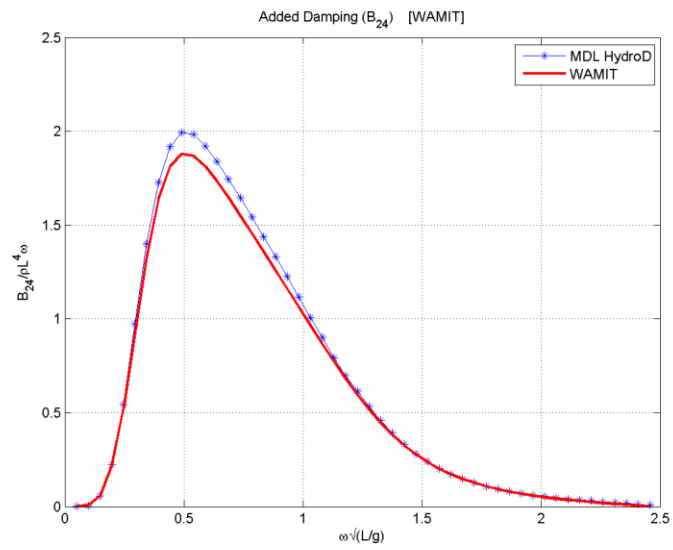
Fig. 97. Spar damping B_{24}
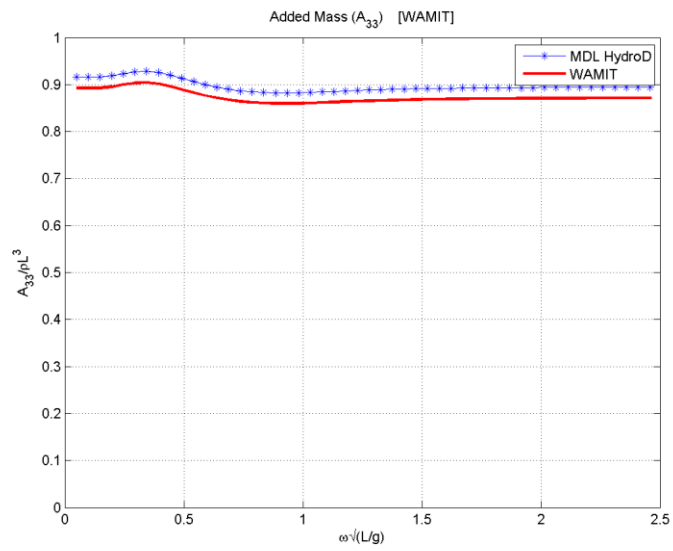
Fig. 98. Spar added mass A_{33}
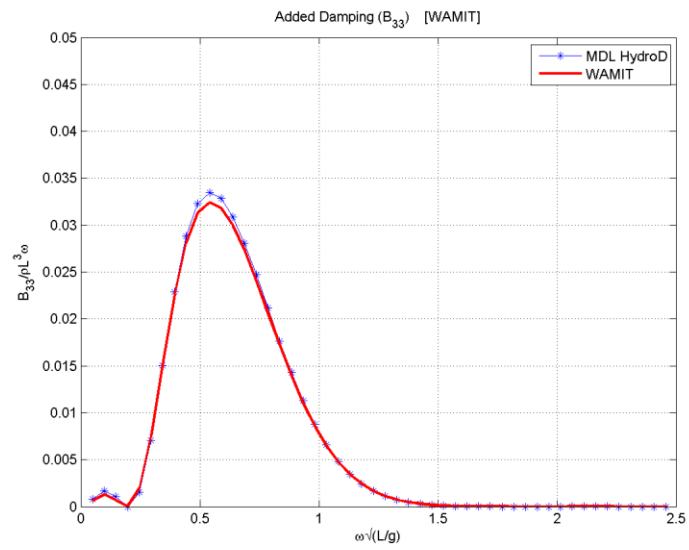
Fig. 99. Spar damping B_{33}
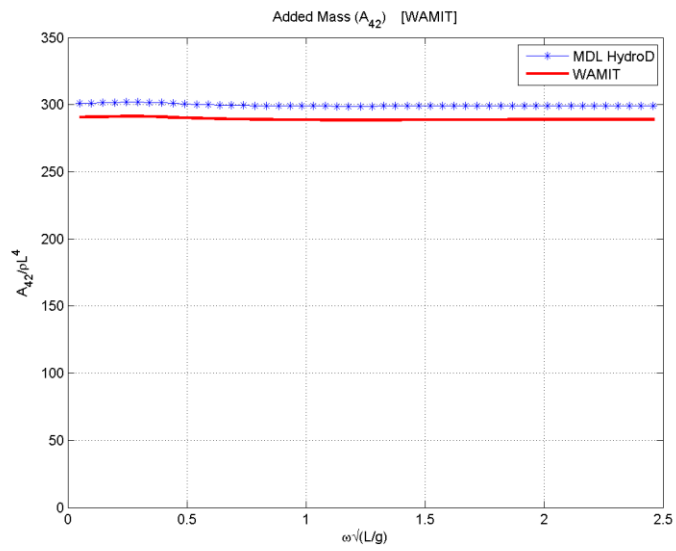
Fig. 100. Spar added mass A_{42}
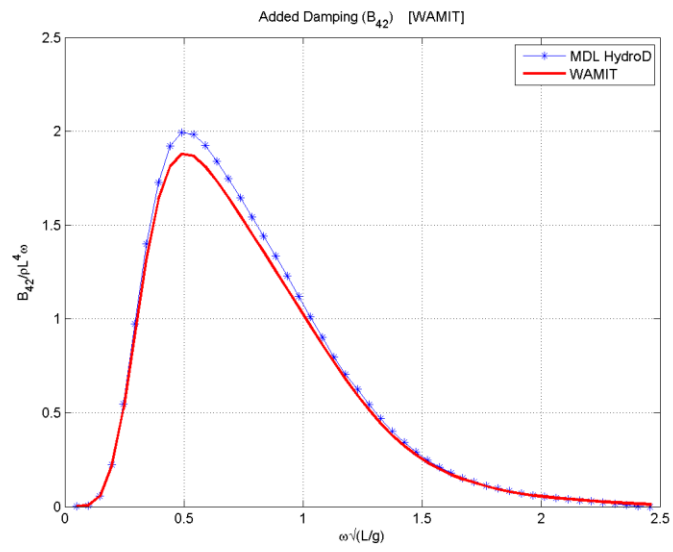
Fig. 101. Spar damping B_{42}
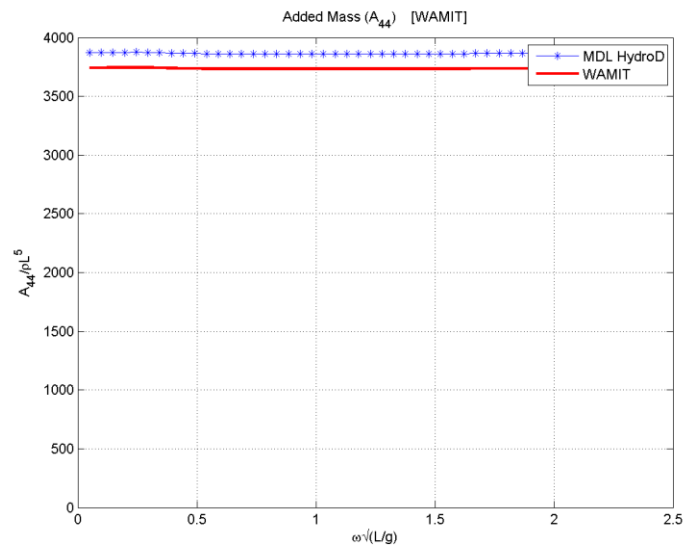
Fig. 102. Spar added mass A_{44}
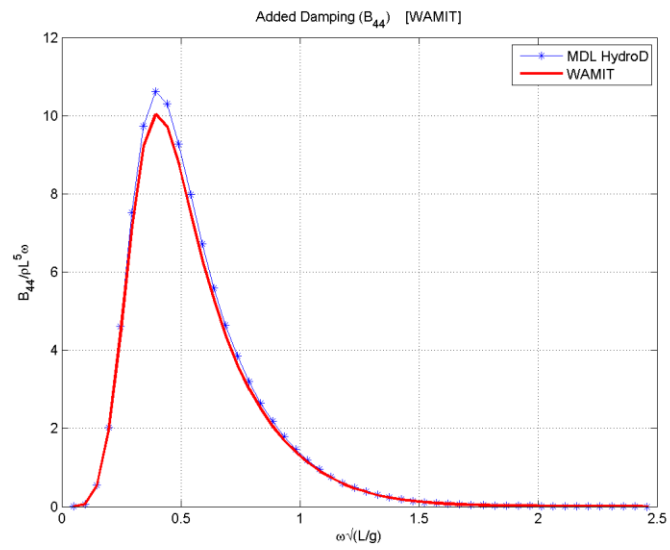
Fig. 103. Spar damping B_{44}
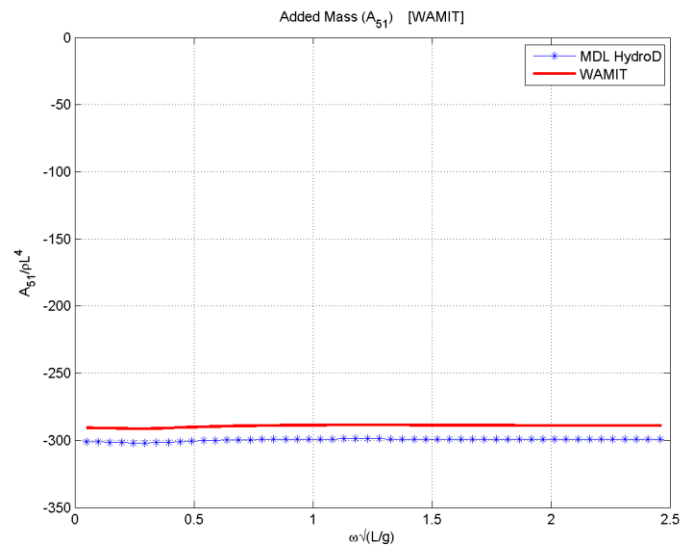
Fig. 104. Spar added mass A_{51}

136
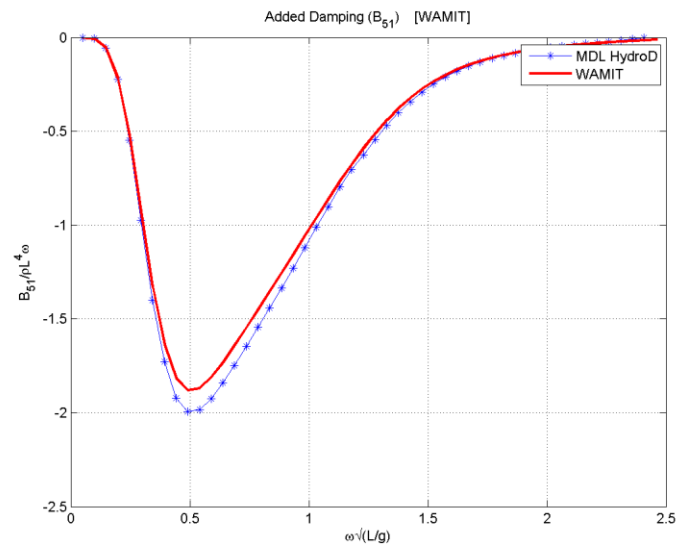
Fig. 105. Spar damping B_{51}
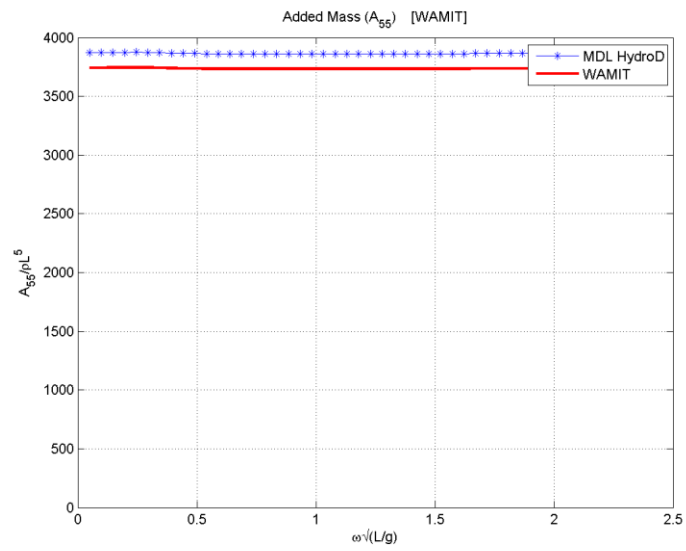
Fig. 106. Spar added mass A_{55}
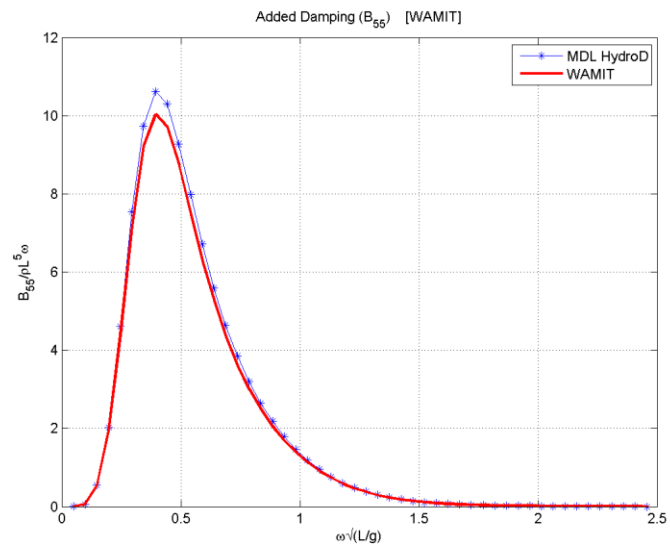
Fig. 107. Spar damping B_{55}

4.4 Forces
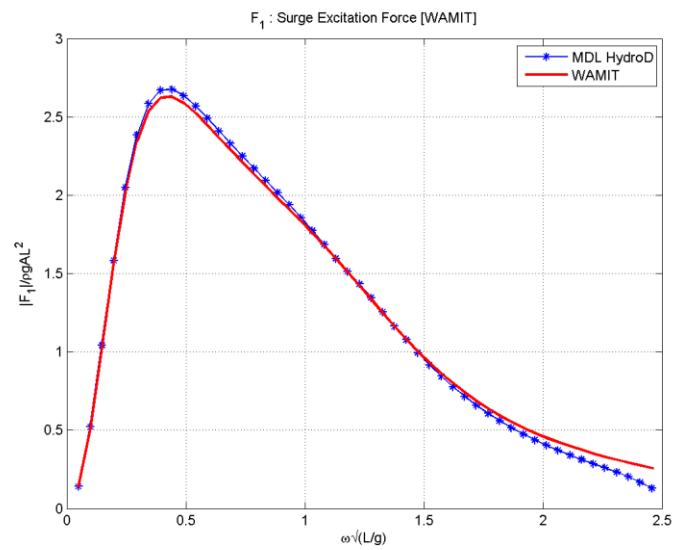
Fig. 108. Spar surge excitation force
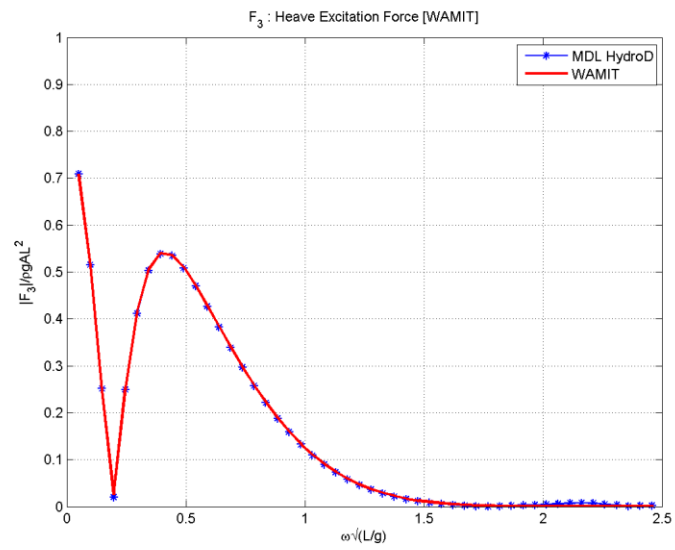
Fig. 109. Spar heave excitation force
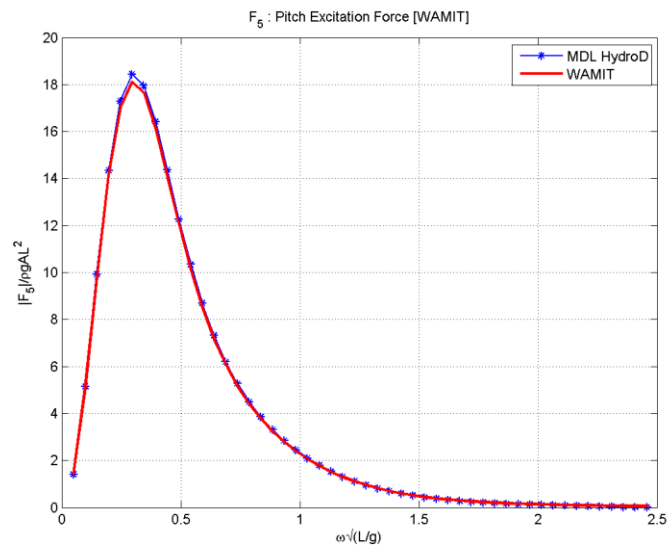
Fig. 110. Spar pitch excitation force

4.5 RAO
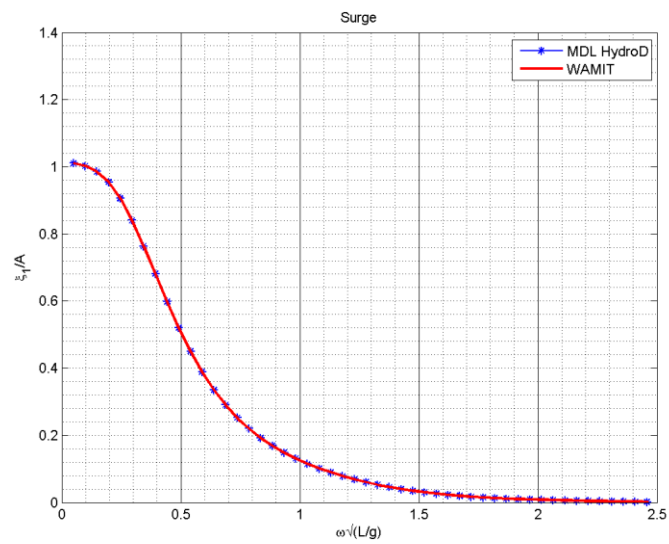
Fig. 111. Spar surge RAO
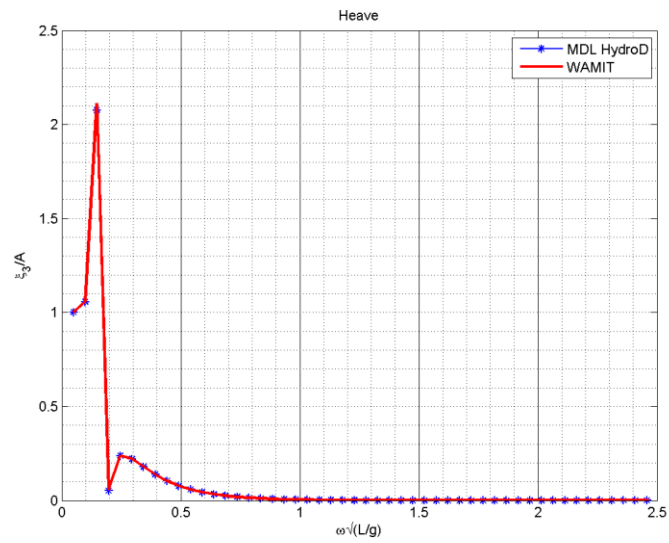
Fig. 112. Spar heave RAO

140
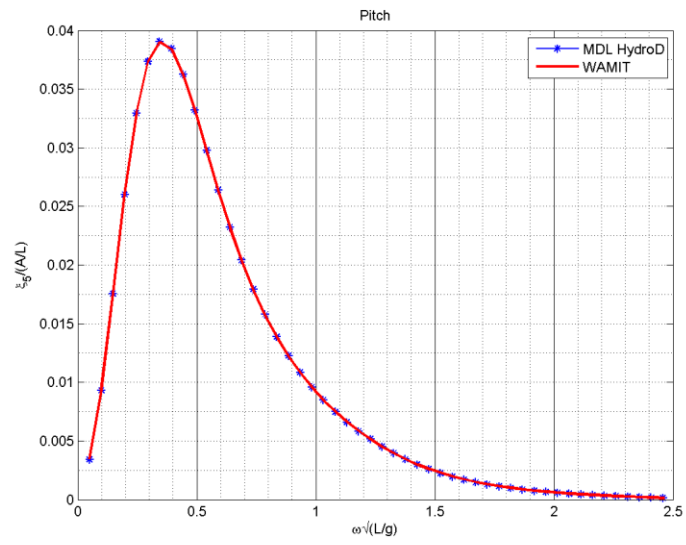
Fig. 113. Spar pitch RAO

5   USN LMSR Ship

5.1 Geometry and Panel Details
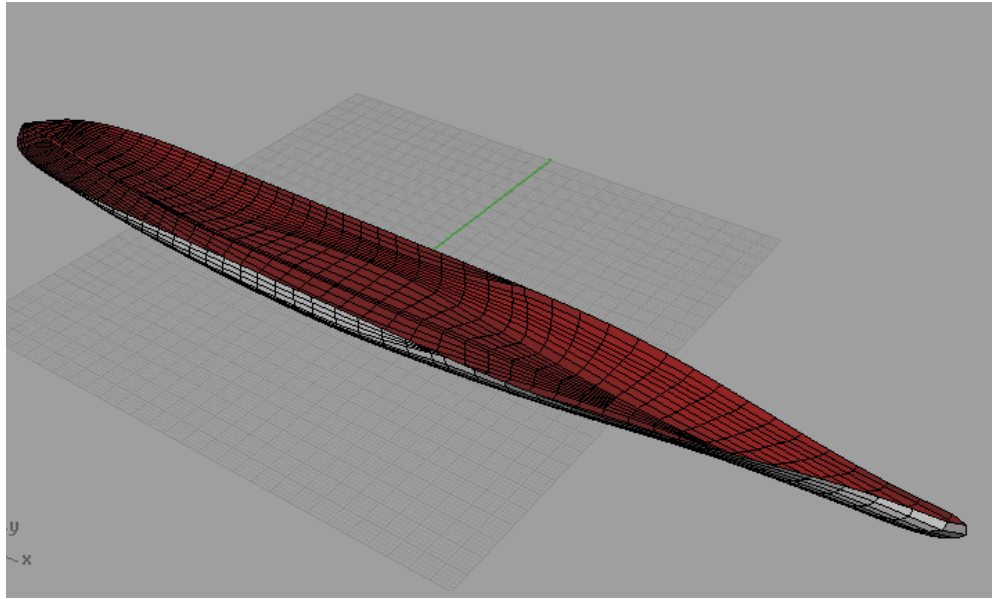
Fig. 114. USN LMSR Ship Bob Hope panel model

Table 19: Ship dimension

Parameter	Value
Length Between Perpendicular, L_{pp}	269.45 m
Breadth molded on waterline, B	32.258m
Draft, T	8.795 m
Number of Panels	1416
Water Depth	Infinite
Non dimensionalizing length	135 m

5.2 Hydrostatics

Parameter	MDLHydroD	WAMIT
Volume	VOLX = 49017.17 VOLY= 48950.77 VOLZ = 49029.09	VOLX = 49012.4 VOLY= 48951.0 VOLZ = 49033.7
Center of Buoyancy	Xb= -9.4776773 Yb= 0.00000 Zb= -3.897359	Xb= -9.485846 Yb= 0.00000 Zb= -3.898955
Hydrostatic Stiffness Terms	C33 = 0.3918698 C35 = 4.2208418E-02 C44 = 6.0625182E-04 C55 = 0.1000643	C33 = 0.39187 C35 = 4.2221E-02 C44 = 6.0621E-04 C55 = 0.10002

5.3 Added Mass and Damping
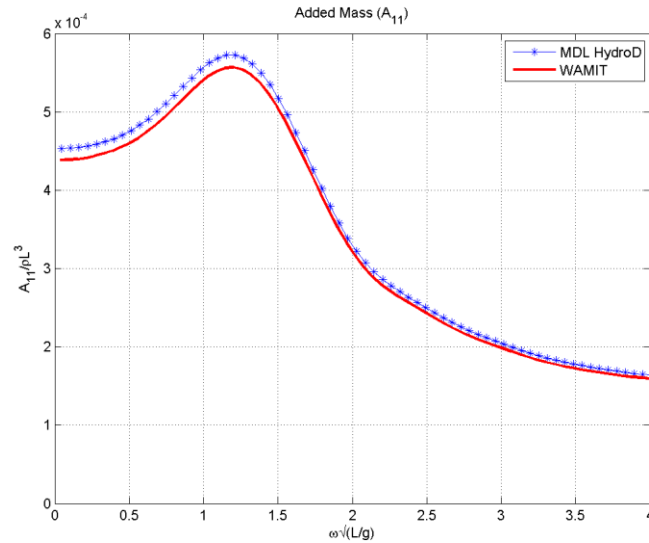
Fig. 115. Ship added mass A_{11}
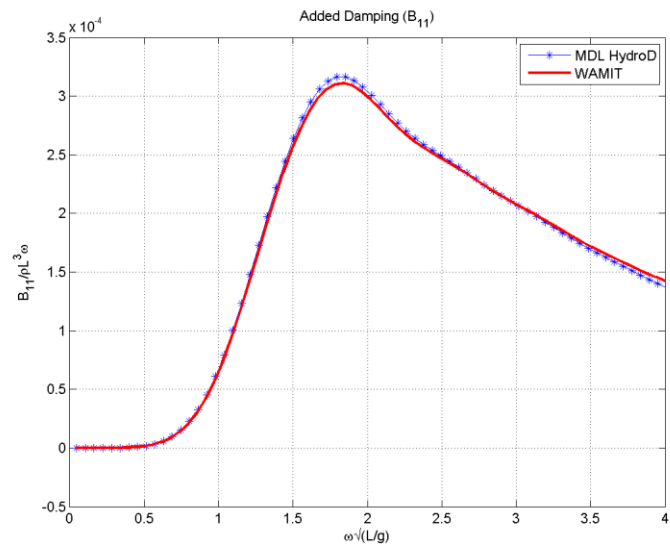
Fig. 116 Ship damping B_{11}
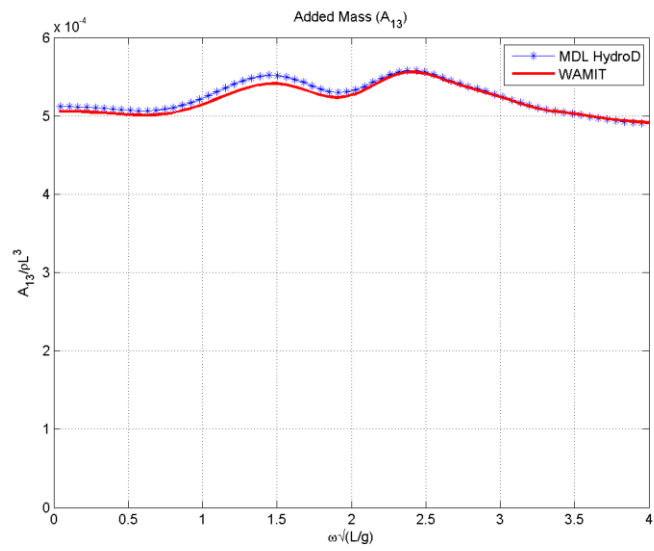
Fig. 117. Ship added mass A_{13}
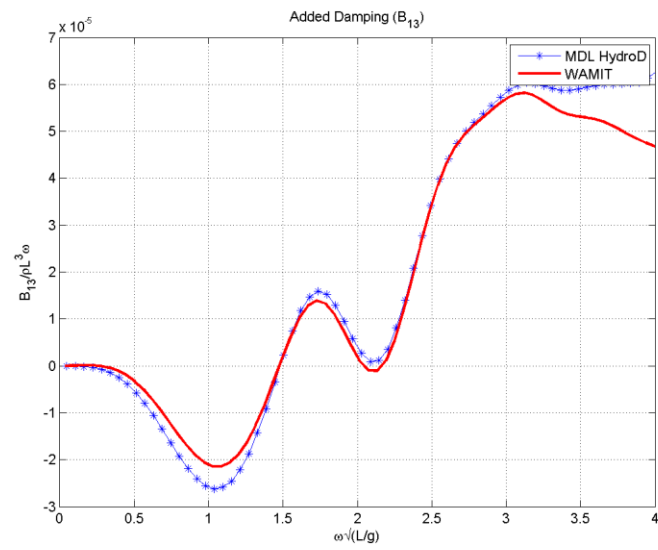
Fig. 118. Ship damping B_{13}
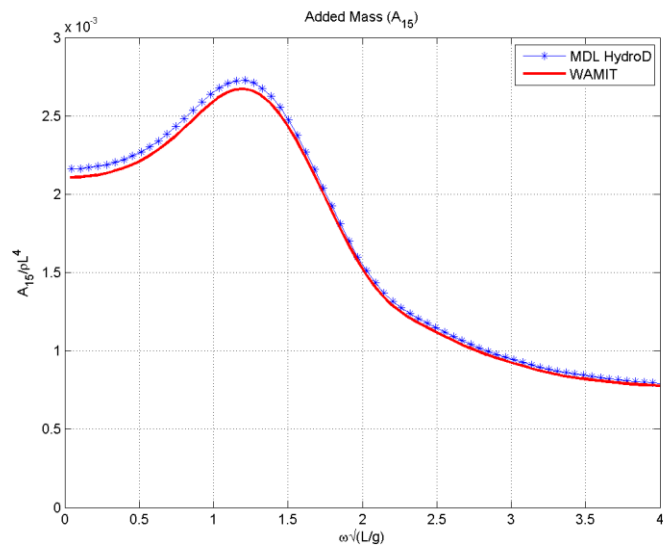
Fig. 119. Ship added mass A_{15}
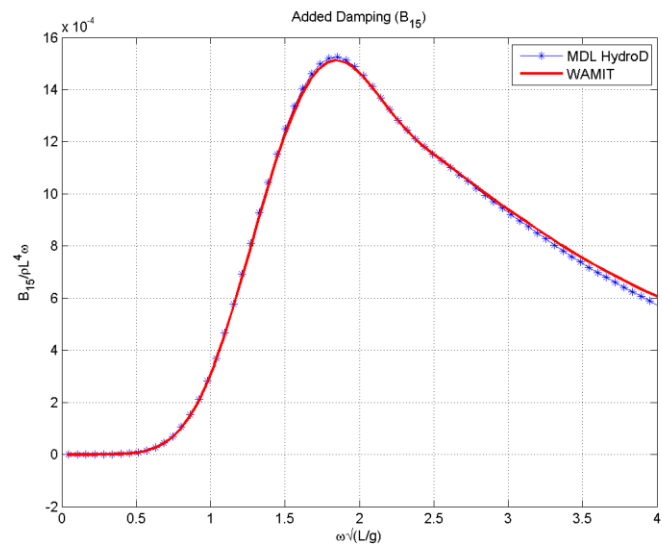
Fig. 120. Ship damping B_{15}
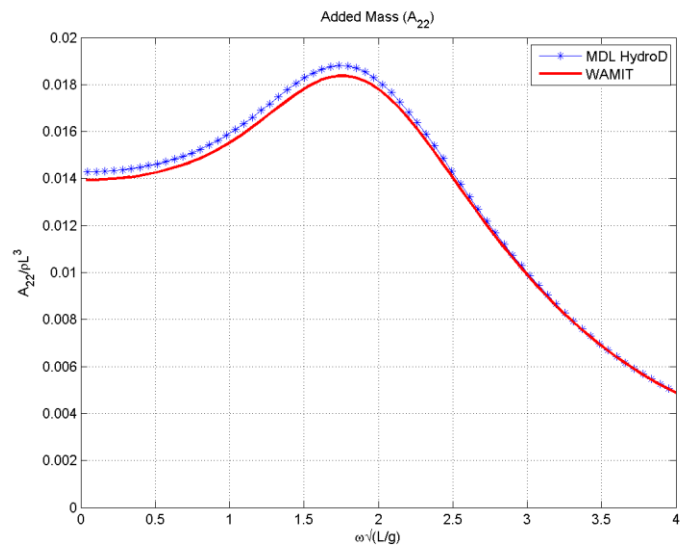
Fig. 121. Ship added mass A_{22}
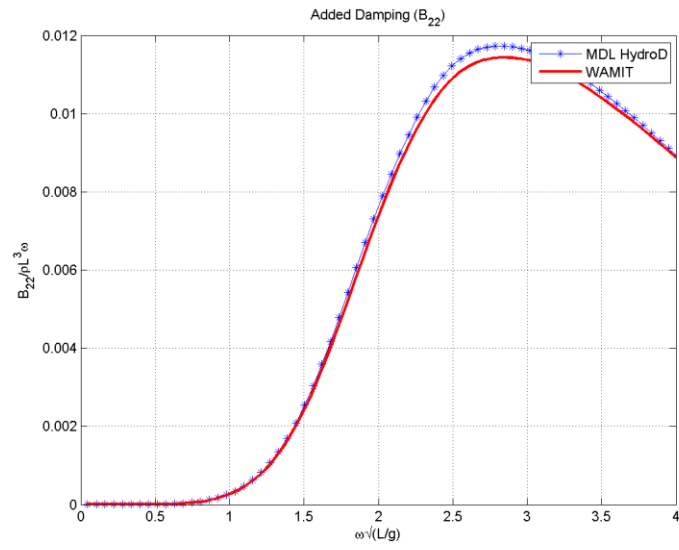
Fig. 122. Ship damping B_{22}
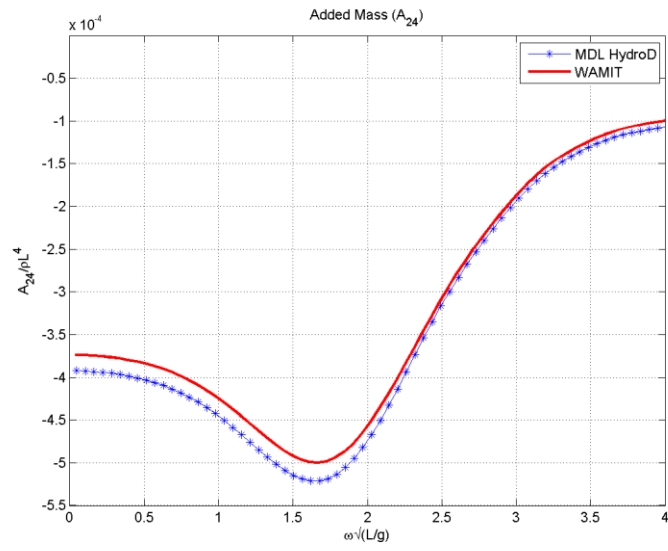
Fig. 123. Ship added mass A_{24}
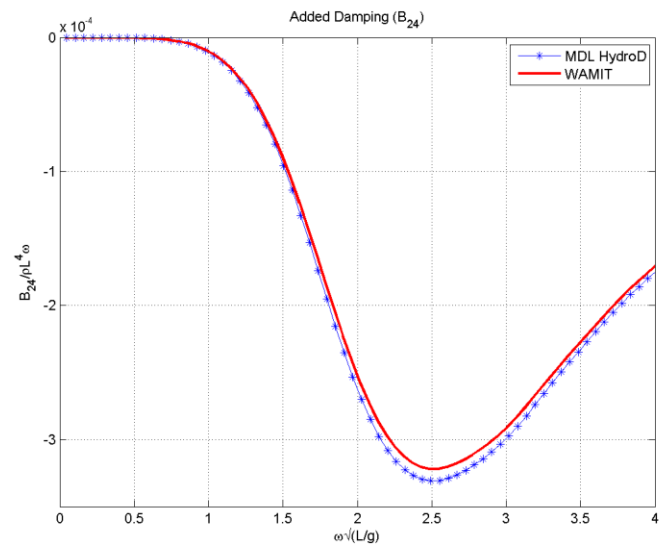
Fig. 124. Ship damping B_{24}
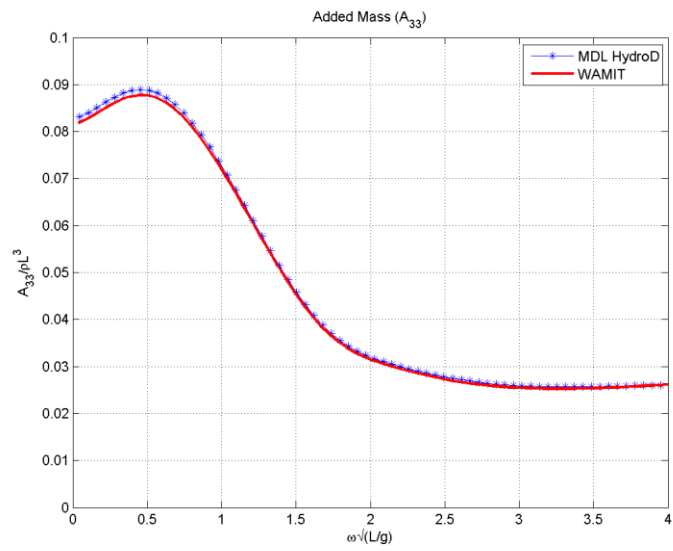
Fig. 125. Ship added mass A_{33}

148
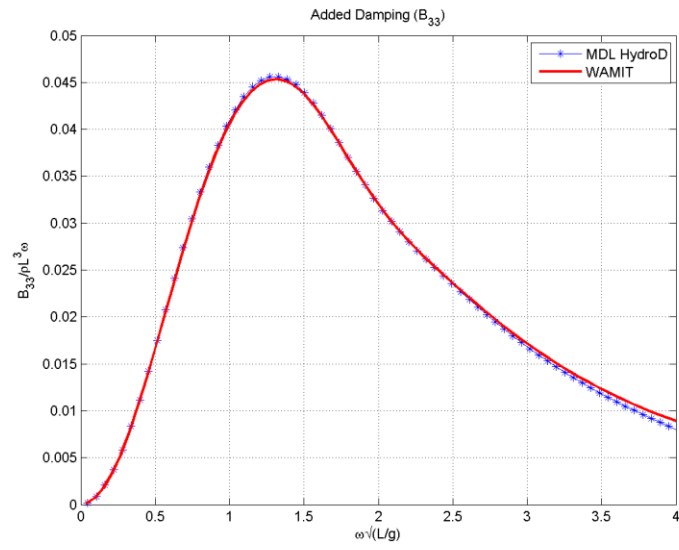
Fig. 126. Ship damping B_{33}
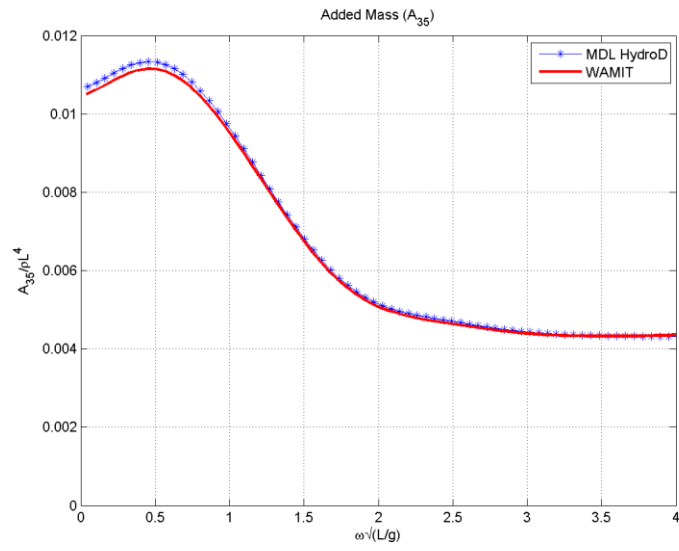
Fig. 127. Ship added mass A_{35}
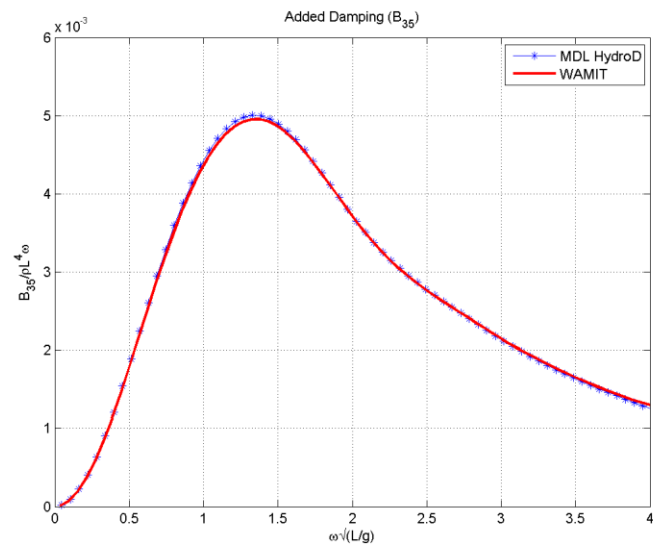
Fig. 128. Ship damping B_{35}
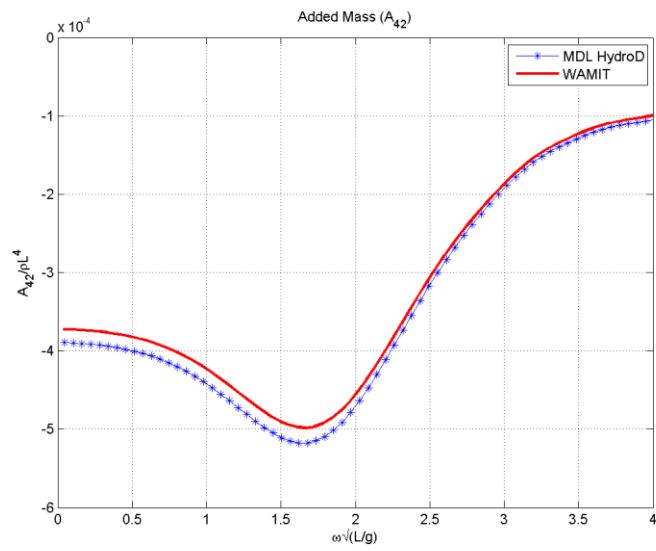
Fig. 129. Ship added mass A_{42}
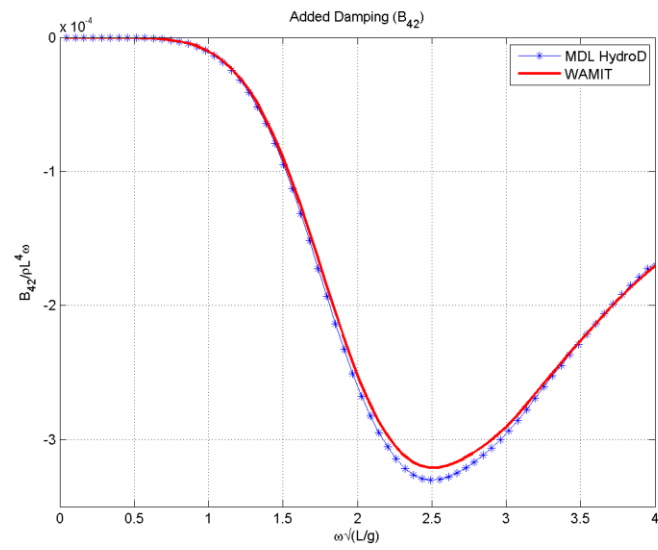
Fig. 130. Ship damping B_{42}
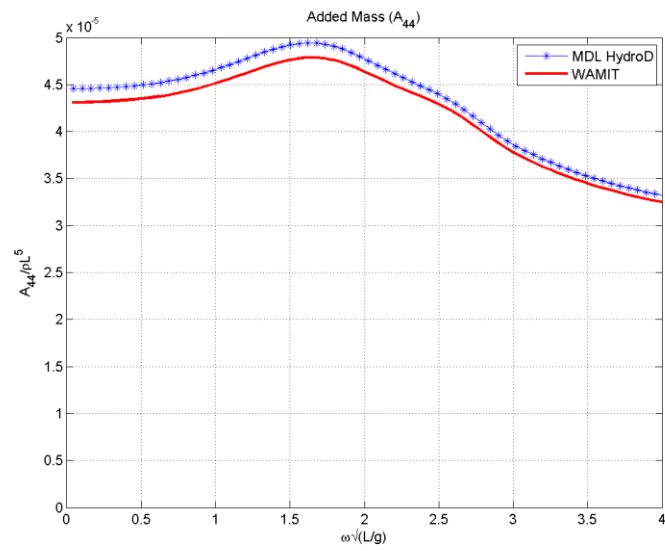
Fig. 131. Ship added mass A_{44}

151
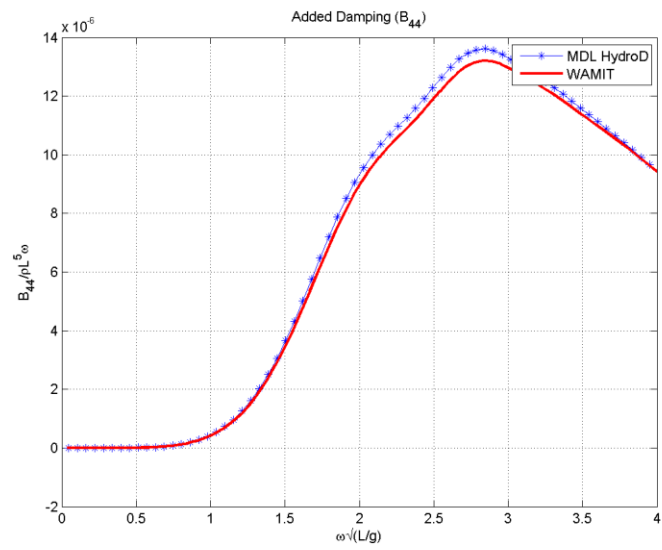
Fig. 132. Ship damping B_{44}
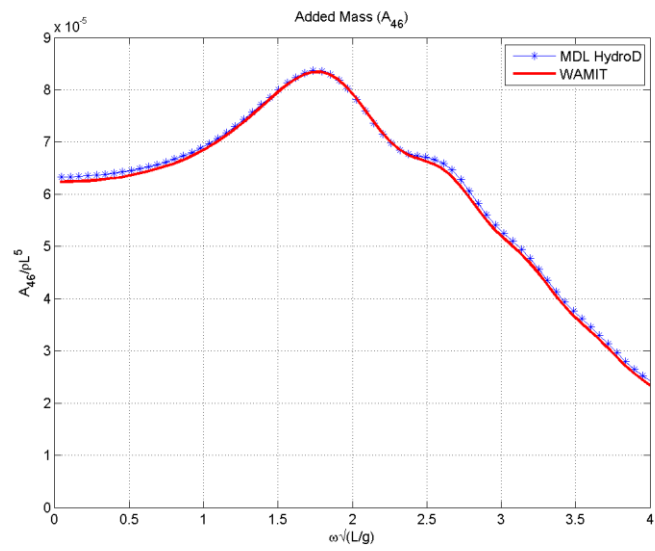
Fig. 133. Ship added mass A_{46}

152
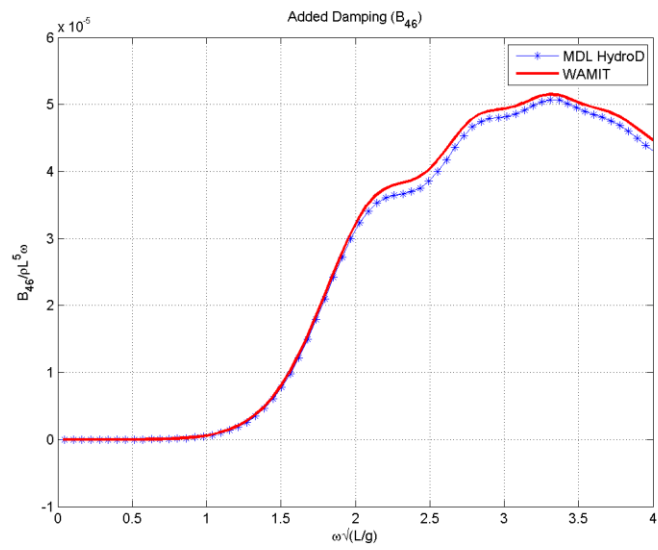
Fig. 134. Ship damping B_{46}
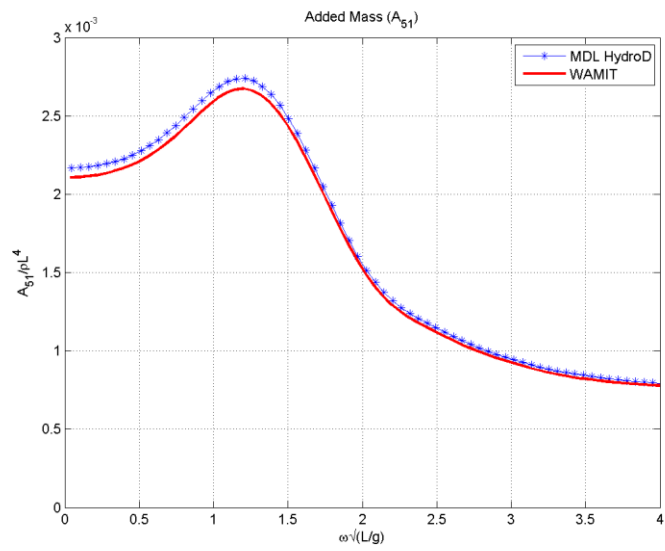
Fig. 135. Ship added mass A_{51}
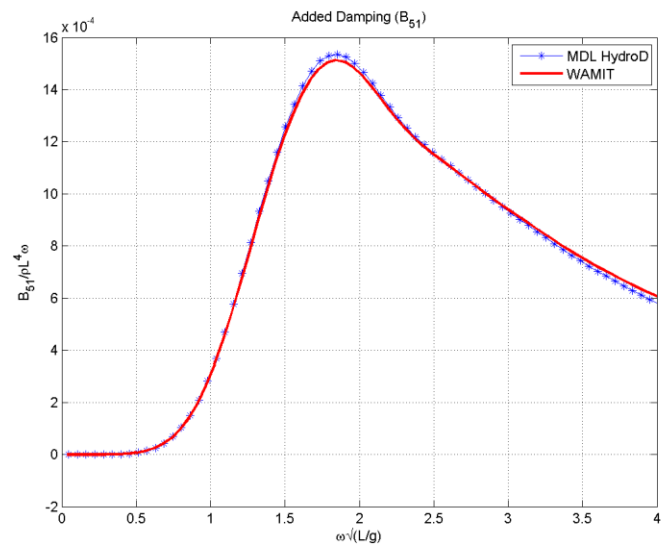
Fig. 136. Ship damping B_{51}
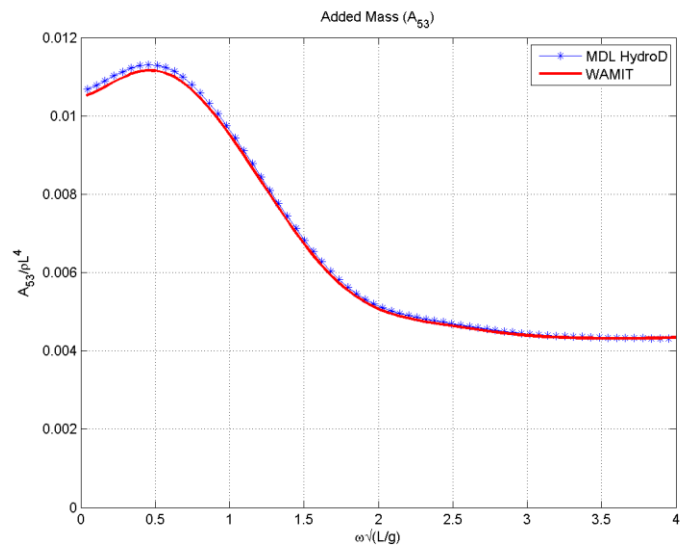
Fig. 137. Ship added mass A_{53}
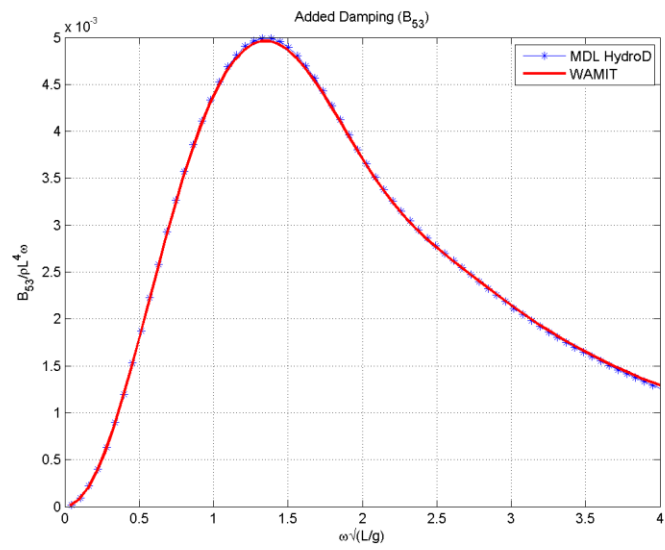
Fig. 138. Ship damping B_{53}
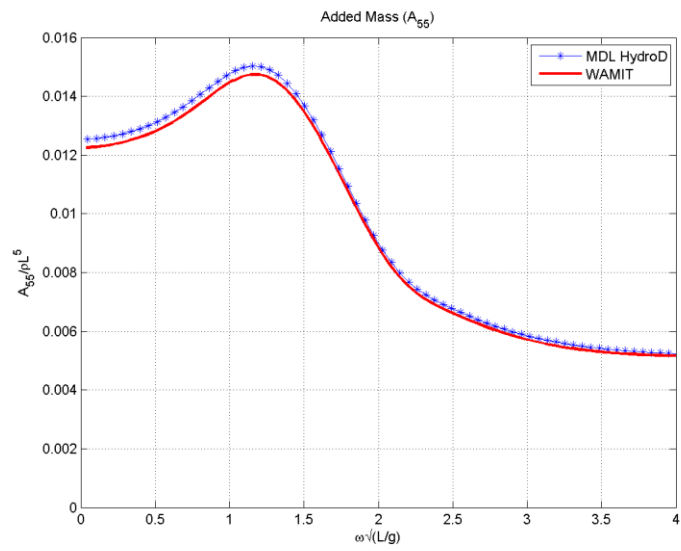
Fig. 139. Ship added mass A_{55}
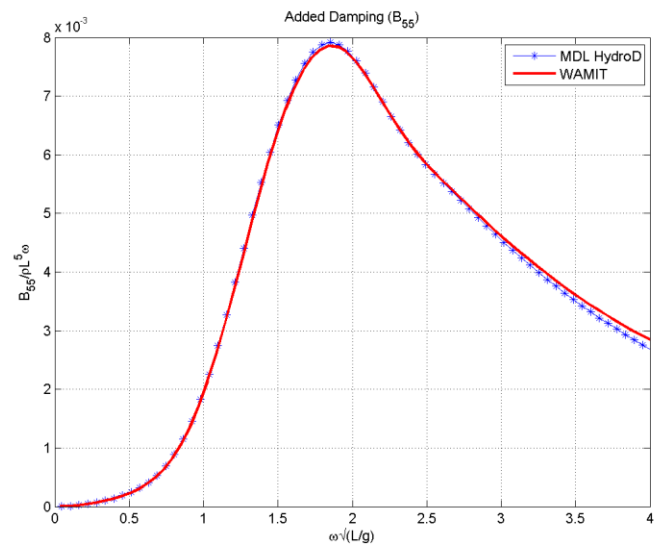
Fig. 140. Ship damping B_{55}
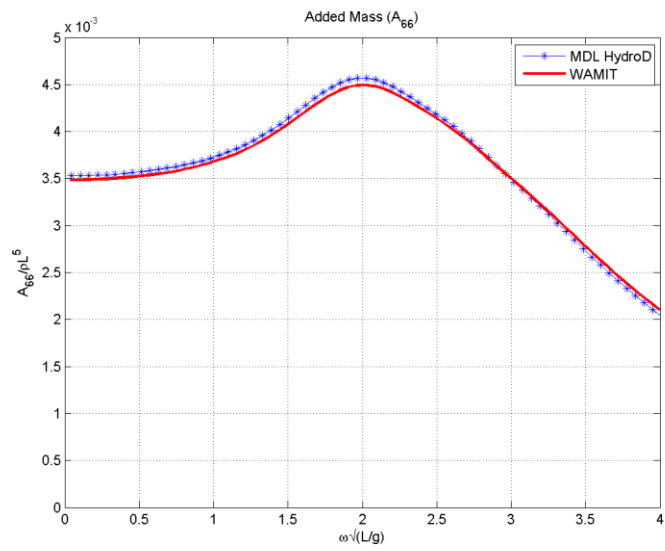
Fig. 141. Ship added mass A_{66}
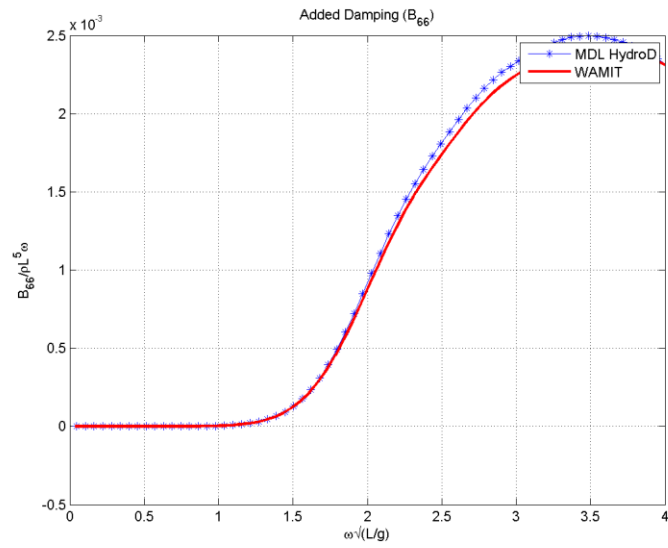
Fig. 142. Ship damping B_{66}

5.4 Forces
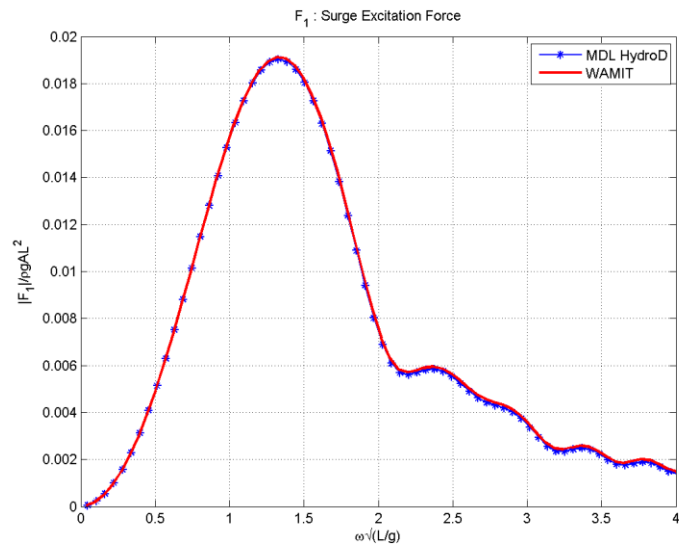
Fig. 143. Ship surge excitation force
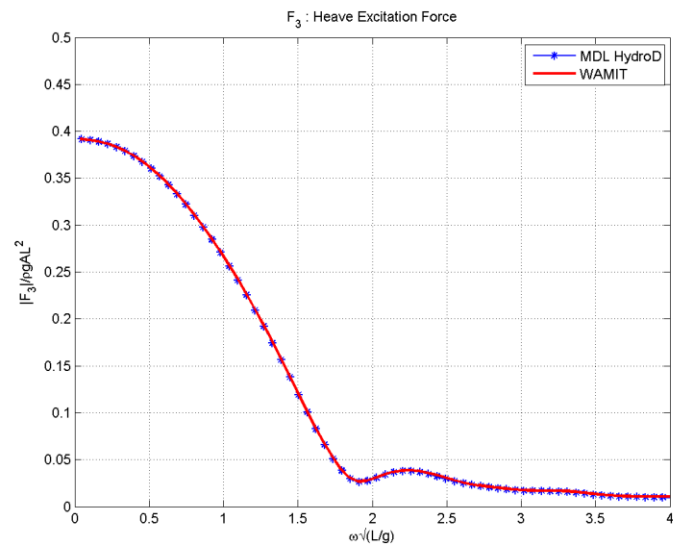
Fig. 144. Ship heave excitation force
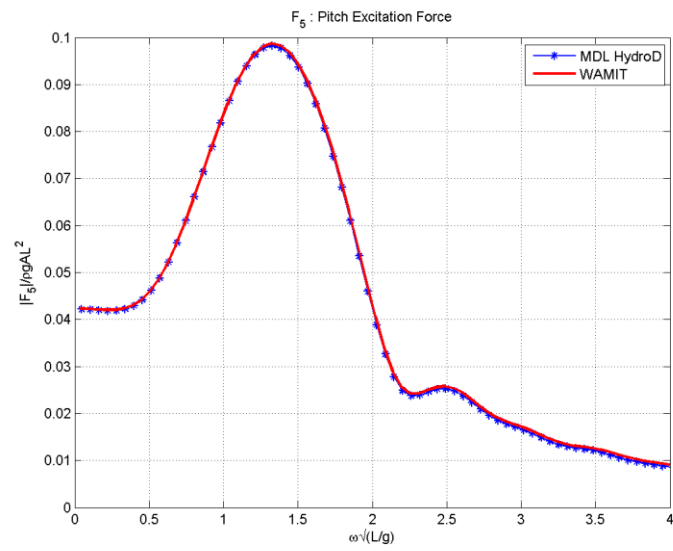
Fig. 145. Ship pitch excitation force

158

5.5 RAO
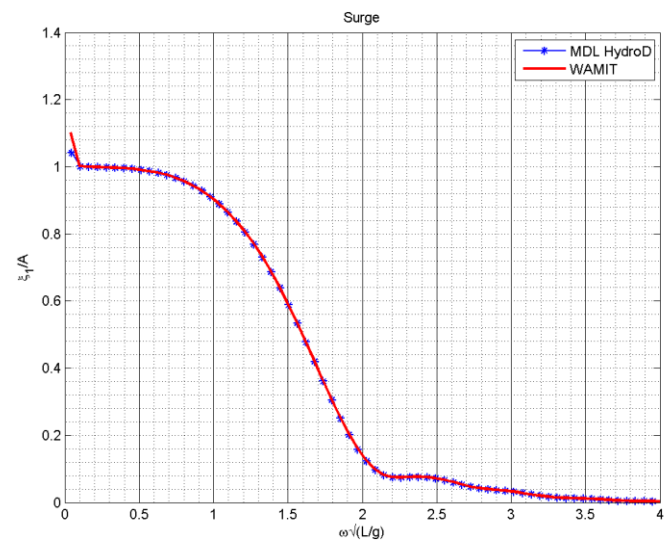
Fig. 146. Ship surge RAO
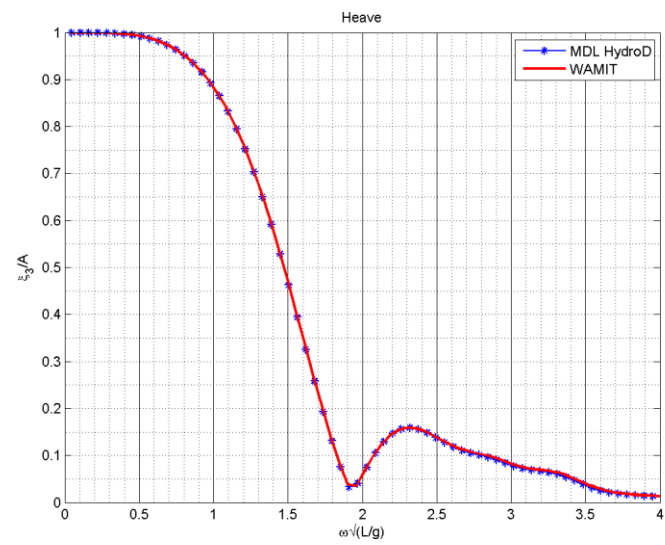
Fig. 147. Ship heave RAO

159
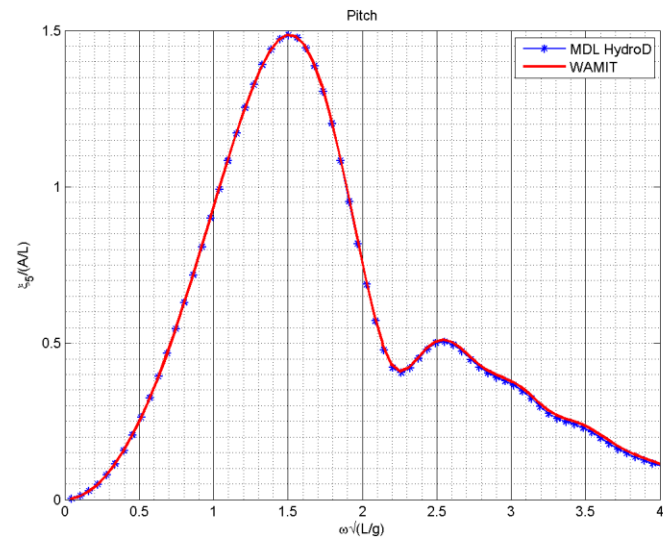
Fig. 148. Ship pitch RAO

6 T-Craft

6.1 Geometry and Panel Details
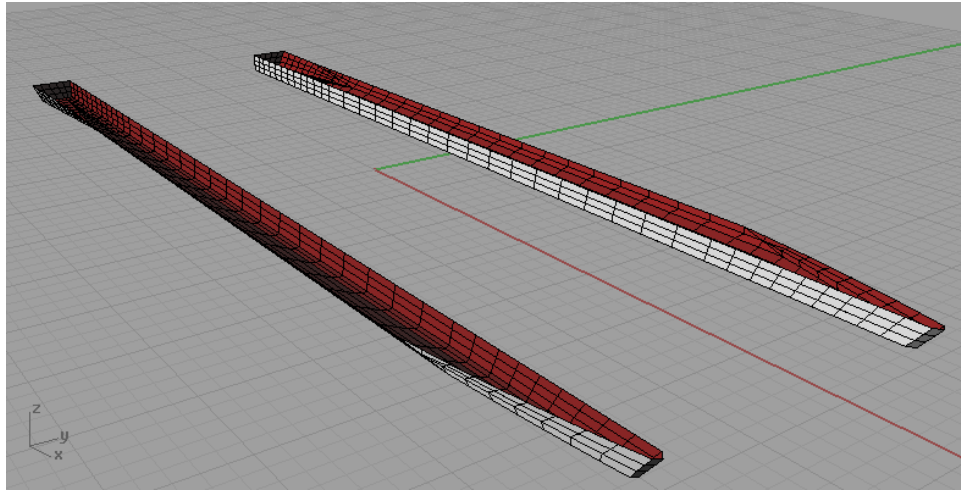
Fig. 149. T-Craft panel model

Table 20: T-Craft dimension

Parameter	Value
Length (On Cusion)	67.52 m
Draft	1.33 m
Cushion width	16.5m
Number of Panels	914
Water Depth	Infinite
Non dimensionalizing Length	1 m

6.2 Hydrostatics

Parameter	MDLHydroD	WAMIT
Volume	VOLX = 350.4449 VOLY= 350.4940 VOLZ = 350.4655	VOLX = 350.466 VOLY= 350.469 VOLZ = 350.470
Center of Buoyancy	Xb= -3.0188 Yb= 0.00000 Zb= -0.5564	Xb= -3.023516 Yb= -0.000003 Zb= -0.556466
Hydrostatic Stiffness Terms	C33 = 358.6418 C35 = 1024.897 C44 = 33522.44 C55 = 128026.5	C33 = 358.64 C35 = 1025.3 C44 = 33522.0 C55 = 0.12801E+06

6.3 Added Mass and Damping
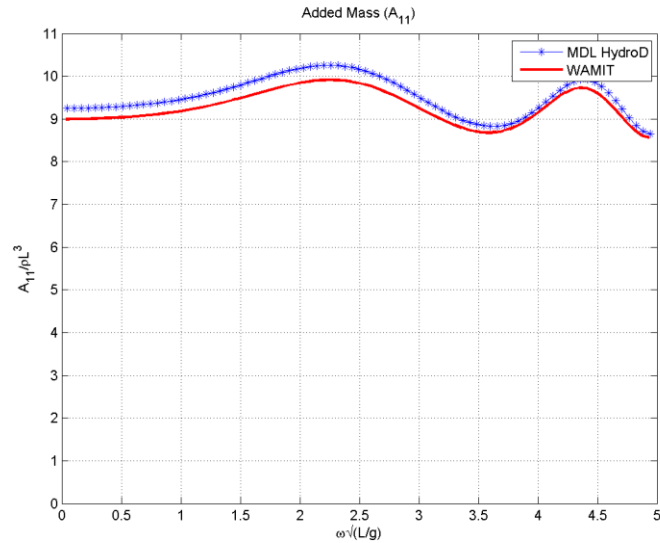
Fig. 150. T-Craft added mass A_{11}
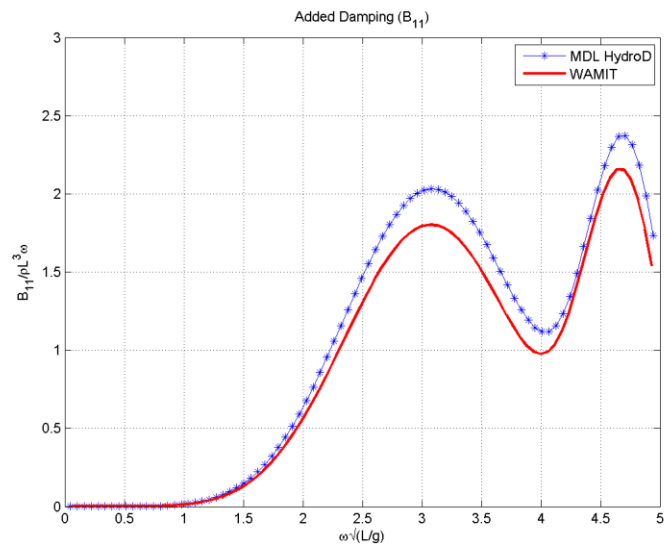
Fig. 151. T-Craft damping B_{11}
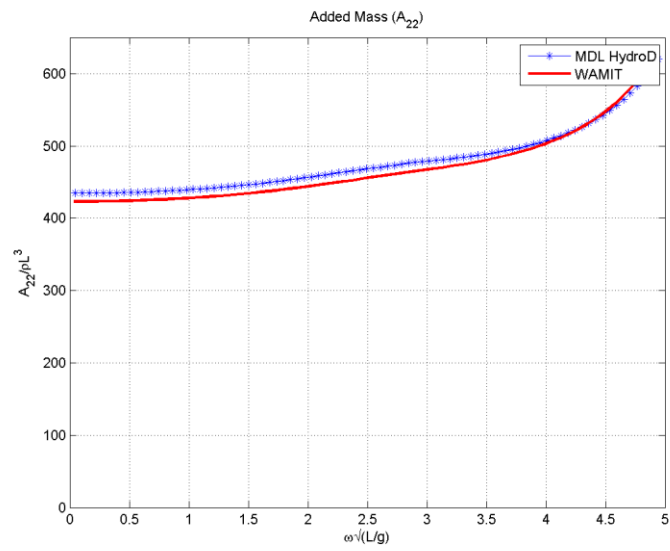
Fig. 152. T-Craft added mass A_{22}

163
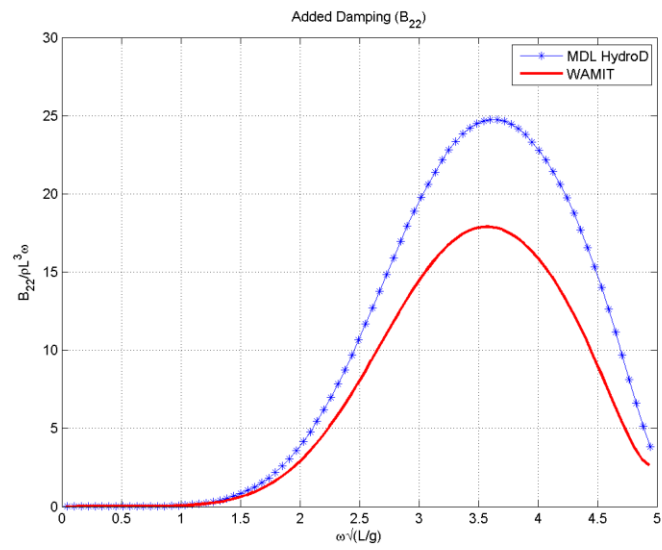
Fig. 153. T-Craft damping B_{22}
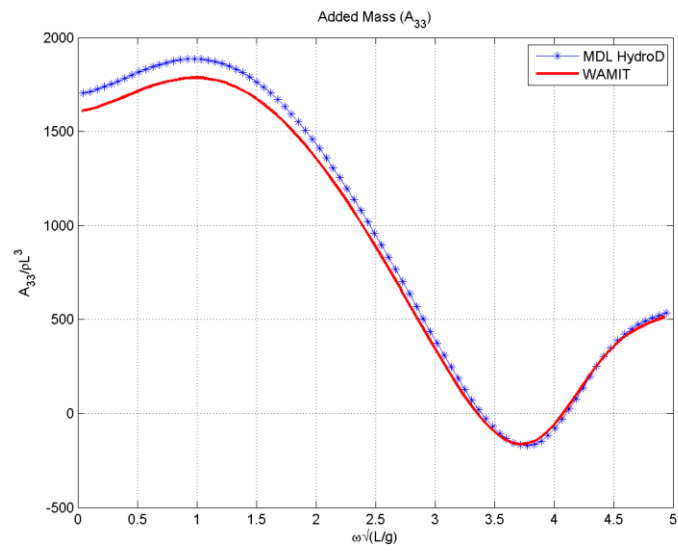
Fig. 154. T-Craft added mass A_{33}

164
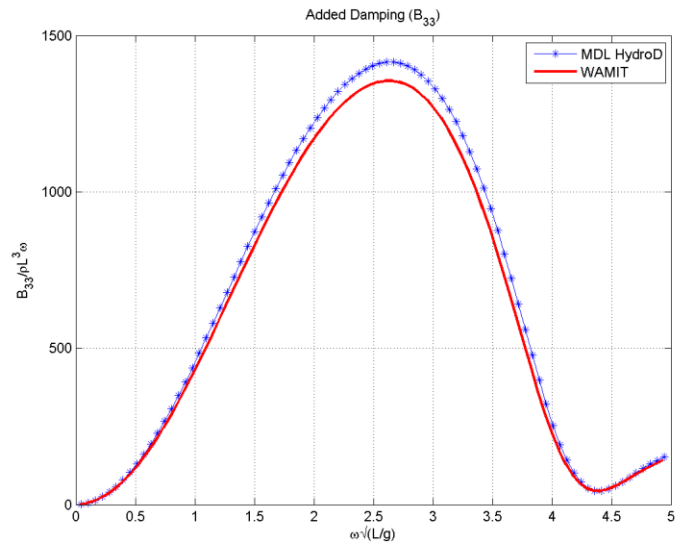
Fig. 155. T-Craft damping B_{33}
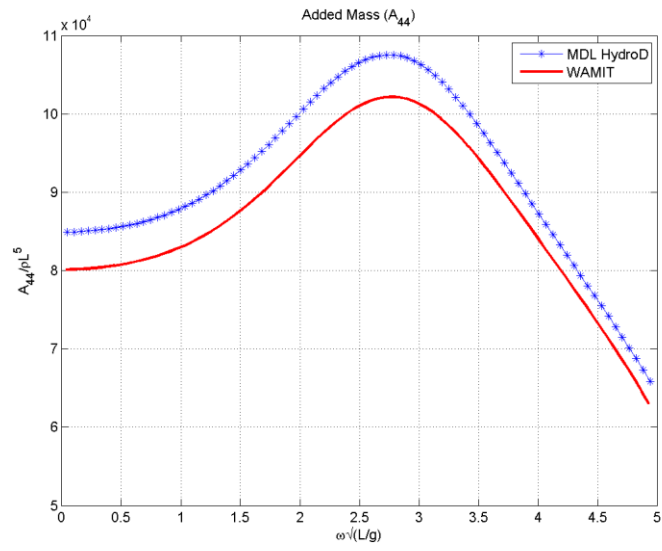
Fig. 156. T-Craft added mass A_{44}
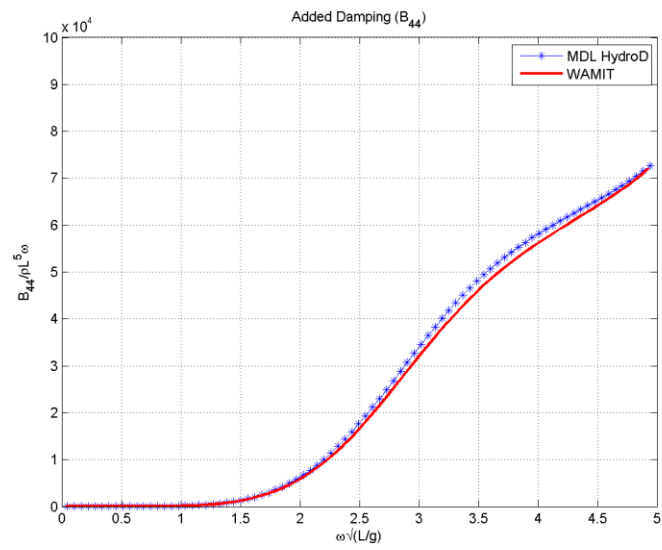
Fig. 157. T-Craft damping B_{44}
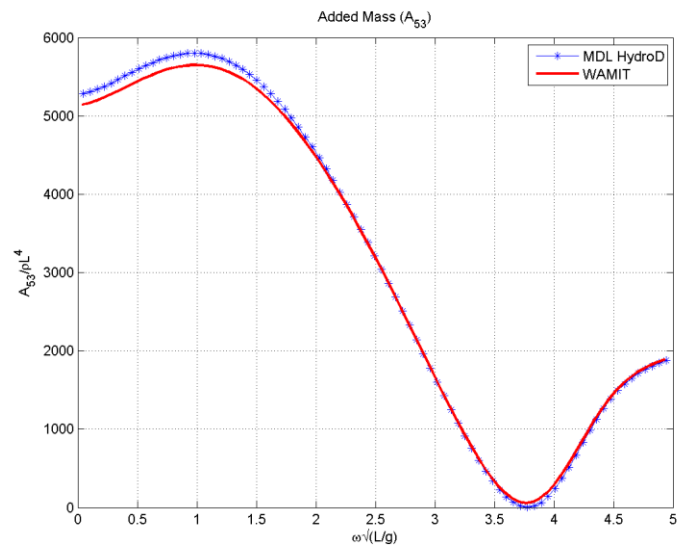
Fig. 158. T-Craft added mass A_{53}

166
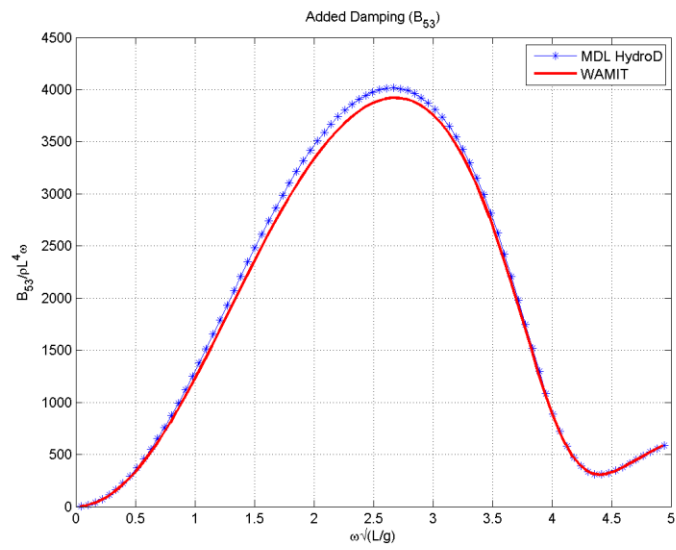
Fig. 159. T-Craft damping B_{53}
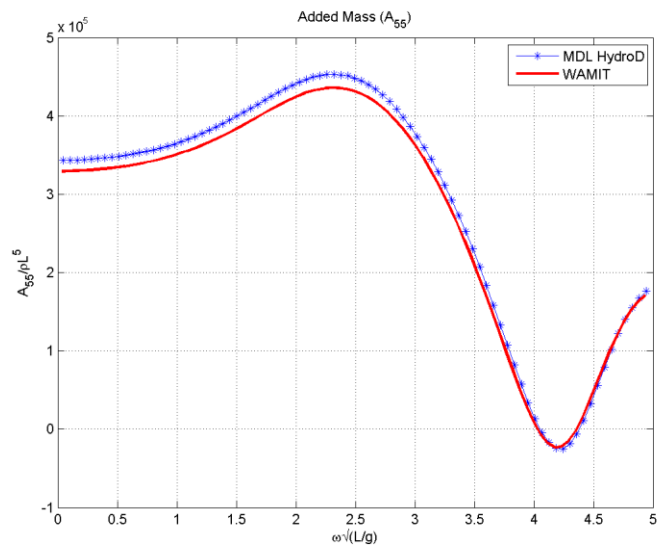
Fig. 160. T-Craft added mass A_{55}
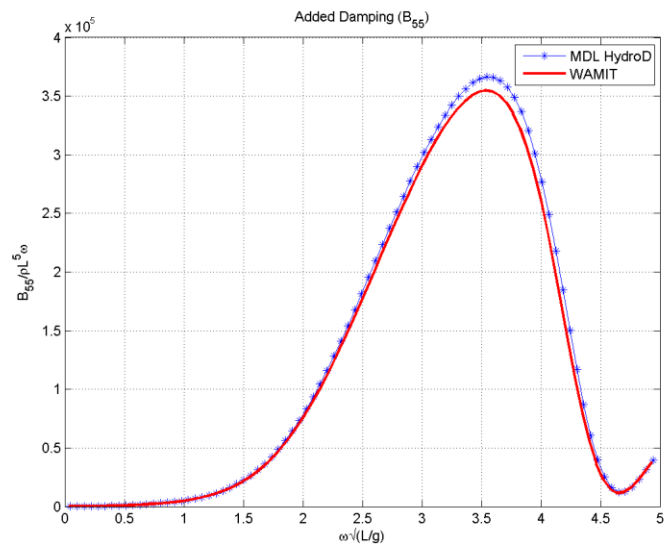
Fig. 161. T-Craft damping B_{55}
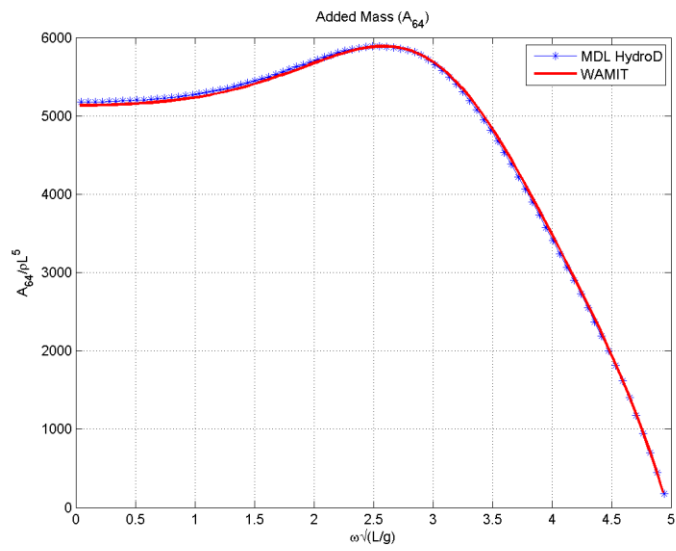
Fig. 162. T-Craft added mass A_{64}

168
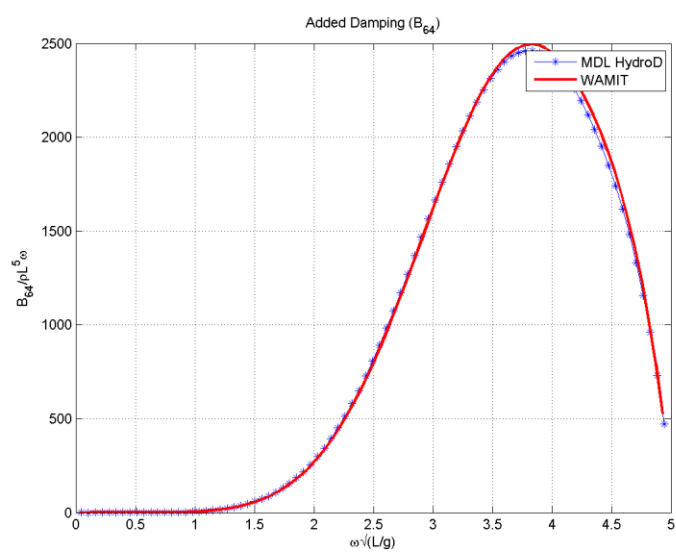
Fig. 163. T-Craft damping B_{64}
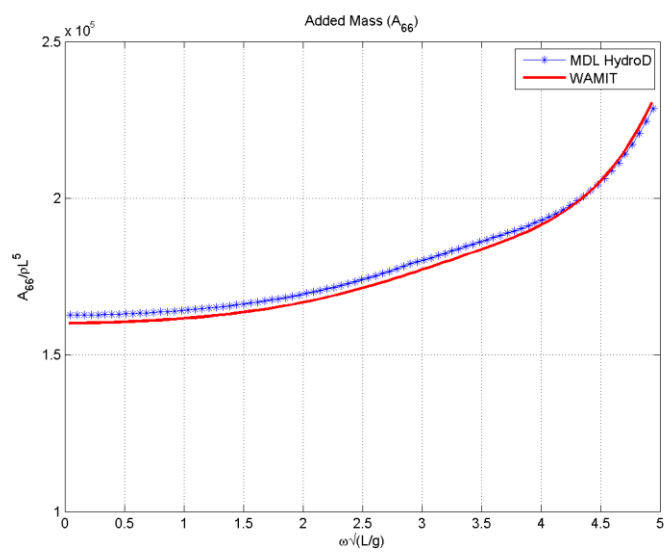
Fig. 164. T-Craft added mass A_{66}
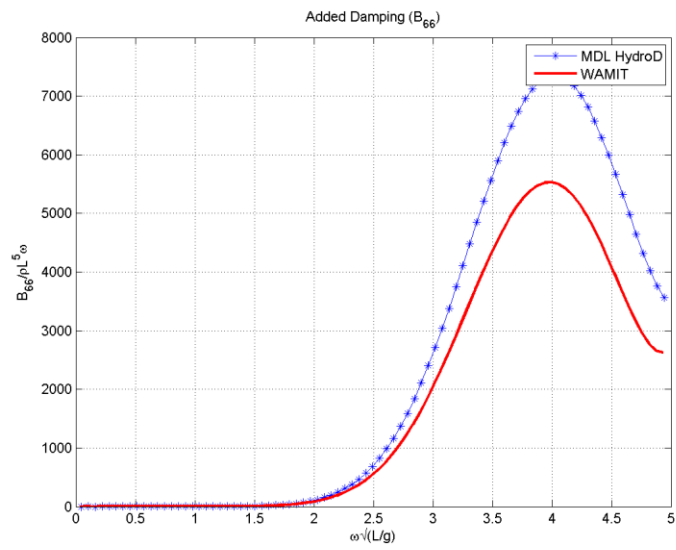
Fig. 165. T-Craft damping B_{66}

6.4 Forces
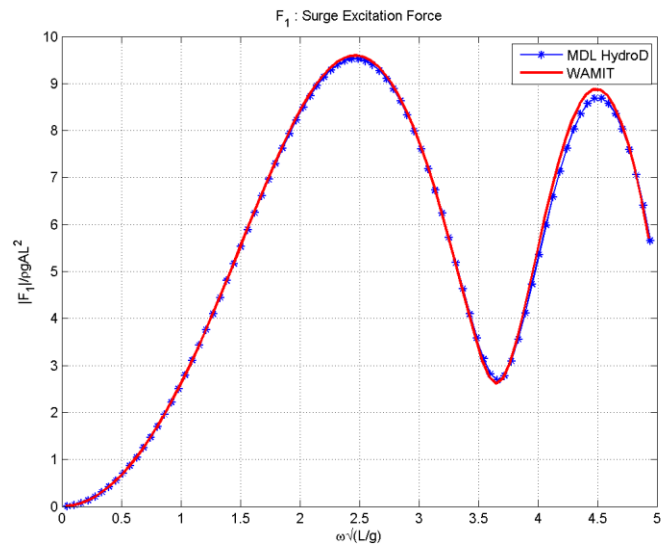
Fig. 166. T-Craft surge excitation force

170
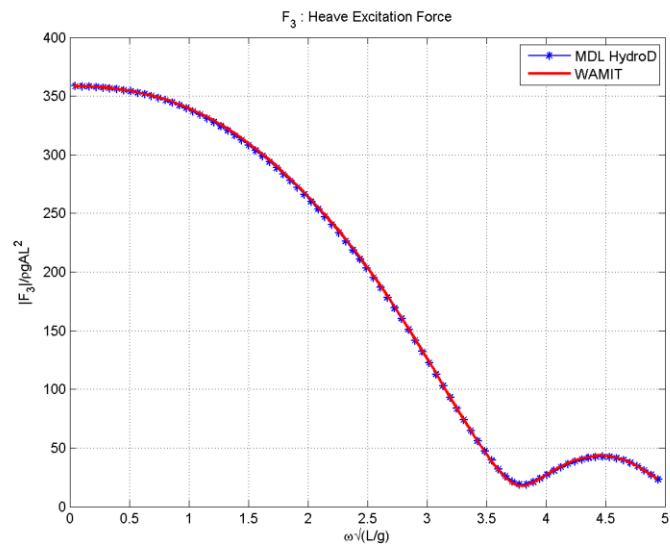
Fig. 167. T-Craft heave excitation force
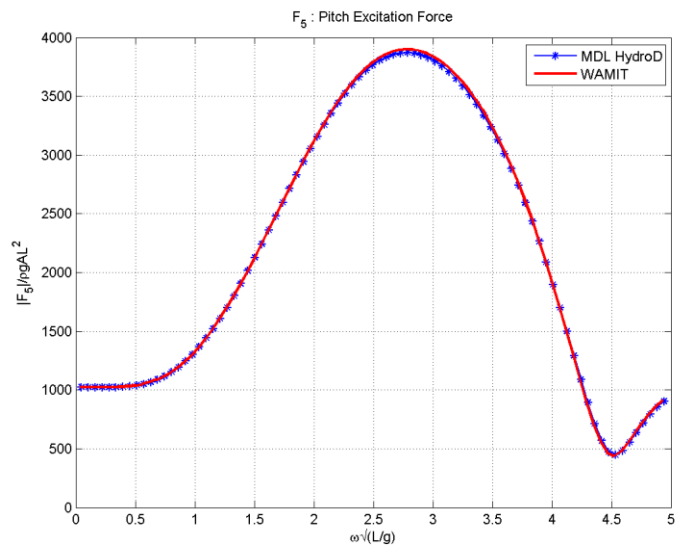
Fig. 168. T-Craft pitch excitation force

171

6.5 RAO
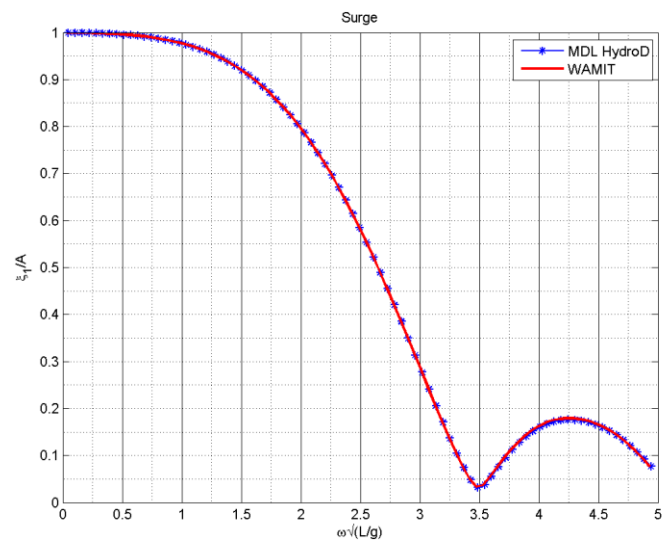
Fig. 169. T-Craft surge RAO
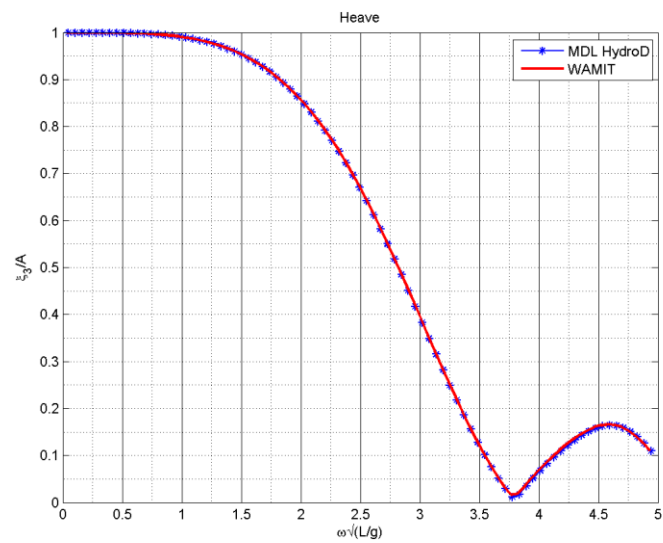
Fig. 170. T-Craft heave RAO

172
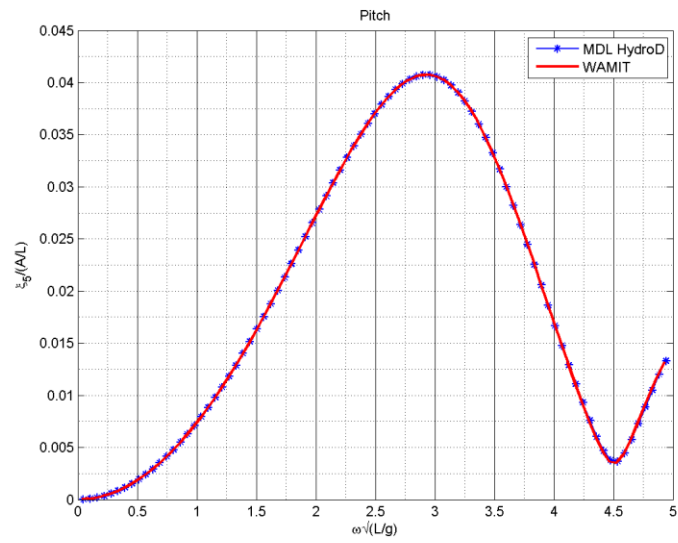
Fig. 171. T-Craft pitch RAO

7 TLP

7.1 Geometry and Panel Details
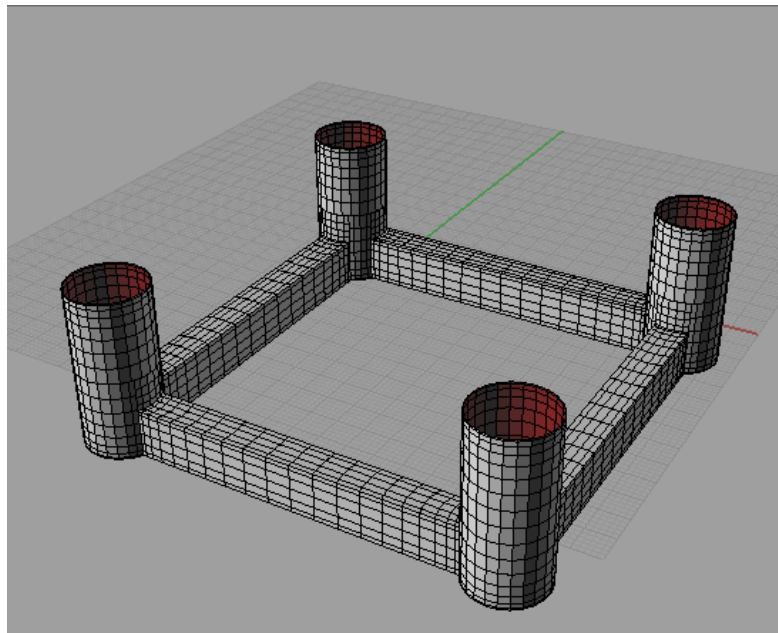
Fig. 172. TLP panel model

Table 21: TLP dimension

Parameter	Value
Cylindrical Column Diameter	17 m
Pontoon Lenght	69.12 m
Number of Panels	4048
Water Depth	Infinite
Non dimensionalizing Length	43.125 m

7.2 Hydrostatics

Parameter	MDLHydroD	WAMIT
Volume	VOLX = 53066.41 VOLY= 53066.43 VOLZ = 53112.37	VOLX = 53066.3 VOLY= 53066.3 VOLZ = 53112.3
Center of Buoyancy	Xb= 6.9180045E-05 Yb= 0.00000 Zb= -22.58567	Xb= -0.000010 Yb= -0.000007 Zb= -22.605247
Hydrostatic Stiffness Terms	C33 = 0.4772040 C35 = -0.62022657E-07 C44 = 8.8613532E-02 C55 = 8.8613532E-02	C33 = 0.47720 C35 = 1.5344E-07 C44 = 8.8593E-02 C55 = 8.8592E-02

7.3 Added Mass and Damping
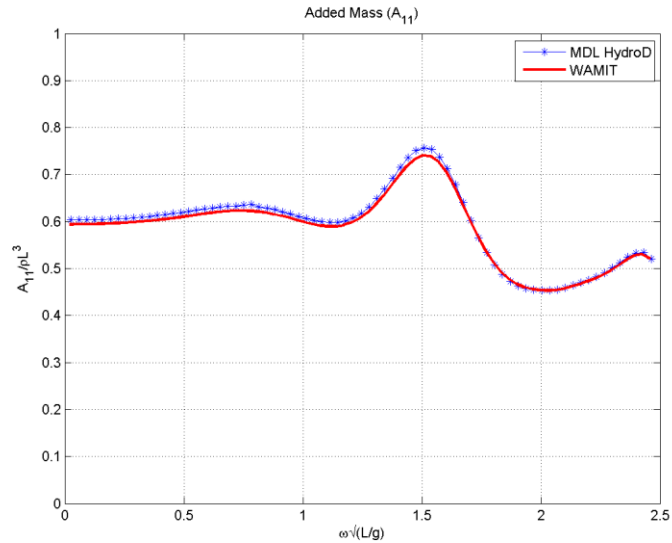
Fig. 173. TLP added mass A_{11}
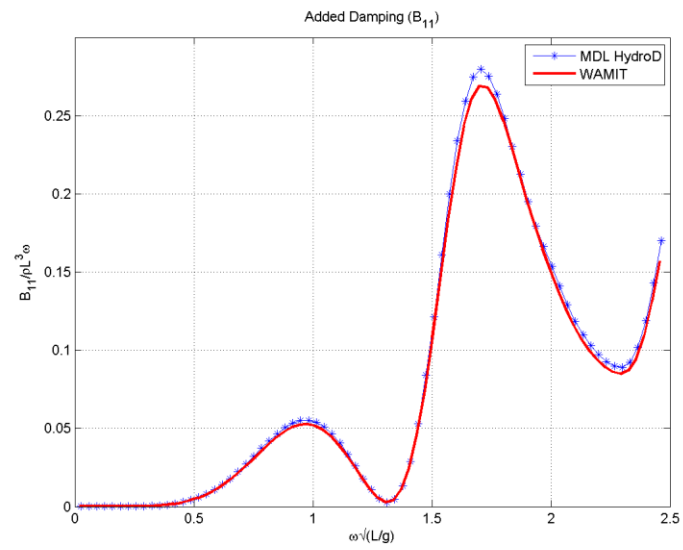
Fig. 174. TLP damping B_{11}
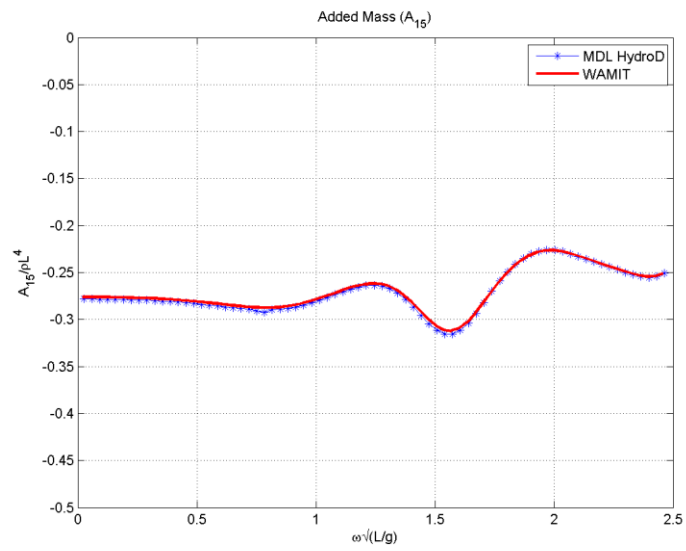
Fig. 175. TLP added mass A_{15}
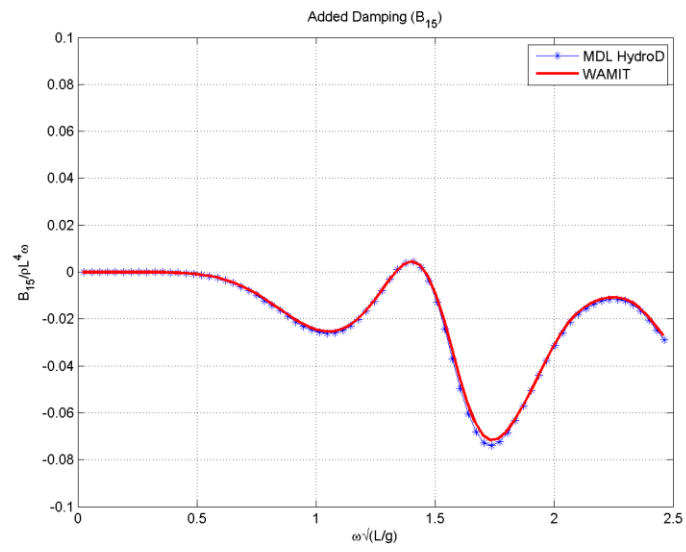
Fig. 176. TLP damping B_{15}
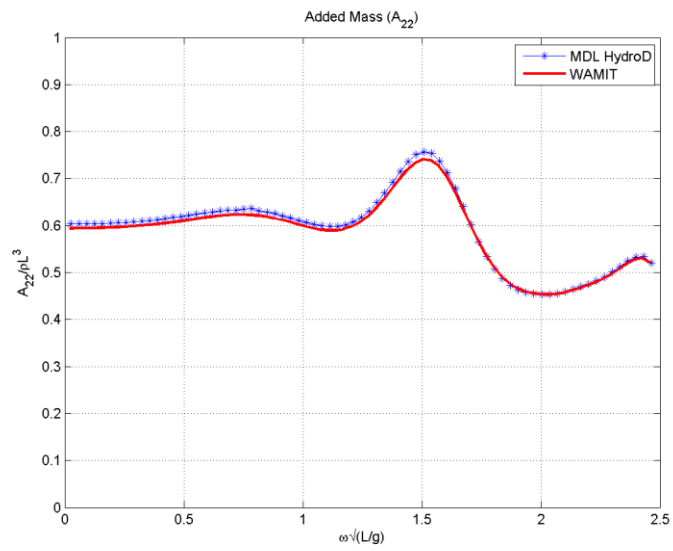
Fig. 177. TLP added mass A_{22}
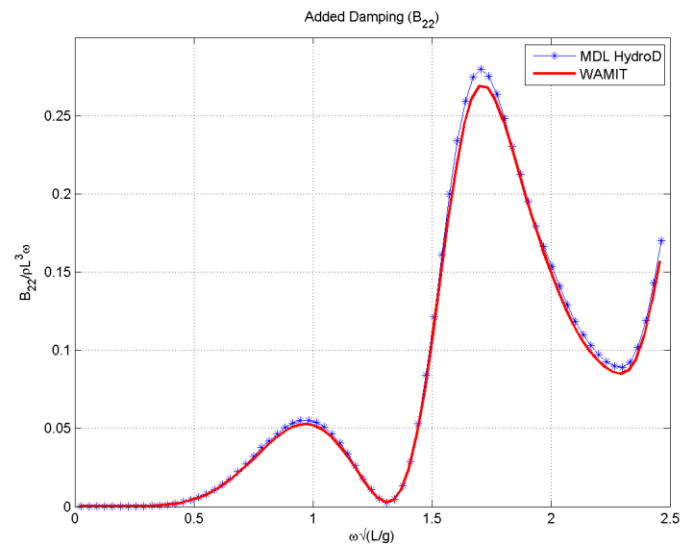
Fig. 178. TLP damping B_{22}
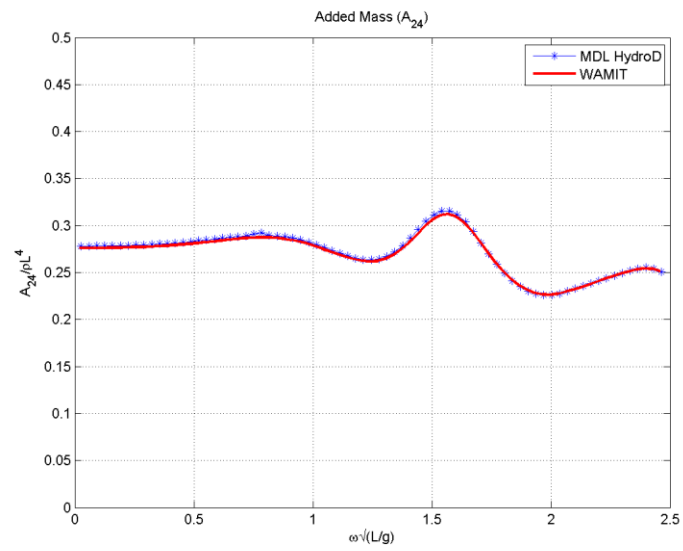
Fig. 179. TLP added mass A_{24}
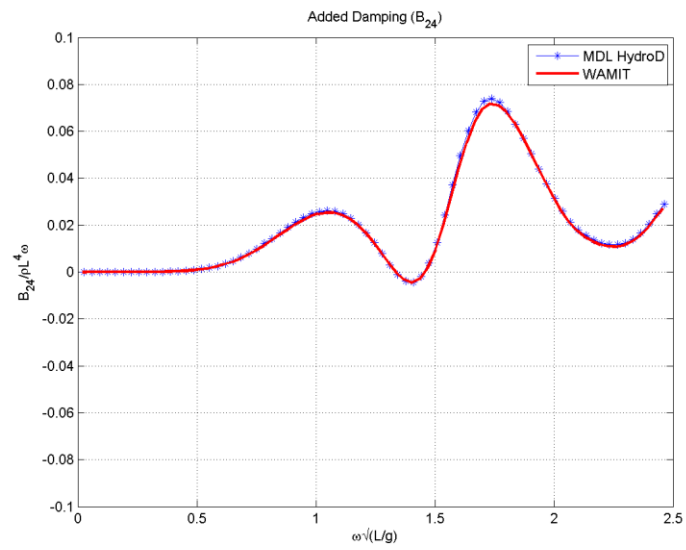
Fig. 180. TLP damping B_{24}
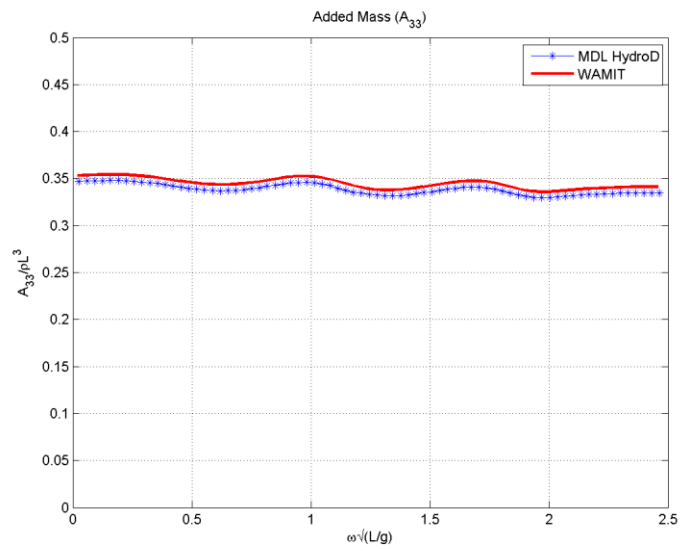
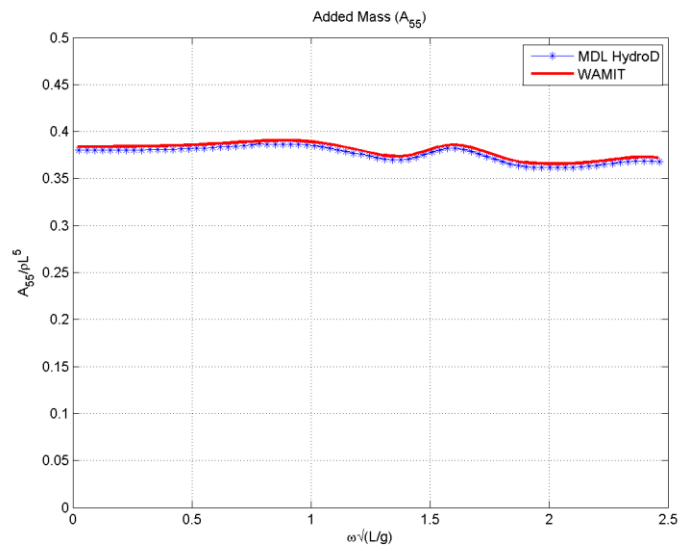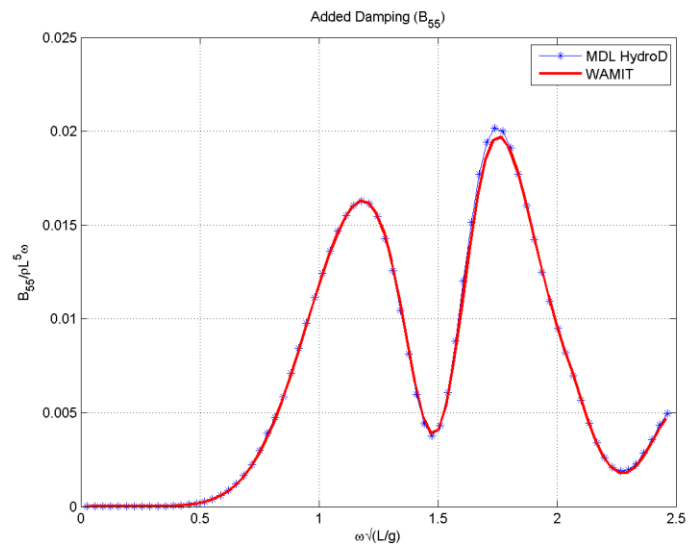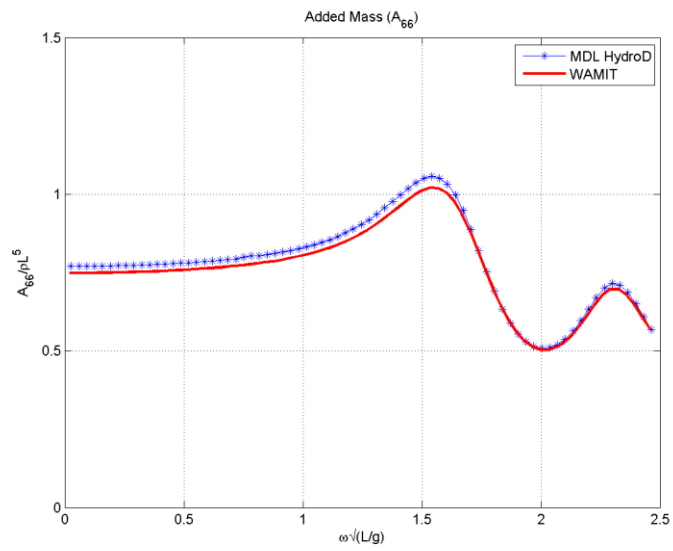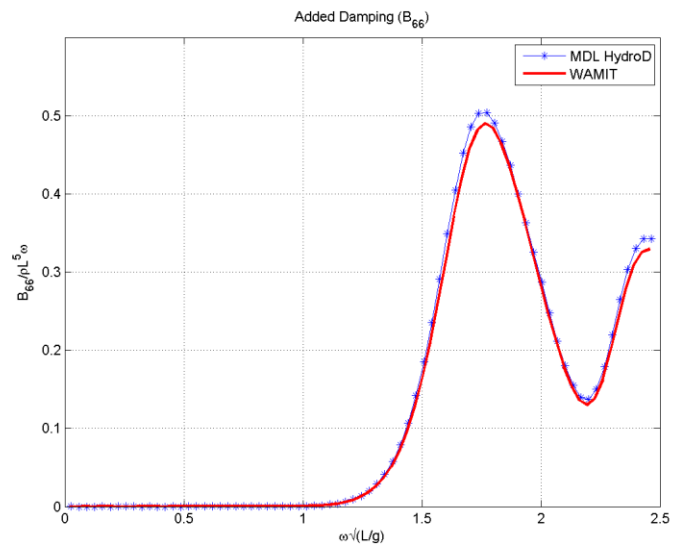Fig. 181. TLP added mass A_{33}
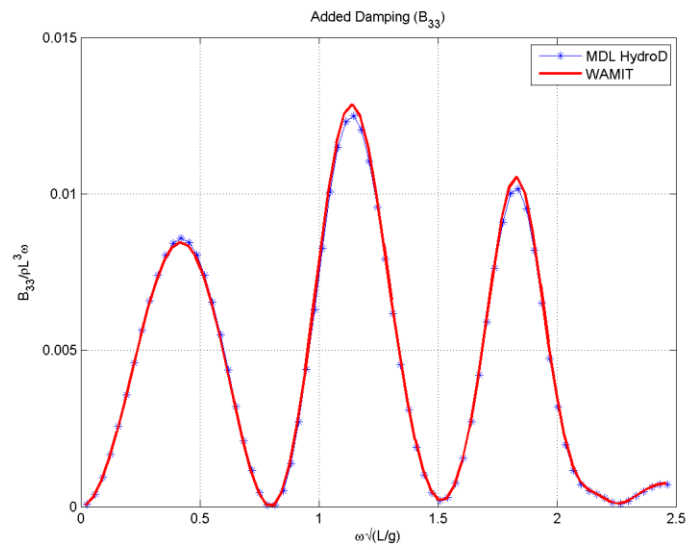
Fig. 182. TLP damping B_{33}
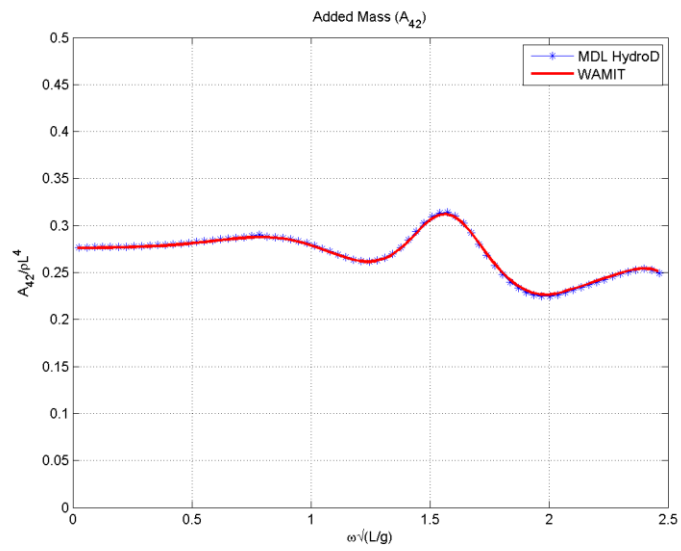
Fig. 183. TLP added mass A_{42}
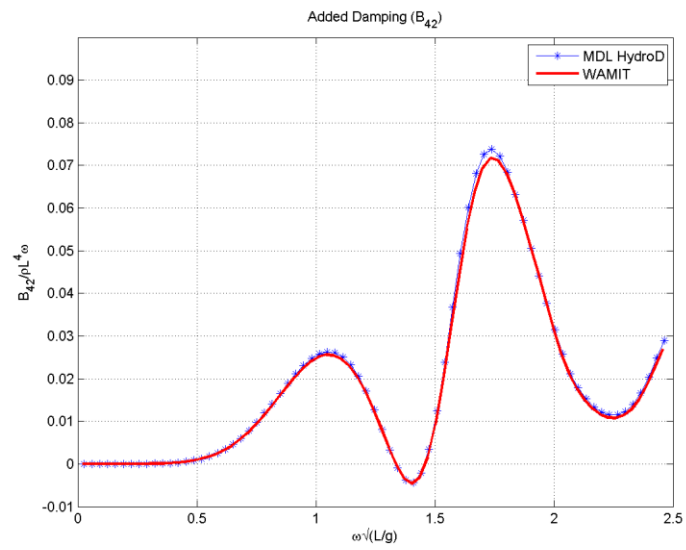
Fig. 184. TLP damping B_{42}
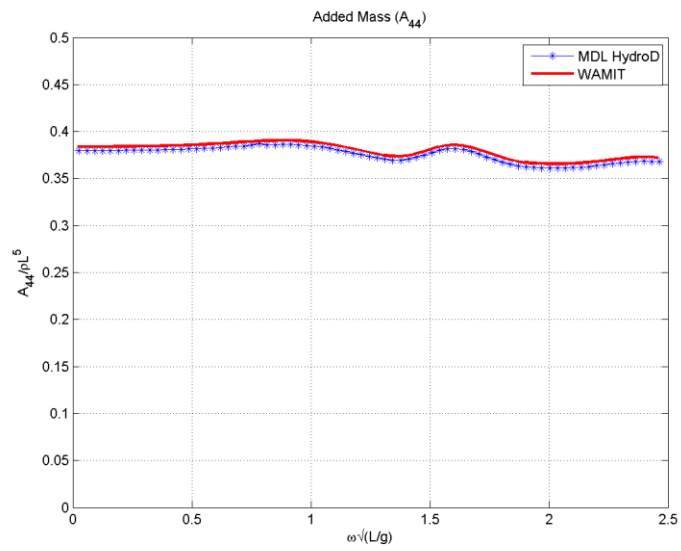
Fig. 185. TLP added mass A_{44}
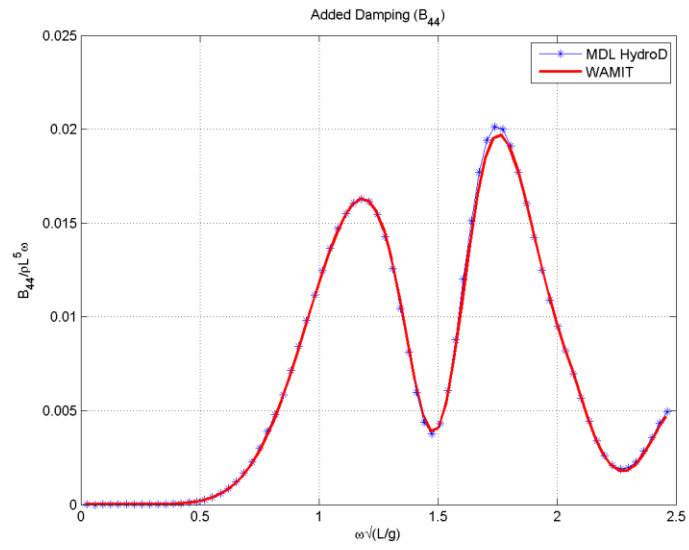
Fig. 186. TLP damping B_{44}
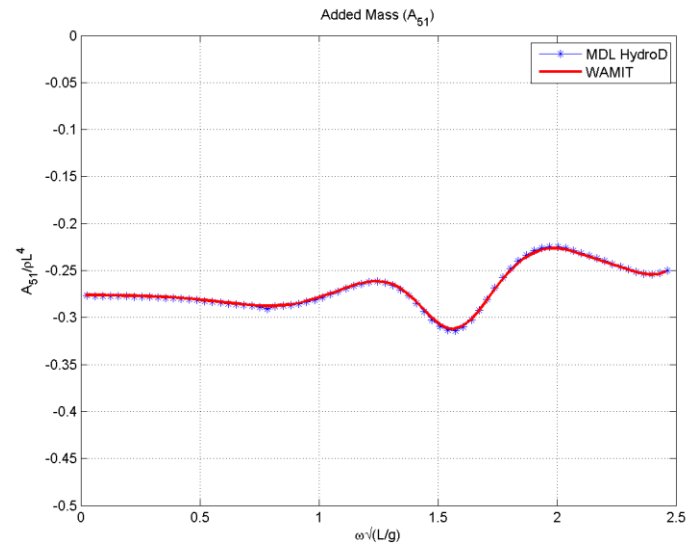
Fig. 187. TLP added mass A_{51}
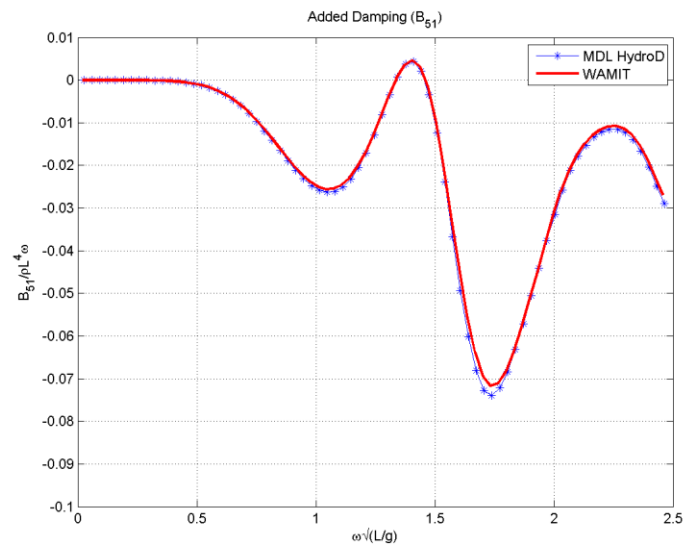
Fig. 188. TLP damping B_{51}

Fig. 189. TLP added mass A_{55}

Fig. 190. TLP damping B_{55}

Fig. 191. TLP added mass A_{66}

184

Fig. 192. TLP damping B_{66}

7.4 Forces
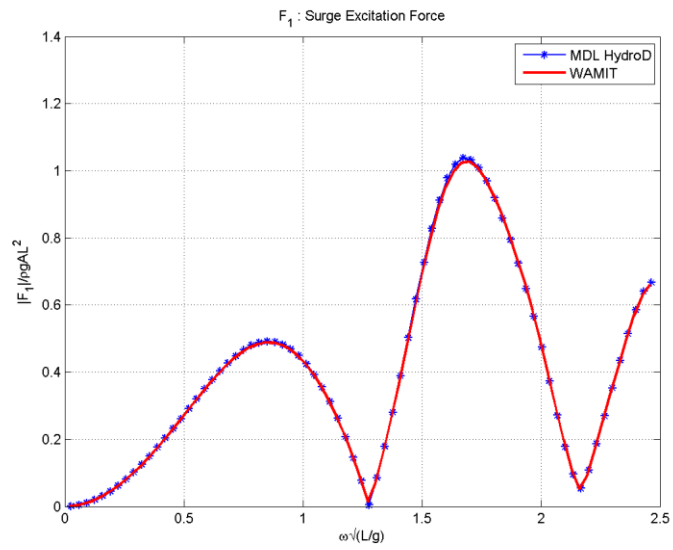
Fig. 193. TLP surge excitation force

185
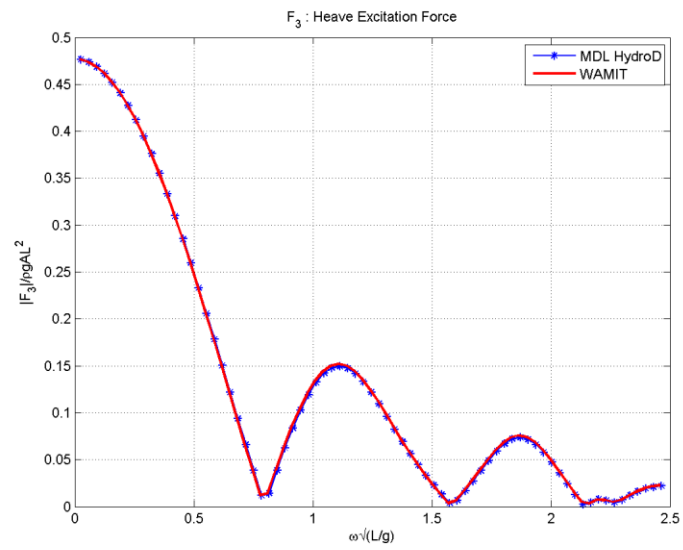
Fig. 194. TLP heave excitation force
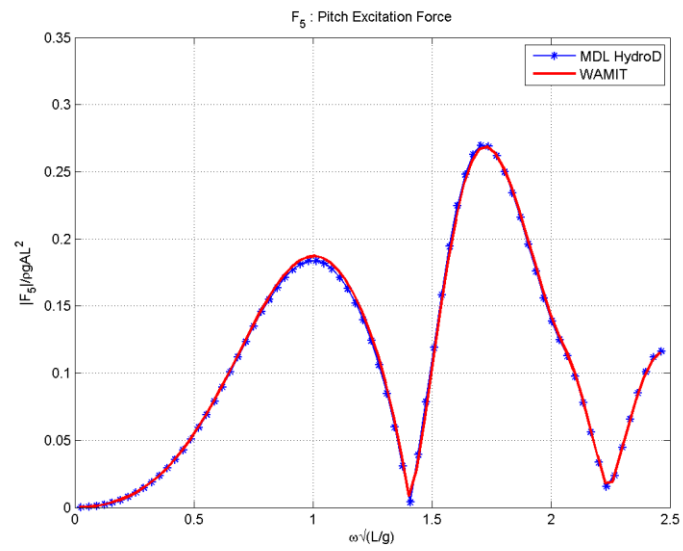
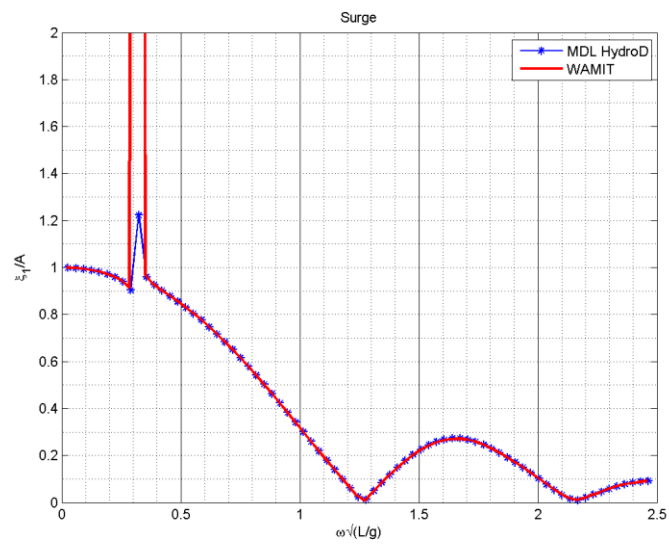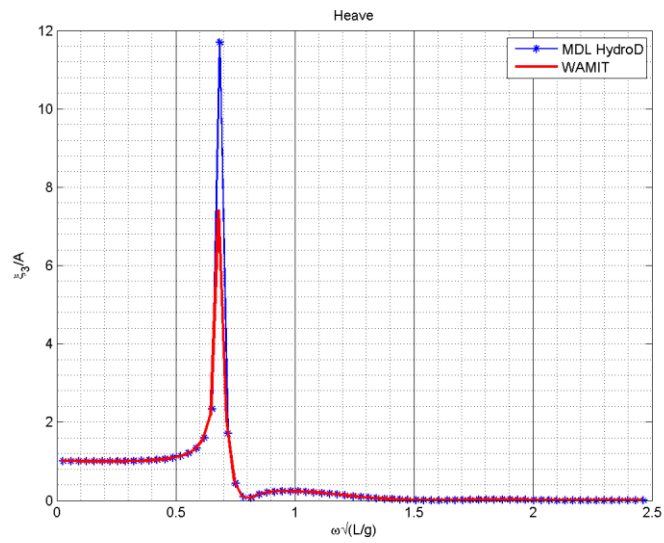Fig. 195. TLP pitch excitation force

7.5 RAO
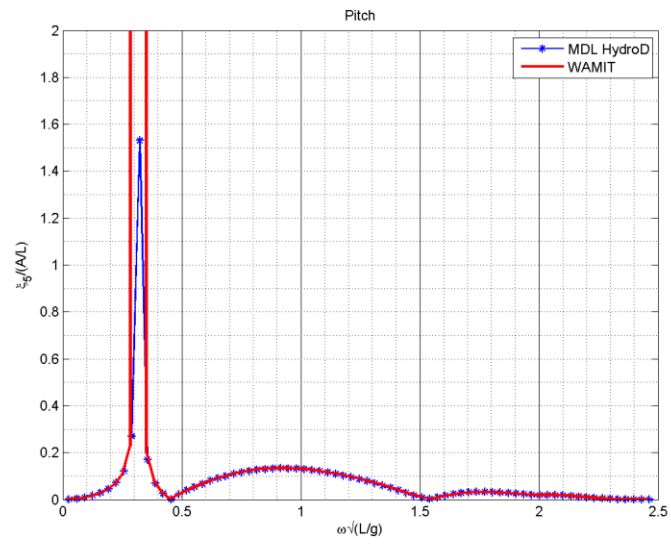

Fig. 196. TLP surge RAO

Fig. 197. TLP heave RAO

Fig. 198. TLP pitch RAO